Enhancing Voltage Regulation in Medium Voltage Distribution Grids in Ghana using Photovoltaic Generation

Desmond Okwabi Ampofo

Universität Bremen 2022

Enhancing Voltage Regulation in Medium Voltage Distribution Grids in Ghana using Photovoltaic Generation

Vom Fachbereich für Physik und Elektrotechnik

der Universität Bremen

zur Erlangung des akademischen Grades

Doktor–Ingenieur (Dr.-Ing.)

genehmigte Dissertation

von

MSc. Desmond Okwabi Ampofo

wohnhaft in Bremen

Referentin:	**Prof. Dr.-Ing. Johanna Myrzik**
Korreferent:	**Prof. Dr.-Ing. Christian Rehtanz**
Eingereicht am:	7th December, 2021
Tag des Promotionskolloquiums:	25th August, 2022

To my family and friends

"We cannot solve our problems with the same thinking we use when we created them"

Albert Einstein (1879-1955)

Acknowledgment

I would like to thank the Almighty God for giving me the strength to finish this thesis. I would like to also convey my deep appreciation to my supervisor, Professor Johanna Myrzik for allowing me to study in Germany and also having confidence in me to pursue a Ph.D. career. In addition, her valuable guidance and support throughout this Ph.D. journey were amazing. Secondly, I am very grateful to Professor Christian Rehtanz for accepting to be my second supervisor and for his valuable support as well. Sincere gratitude goes to Professor Kai Michels and Professor Emmanuel Frimpong who were the examiners of this thesis and by extension members of the Doctoral Committee. I am very grateful to both of them for taking the time to evaluate the thesis and the oral examination. This journey would not have been possible without the funding support from DAAD (German Academic Exchange Service), I am grateful to them.

I owe a lot of gratitude to all my colleagues (Ahmed Abdelsamad, Holm Hinners, Sergio Contreras, Nasratullah Mohseni, Adnan Shihab, and Tom Warendorf) in the institute for their friendship and support along this journey. Special gratitude to Marilyn Asmah for her encouragement and for making time to proofread the entire thesis and offer valuable criticisms. I am grateful to Samuel Osei Fobi and Asare Koduah for also proofreading part of this thesis.

My gratitude also goes to my adopted German family, Mr. and Mrs. Baumann for their emotional support and for always welcoming me into their home, especially during the Christmas periods. My stay in Germany would have not been complete without them. My profound gratitude also goes out to the Ghanaian community in Bremen for their friendship and support, especially to Micheal Kyei Agyekum, Nicholas Adjei, and James Ziemah.

Lastly, I would like to thank my parents and siblings in Ghana for their valuable support and for always being there for me.

Abstract

It is estimated that the photovoltaic (PV) generation capacity in distribution grids in Ghana will increase to 200 MW by the year 2030. According to the number of licenses issued by the Energy Commission of Ghana, 80% of this capacity will be located in the northern part of the country. This will have a significant impact on voltage regulation as two main issues arise. First, the distribution grid in the northern and middle parts of the country experiences low voltages especially during the peak demand period as a result of the transmission of power over long distances from the southern part of the country, where about 90% of the total generation capacity is located. The expected integrations of PVs mostly in the northern part of the country will therefore improve the voltage profiles but only during the solar generation period as it reduces the power transfer from the south to the north. The second issue is that the northern parts of the country account for about 10% of the national load demand. Thus, the expected high increase in PV units will potentially lead to a voltage rise on the grid especially as the peak solar hours coincide with the low demand period on a typical day in Ghana. Mitigating these issues requires the active participation of PV units in voltage regulation, which the national grid code allows in the form of local reactive power control methods.

Each reactive power control method has a varied impact on the network performance. A comparative assessment of the $Q(U)$ and $cos\varphi(P)$ local voltage control methods based on genetic algorithm (GA) optimal power flow is therefore carried out using probabilistic models for both load (demand) and generation to account for their stochastic nature. Simulation results reveal the effectiveness of the $Q(U)$ control in reducing power loss on the grid, improving voltage profile, and minimizing the tap movements of the on-load tap changer and voltage regulator as compared to the $cos\varphi(P)$ voltage control method when implemented on a medium voltage distribution network. Notwithstanding, its performance depends on its control parameters and how it can change its reactive power compensation with the changing load and generation conditions.

Therefore, this research proposes an innovative concept to change the reactive power compensation to the changing grid conditions by incorporating an adaptive functionality made up of voltage stability and sensitivity blocks into the $Q(U)$ control method. Different load and generation scenarios are used to

demonstrate the effectiveness and robustness of this proposed concept to improve the voltage profiles, especially during both peak demand and solar hour periods by keeping the voltages within the regulatory grid code range using only locally measured variables (voltage and DG active and reactive power) at the PCC. This scheme was furthermore compared with $Q(U)$ control operating with fixed control parameters and fully centralised voltage control. In all the comparisons, the proposed concept performed better than the $Q(U)$ control with fixed control parameters and achieved comparable performance with the fully centralised scheme which uses communication facilities.

Keywords: Medium voltage distribution network, Ghana, local voltage control, photovoltaic, Q(U) control.

Kurzfasszung

Schätzungen zufolge wird die Photovoltaik (PV)-Erzeugungskapazität in den Verteilernetzen in Ghana bis zum Jahr 2030 auf 200 MW ansteigen. Nach der Anzahl der von der ghanaischen Energiekommission erteilten Lizenzen werden 80% dieser Kapazität im nördlichen Teil des Landes angesiedelt sein. Dadurch ergeben sich zwei Hauptprobleme, die erhebliche Auswirkungen auf die Spannungsregulierung haben. Erstens ist das Verteilernetz im Norden und in der Mitte des Landes vor allem während der Nachfragespitzen von niedrigen Spannungen betroffen, da der Strom über weite Strecken aus dem Süden des Landes übertragen wird. Hier befinden sich etwa 90 % der gesamten Erzeugungskapazität. Die erwartete Integration von PV-Anlagen vor allem im Norden des Landes wird daher die Spannungsprofile verbessern, allerdings nur während der solaren Erzeugungsperiode, da die Stromübertragung vom Süden in den Norden reduziert wird. Zweitens entfallen auf die nördlichen Landesteile etwa 10 % des nationalen Lastbedarfs. Daher wird der erwartete starke Anstieg der PV-Anlagen möglicherweise zu einem Spannungsanstieg im Netz führen, zumal die Spitzenzeiten der Solarenergie mit den Zeiten geringer Nachfrage an einem typischen Tag in Ghana zusammenfallen. Um diese Probleme abzuschwächen ist eine aktive Beteiligung von PV-Anlagen an der Spannungsregulierung erforderlich, die der nationale Netzcode in Form von lokalen Blindleistungsregelungsmethoden zulässt.

Jede Methode der Blindleistungsregelung hat einen unterschiedlichen Einfluss auf die Netzleistung. Daher wird eine vergleichende Bewertung der lokalen Spannungsregelungsmethoden $Q(U)$ und $cos\varphi(P)$ auf der Grundlage eines optimalen Leistungsflusses mittels genetischer Algorithmen (GA) durchgeführt, wobei probabilistische Modelle sowohl für die Last (Nachfrage) als auch für die Erzeugung verwendet werden, um deren stochastischen Charakter zu berücksichtigen. Die Simulationsergebnisse zeigen die Wirksamkeit der $Q(U)$-Regelung bei der Verringerung der Leistungsverluste im Netz, der Verbesserung des Spannungsprofils und der Minimierung der Stufenschaltungen von Laststufenschaltern und Spannungsreglern im Vergleich zur $cos\varphi(P)$-Spannungsregelungsmethode,wenn sie in einem Mittelspannungsverteilungsnetz eingesetzt wird. Allerdings hängt die Leistung von den Regelungsparametern ab und davon, wie die Blindleistungskompensation bei sich ändernden Last- und Erzeugungsbedingungen angepasst werden kann.

Daher wird in dieser Studie ein innovatives Konzept zur Anpassung der Blindleistungskompensation an die sich ändernden Netzbedingungen vorgeschlagen, indem eine adaptive Funktionalität aus Spannungsstabilitäts- und Empfindlichkeitsblöcken in die $Q(U)$-Regelmethode integriert wird. Verschiedene Last- und Erzeugungsszenarien werden verwendet, um die Wirksamkeit und Robustheit dieses vorgeschlagenen Konzepts zur Verbesserung der Spannungsprofile insbesondere während der Spitzenlast und der Sonnenstunden zu demonstrieren, indem die Spannungen innerhalb des regulatorischen Grid-Code-Bereichs gehalten werden, wobei nur lokal gemessene Variablen (Spannung und DG-Wirk- und Blindleistung) am PCC verwendet werden. Dieses System wurde außerdem mit der $Q(U)$-Regelung, die mit festen Regelparametern arbeitet, und einer vollständig zentralisierten Spannungsregelung verglichen. Bei allen Vergleichen schnitt das vorgeschlagene Konzept besser ab als die $Q(U)$-Regelung mit festen Regelparametern und erreichte eine vergleichbare Leistung wie die vollständig zentralisierte Regelung, die Kommunikationseinrichtungen nutzt.

Contents

Contents

List of Figures

List of Tables

List of Abbreviations and Symbols

Abbreviations

Abbreviations	Definition
AD	Adaptive
AnDar	Anderson-Darling
ANN	Artificial Neural Network
CB	Capacitor Bank
CCU	Centralised Control Unit
CIGRE	International Council on Large Electric Systems
CT	Current Transformer
DG	Distributed Generation
DNO	Distribution Network Operator
DMS	Distribution Management System
EC	Energy Commission
ES	Energy Storage
FIT	Feed-In-Tariffs
GA	Genetic Algorithm
IEEE	Institute of Electrical and Electronics Engineers
LDC	Line Drop Compensation
LV	Low Voltage Distribution Network
MAS	Multi-Agent System
MF	Membership Function
MPC	Model Predictive Control
MRP	Mines Reserve Power
MV	Medium voltage

Abbreviations	Definition
NMS	Network Management System
OLTC	On-load Tap Changer
OPF	Optimal Power Flow
PCC	Point of Common Coupling
PDF	Probability Density Function
PF	Power Factor
PT	Potential Transformer
PURC	Public Utilities Regulatory Commission
PV	Photovoltaic
RA	Resource Agent
RE	Renewable Energy
REPO	Renewable Energy Purchase Obligation
RTU	Remote Terminal Unit
SCADA	Supervisory Control and Data Acquisition
SVC	Static Var Compensators
SVO	System Voltage Optimisation
TAPCO	Takoradi Power Company
TICO	Takoradi International Company
TT1PP	Tema Thermal 1 Power Plant
TT2PP	Tema Thermal 2 Power Plant
VR	Voltage Regulator
VRD	Voltage Regulating Device
VSCI	Voltage Source Inverters
VSI	Voltage Stability Index
WAGP	West Africa Gas Pipeline

Symbols

Photovoltaic Parameters

Symbol	Term	Unit SI
I_{MPP}	Current at maximum power point	A
U_{MPP}	Voltage at maximum power point	V
S_{RAD}	Solar irradiance values for that hour	W/m^2
S_{STC}	Solar irradiance at standard test conditions	W/m^2
I_{SH}	Short-circuit current of the module	A
K_C	Current temperature coefficient	A/°C
T_{CT}	Cell temperature	°C
U_{OP}	Open-circuit voltage of the module in volts	V
K_U	Voltage temperature coefficient	V/°C
T_{AC}	Cell ambient temperature	°C
N_T	Cell nominal operating temperature	°C
FF	Photovoltaic fill factor	-
I_{PV}	Photovoltaic output voltage	A
U_{PV}	Photovoltaic output current	V

Probability density function

Symbol	Term	Unit SI
μ	Mean of the normal distribution	-
σ	Standard deviation of the normal distribution	-
c	Scale factor of the Weibull distribution	-
k	Shape factor of the Weibull distribution	-
α	Shape parameter of Beta distribution	-
β	Shape parameter of Beta distribution	-

Local control parameters

Symbol	Term	Unit SI
P_0	Active power value for reactive power compensation to begin	p.u.
P_1	Active power value for maximum reactive power compensation	p.u.
Q_{MAX}	Maximum allowable reactive power	MVAr
U_1	Voltage value at maximum reactive power (capacitive region)	p.u.
U_2	Voltage value for lower dead band	p.u.
U_3	Voltage value for upper dead band	p.u.
U_4	Voltage value at maximum reactive power (inductive region)	p.u.

Optimization parameters

Symbol	Term	Unit SI
P_{DEM}	Active power demand (load) at a bus	p.u.
P_{GEN}	Active power generation at a bus	p.u.
Q_{DEM}	Reactive power demand (load) at a bus	p.u.
Q_{GEN}	Reactive power generation at a bus	p.u.
G_{ij}	Conductance between bus i and j	p.u.
B_{ij}	Susceptance between bus i and j	p.u.
U_i	Magnitude of bus voltage	p.u
δ_i	Angle of bus voltage	degree
L_{TD}	Total load on the grid	MVA
L_i	Load magnitude at a bus	MVA
k_i	Weight factor of a bus	-
V_{INDEX}	Voltage profile improvement index	p.u.

Voltage sensitivity function parameters

Symbol	Term	Unit SI
P_{DG}	Active power output of DG	p.u.
Q_{DG}	Reactive power output of DG	p.u.
U_{PCC}	Voltage at the point of common coupling	p.u.
P	Active power injection into a bus	p.u.
Q	Reactive power injection into a bus	p.u.
$\partial U_{PCC}/\partial Q$	Voltage sensitivity with respect to reactive power injection	-
$\partial U_{PCC}/\partial P$	Voltage sensitivity with respect to active power injection	-
Q_{SF}	Required reactive power	p.u.
U_{TARGET}	Desired voltage at the point of common coupling	p.u
S_{lim}	Rating of the inverter	MVA
Q_{new}	Reactive output of adaptive control	MVAr

Artificial neural network parameters

Symbol	Term	Unit SI
x_i	Input data	-
y_i	Output value	-
w_i	Connection weights of the hidden layer	-
v_i	Connection weights of the output layer	-
h_i	Hidden layer	-
d_i	Desired output	-
E	Root mean square error signal	-
α	Activation function	-

Chapter 1 Introduction

Globally, there are exciting times for renewable energy (RE) as conscientious initiatives have been launched by world leaders to decrease the discharge of greenhouse gases such as carbon dioxide, nitrous oxide, methane, etc. These gases are the main causes of global warming and the resulting climate change. One such initiative, spearheaded by the United Nations under the United Nations Framework Convention on Climate Change, is the Paris Agreement. This agreement was adopted in December 2015 by heads of state and various country delegates [1]. A primary objective of this agreement is to keep the average global temperature rise below 2 degrees Celsius. One sure way of achieving this target is to focus on clean energy as an alternative to fossil fuel as suggested by authors of [2], who provided an aggressive approach to achieve this target after studying the energy sector, which includes transportation, heating, cooling, agriculture, and industry in 139 countries. The research concluded that zero-emissions energy should be 80% by 2030 and 100% by 2050 to keep global warming from rising above 1.5 degrees Celsius. This, in turn, favours the adoption of RE technologies, requiring a paradigm shift in the global energy system from fossil fuels that are hazardous to the environment to RE sources that are environmentally friendly and sustainable.

This global energy transformation which is also known as energy transition [3] has triggered technological research in the field of RE, which is summarised mainly into technical and policy research. The technical research focuses on implementing new designs and modernising existing energy infrastructure like the electrical power system to accommodate renewable energy integration. The policy research however focuses on initiatives and incentives that will increase the adoption of RE technologies as a plausible alternative to fossil fuels. In this regard, various countries have come up with new regulations and initiatives aimed at meeting defined targets. An example is Germany, where under the Erneuerbare-Energien-Gesetz translated in English as “Renewable Energy Sources Act (EEG 2017)”, the target is to increase the percentage share of renewable energy in the gross electricity consumption to 40-45% by 2025, 55-60% by 2035 and at least 80 percent by 2050 [4]. In driving this target, policies such as Feed-in Tariff was included in this Act to provide incentives to owners of RE sources. Furthermore, in the United Kingdom, the government had a target of achieving 15% of renewable energy penetration in the final total energy consumption (electricity, heating, cooling, and transport) by the end of 2020. At the end of 2019, 12.3% had been achieved [5]. This achievement can partly be attributed to the Feed-in Tariffs policy. Under this policy, the government is to

provide financial incentives to owners of renewable generation, which is limited to solar photovoltaic (PV), wind, micro combined heat and power, hydro and anaerobic digestion up to a capacity of 5MW [6].

The energy transition is however not only limited to industrialised countries like Germany and the United Kingdom, but several other countries including all the countries in Africa signed the Paris Agreement and have committed to the global effort to reduce the emissions of greenhouse gases [7]. Consequently, individual African countries have started introducing policies in this direction, whose results have been reflected in the overall energy outlook as reported in [8]. According to this report, the renewable energy capacity, including hydropower increased from 28 GW to 50 GW from 2010 to 2018. This increase accounts for 20.41% of the total installed generation capacity on the African continent which was 245 GW in 2018 [8]. In Ghana, hydropower and thermal energy are the main sources of electricity generation as shown in figure 1.1. This figure shows the increasing trend of thermal generation over the last few years. In 2019, thermal generation accounted for 59.8% of the generation mix with hydropower and other RE sources accounting for the remaining 39.9% and 0.3% respectively [9]. The thermal generators use natural gas, light crude oil, heavy fuel oil, and diesel as fuel. There is currently, a gradual attempt to diversify the energy sources for power generation from an over-reliance on thermal energy to renewable sources like PV and wind.

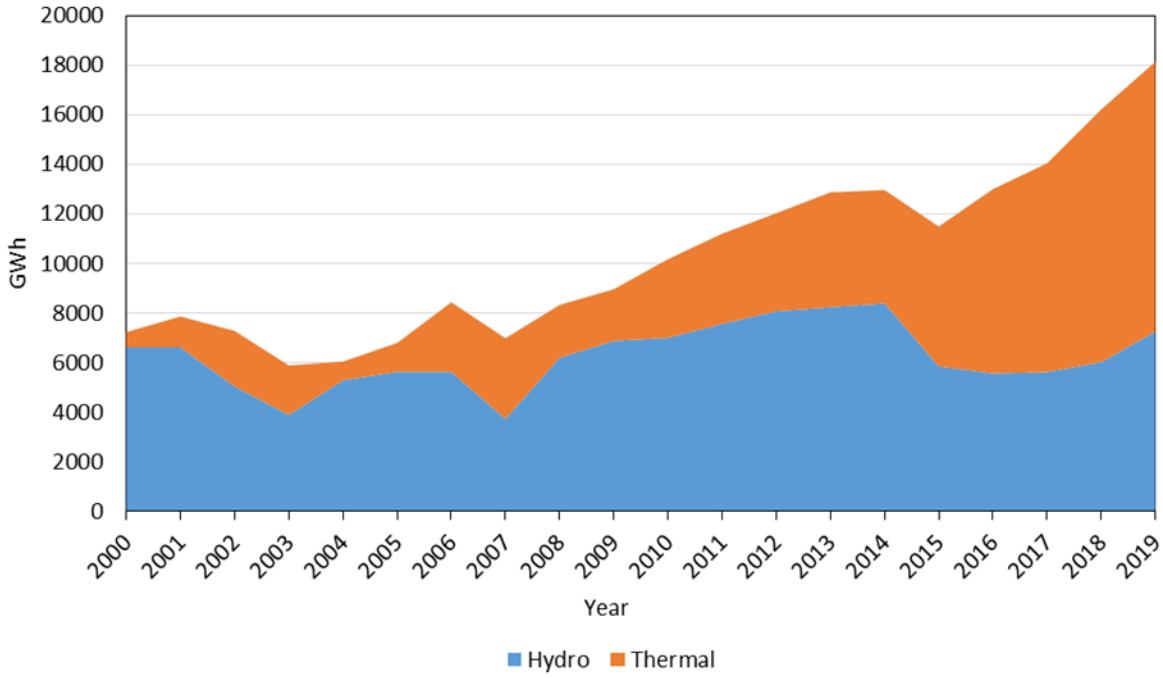

Figure 1.1 Electricity generation trend in Ghana [9]

The main driving force for this diversification is not just to reduce greenhouse emissions but also to enhance electricity security. Natural gas accounts for about

69.82% of the total amount of fuel used to power the thermal plants in Ghana as shown in table 1.1 [10], [11]. The natural gas supply imported from Nigeria through the West Africa Gas Pipeline (WAGP) accounts for 42% of the total gas used to power the thermal plants in the country [11]. WAGP is a gas distribution network connecting Ghana, Togo, and Benin to gas supplies from Nigeria Gas Company (N-Gas). Unfortunately, the gas supply from this pipeline has not been reliable, due to the fact that N-Gas has limited the volume of the gas supply to Ghana to 123 million standard cubic feet per day (mmscfd) instead of the contractual agreement of 440 mmscfd [11]. The limitation is because of the internal situation in Nigeria where the government is scaling up the thermal generation capacity to meet the additional 40,000 MW needed to address the energy challenges in that country [11]. This put a strain on N-Gas as it is unable to meet its contractual obligations to Ghana, resulting in a deficit in the volume of gas from WAGP which negatively affects the electricity supply in the country. This sometimes leads to shedding of load because of insufficient power generation from the thermal plants.

Table 1.1 Percentage breakdown of fuel consumption by thermal plants [10], [11]

Fuel type	Percentage
Natural gas	69.82
Heavy fuel oil	21.68
Light crude oil	4.73
Diesel	3.77

Yet, the country has a potential for other sources of RE like PV as highlighted by Asmah et al [12]. Figure 1.2 shows the average global solar irradiance potential of the entire country. It ranges from 4.5-5.6 kWh/m^2-day, with average values of irradiance for the northern parts of the country being higher than the south. These values are subject to seasonal variations. Ghana has three main seasons, namely, dry, harmattan, and rainy seasons. The rainy season is a period characterised by heavy rains starting from June to October. The harmattan, sometimes considered part of the dry season, is a period characterised by dry and dusty winds blowing from the Sahara desert. Harmattan starts from November to January. The dry season on the other hand is a period of a long drought, very low humidity, and very sunny, which starts from February to May. Higher values of solar irradiance thus occur in the dry season. This is very significant since the water level in the hydropower dams which determines the amount of power generation drops very low during this season because of the drought, leading to a reduction in the hydropower output. This

reduction will result in load shedding in parts of the country if there is not enough thermal generation to compensate for the shortfalls in hydropower generation as was the case in 2015 [12]. PV can thus be harnessed and used to compensate for the shortfalls in hydropower generation during the dry season. Whereas the wind potential energy in Ghana has been estimated to be a total of 5,600 MW out of which 200-400 MW are deemed exploitable due to geographical constraints [13], [14].

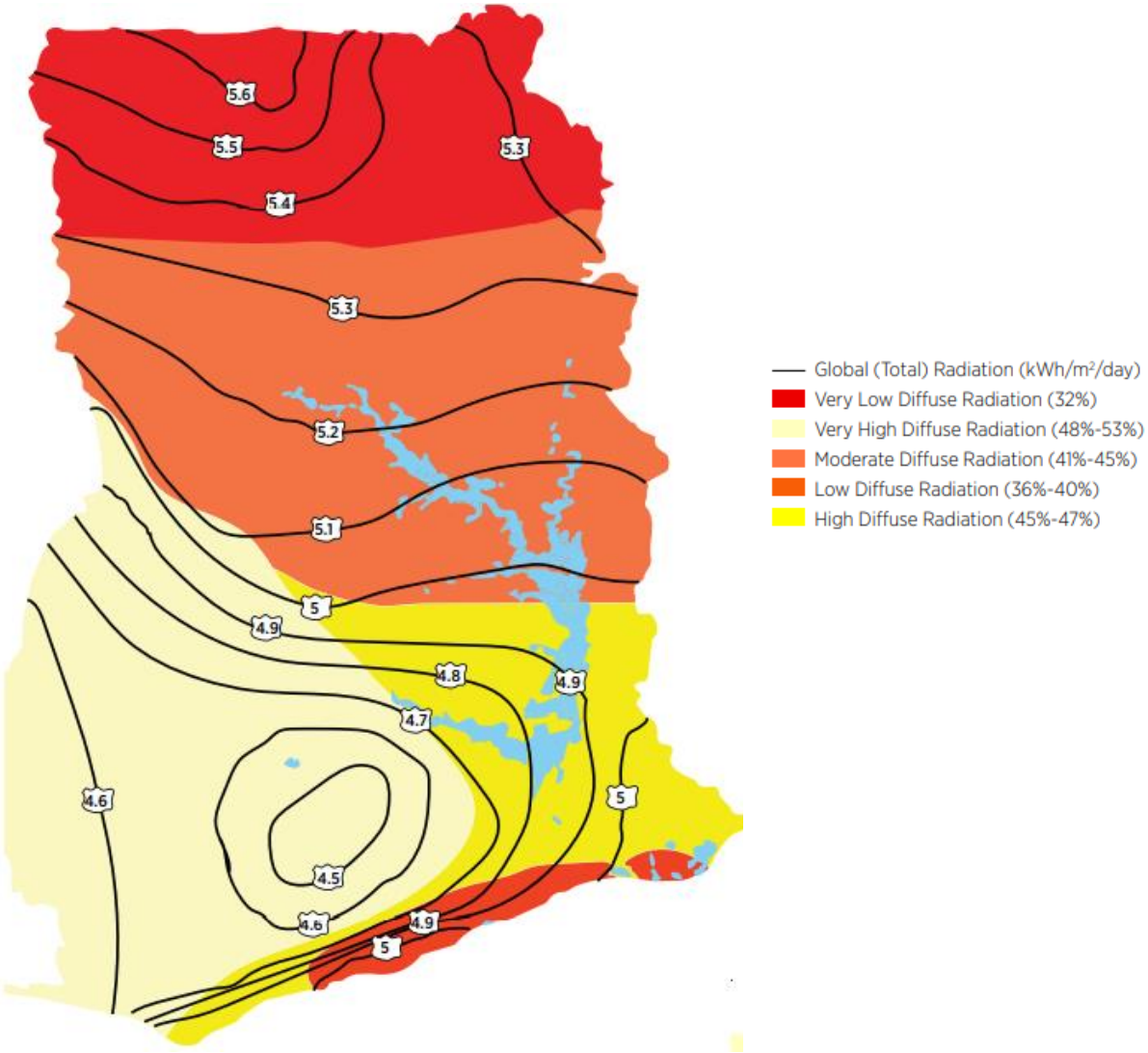

Figure 1.2 Ghana's Global solar Irradiation Map [15]

1.1 Status of renewable energy development in Ghana

To fully exploit the RE potential, the government of Ghana passed the Renewable Energy Act, 2011 (Act 832) [16] to lay the foundation for the deployment, utilization, and management of RE resources, thereby creating an

enabling environment for their integration into the Ghanaian power grid. RE as defined in the Act includes wind, solar, biomass, hydro, geothermal, and biofuel. The government institutions responsible for implementing this Act are the Energy Commission (EC) and the Public Utilities Regulatory Commission (PURC). EC is responsible for implementing all the provisions made in the Act, advising the government on matters concerning RE, and engaging all the stakeholders in the RE sector in developing and implementing policies for the promotion of RE in the country. PURC is an independent institution that regulates utility services in the country. Under this Act, PURC is responsible for the pricing of electricity from RE sources, including charges for grid connection.

Included in Act 832 are measures and policies to facilitate and attract investment into the RE sector. These measures are explained as follows.

- Feed-in-Tariff scheme: This scheme governs and provides security for the sale of electricity from RE sources. It is made up of Renewable Energy Purchase Obligation (REPO), Feed-In-Tariffs (FIT) rate, and guidelines for connecting REs to transmission and distribution systems. The REPO mandates all distribution network operators to procure a specific percentage of their total electricity purchase from RE sources. The percentage to be procured is determined by the (PURC) in conjunction with EC. The rate of FIT can only be approved by the PURC in collaboration with the utility company and the consumer. This agreed approved rate is effective for ten years and is subjected to reviews biennially. The guidelines for RE connections mandate transmission and distribution network operators to grant easy access to RE connections. Furthermore, the guidelines encourage network operators to invest and upgrade their network infrastructure at a reasonable economic expense to make the network accommodate RE sources. The only exception is at the metering point where the cost of the upgrade is borne by the RE owner or investor.
- The Tax and Excise exemption: This waives import duties and taxes on PV and wind equipment and their related accessories. The exemption is to be approved by the EC [12].
- Renewable energy fund: this was set up under the Act to generate the needed financial resources for the adoption, development, and utilisation of RE sources. Monetary resources accrued from this fund are to support innovative scientific research into RE sources, support the development of standards regarding the utilisation of RE, and build the capacity of personnel involved in the RE sector. Sources of this fund include

government levies, donations, and grants from local and other international key stakeholders in the RE sector.

- Updating the existing national grid code: The Act recommended for new sub-codes which focus only on RE to be developed and incorporated into the national electricity grid code. This is to accommodate and promote grid-connected RE sources by providing guidelines about their integration into the power grid. In this regard, two sub-codes were developed, one for the transmission network and the other for the medium voltage (MV) distribution network.

The government has furthermore set a target of increasing REs (excluding hydro generation) from 42.5 MW in 2015 to 1363.63 MW by 2030 in the national energy mix according to the Ghana renewable energy master plan [17]. The breakdown of these figures with emphasis on wind and PV is shown in table 1.2. In this master plan, utility-scale PV is expected to increase from 22.5 MW in 2015 to 447.5 MW in 2030. The 22.5 MW in 2015 was made up of a 2.5 MW plant owned by Voltage River Authority (a power generation company in Ghana) and a 20 MW plant which is operated by Beijing Xiaocheng Company. Utility-scale wind energy is expected to increase from 0 MW in 2015 to 325 MW in 2030. The amount of PV-based distributed generation (DG) is expected to increase from 2 MW to 200 MW by 2030 and is likely to be made up of households and institutions with grid-connected PV systems. Stand-alone solar systems are also expected to increase to 45 MW by 2030 from 5 MW in 2015. These stand-alone systems consist mostly of street and community lighting projects.

Table 1.2 Installed RE capacity for electricity purposes in Ghana as of 2015 [16]

Technology type	Unit	Reference (2015)	2020	2025	2030
Utility-scale RE (PV)	MW	22.5	152.5	347.5	447.5
Utility-scale RE (wind)	MW	0	0	275	325
Distributed generation (PV)	MW	2	20	100	200
Mini or microgrid	MW	0.2	2.2	5.5	13
Off-grid (stand-alone solar)	MW	5	17	26	45

It is evidenced from table 1.2 that much of the expected wind and PV RE generation by the end of 2030 will be grid-connected as summarised in figure

1.3. Grid-connected will account for 95%, while off-grid and mini or microgrid generations account for 4% and 1% respectively.

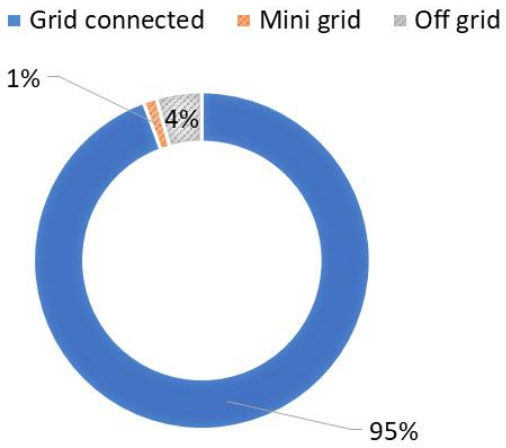

Figure 1.3 Expected installed renewable capacity by the year 2030 [9]

It is expected that these policy measures under the RE Act will drive the set target of 2030. In this regard, the Energy Commission has issued 130 provisional renewable energy licenses to several companies with a total capacity of 7,000 MW as of November 2019, out of which 63.8% are solar photovoltaic [10]. 40 of these provisional licenses have moved to the Sitting Permit stage with construction permits being issued to 13 companies. 11 out of the 13 companies are into solar photovoltaic development. This expected increase in REs, especially grid-connected both at the distribution and transmission network level, will significantly impact the operations of the existing power grid infrastructure. REs connected to the distribution network is technically termed DG [17]. The reverse power flow from these DGs changes the power flow across the distribution network from unidirectional to a bidirectional flow, affecting the performance and operation of the network.

1.2 Research Background

The structure of the National Interconnected Transmission System (NITS), a network of transmission lines linking all the power generating plants to the various load centers in Ghana, is longitudinal because of the topology of the country. The network spans a total of 6,475 km of transmission lines from the south to the north of the country as of 2019, of which more than 20% of these lines are longer than 80km [10]. With these long lines, the main limiting barrier for power transmission becomes the voltage instead of the thermal capacity. Furthermore, more than 90% of the 5172 MW total generation capacity is located in the southern part of Ghana, because of its proximity to fuel for thermal generation which accounts for 67% of the total installed generation

capacity [9]. A pictorial view of the location of the various hydro and thermal generation units in Ghana is shown in figure 1.4, showing thermal generations; Takoradi International Company (TICO), Mines Reserve Power (MRP) plant, Tema Thermal 1 Power Plant (TT1PP), Tema Thermal 2 Power Plant (TT2PP) and Takoradi Power Company (TAPCo) being located along the coast. The two major hydropower generation are the Kpong and Akosombo dams which have a capacity of 160 MW and 1020 MW respectively.

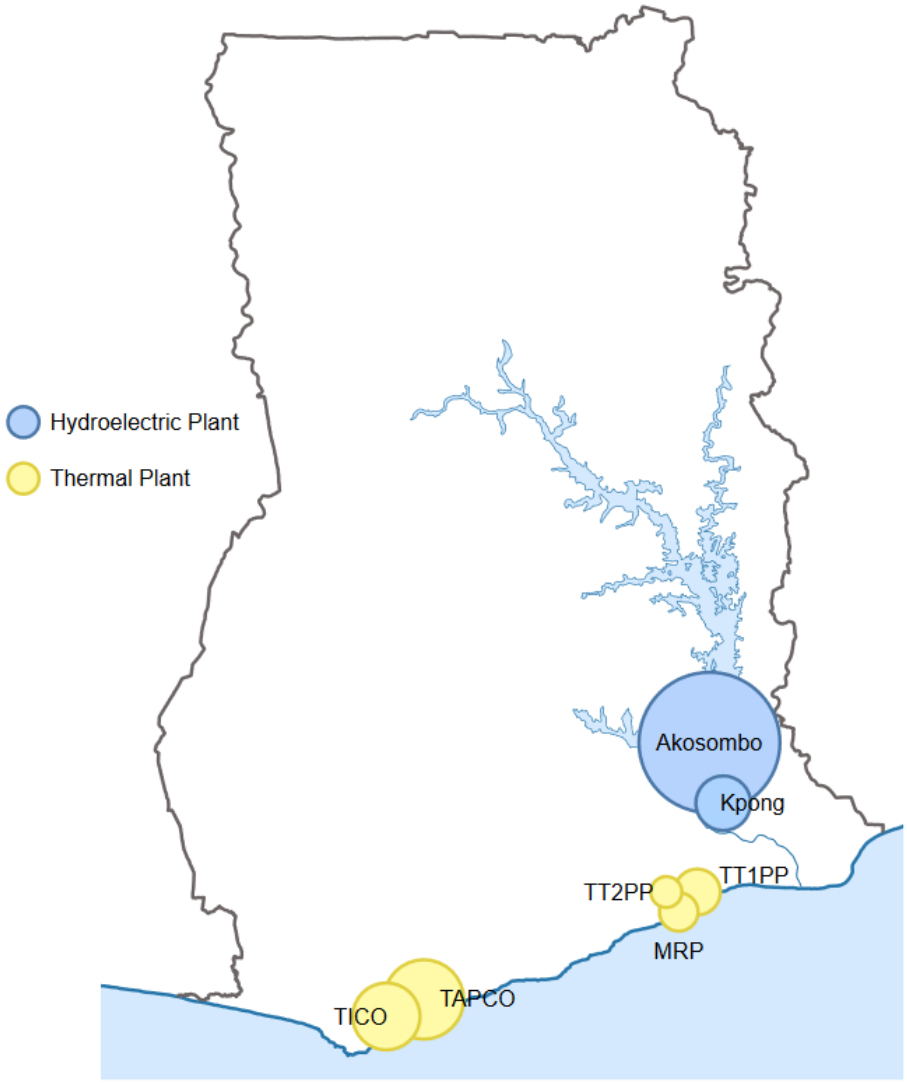

Figure 1.4 Location of thermal and hydro generation in Ghana [18]

Voltage regulation challenges subsequently emerge when power is being transmitted from the south where most of the generation capacity is located to the middle and northern parts of the country as highlighted in [19]. Figure 1.5 shows the main transmission (161 kV) and MV distribution (34.5 kV) lines for the northern part of Ghana. The bulk supply point (BSP) is the point where the 161 kV line connects the 34.5 kV line through a step-down voltage transformer.

The primary substations are where the 34.5 kV line is stepped down to either 11 kV or 415 V line for power distribution.

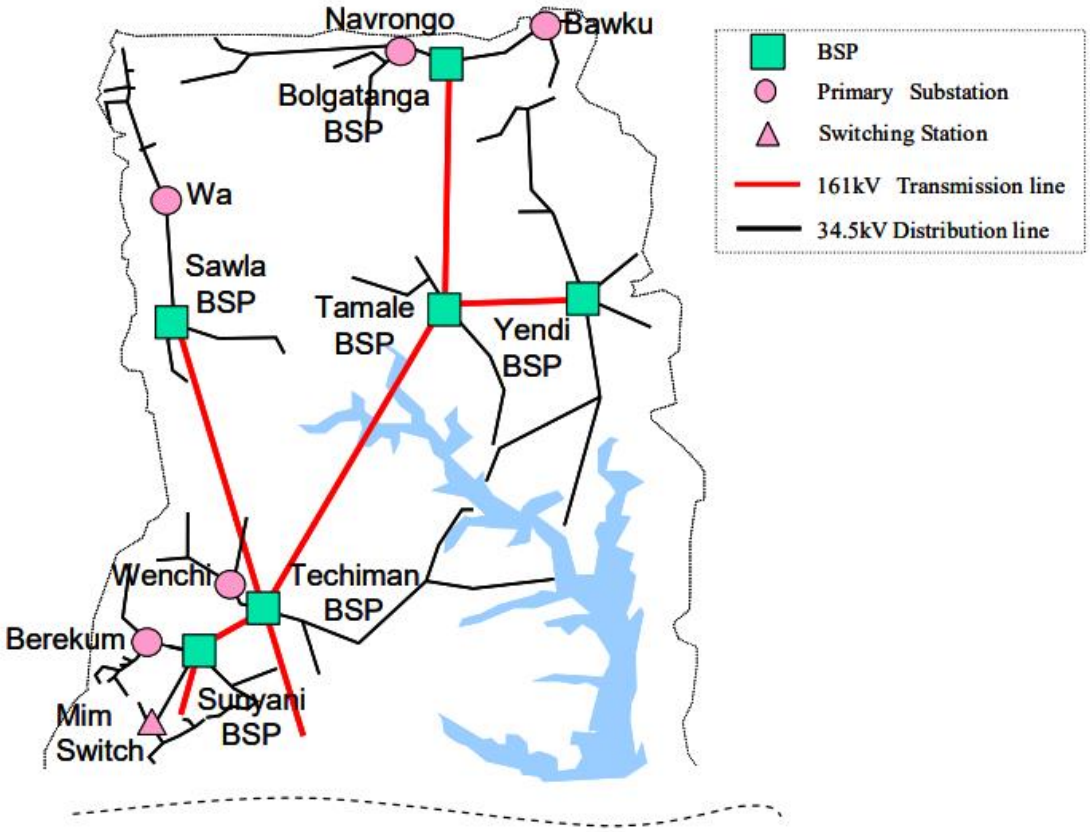

Figure 1.5 Power network diagram of northern Ghana [20]

The long transmission of power from the south to the north results in severe voltage drops which subsequently leads to a situation where the voltage profiles in the middle and northern parts of the country exceed the national electricity grid code voltage variation limit of ±5% of the nominal voltage. For instance, there have been situations where the voltage profile variation margin in the northern parts of the country can get as worse as 17% of the nominal voltage [21], leading to periodic load shedding to restore the voltage to the regulatory limit. This voltage situation reflects also in the distribution network as low voltages are observed on the network as highlighted in table 1.3 from the report of Northern Distribution Company, the utility company in charge of power distribution in the northern part of Ghana [20]. Table 1.3 shows the MV distribution lines linking some towns with severe voltage drops such as the Sawla – Wa MV distribution line which recorded a 32.5% of voltage drop which is above the grid code limit of ±5%. These low voltages worsen during peak demand periods, which start from 17:00 to 20:00 hours daily. Consequently, voltage regulation is a major issue in distribution network planning in Ghana. This requires adequate reactive power provisioning to be available on the grid at

all times. In dealing with this issue, Ghana's main distribution company, Electricity Company of Ghana deploys several voltage regulators on its 33 kV and 11 kV networks to enhance the voltage profile as highlighted in the 2020 electricity supply plan report [10]. The expected integration of DGs will have an impact on this existing voltage regulation challenge.

Table 1.3 Voltage drop of selected medium voltage lines in northern Ghana [20].

Transmission line	Voltage drop (%)
Sunyani - Berekum line	19.3
Sunyani - Mim line	29.5
Techiman – Wenchi line	3.5
Sawla – Wa line	32.5
Bolgatanga – Bawku line	16.0
Bolgatanga – Navrongo line	1.0

As per the number of licenses issued by the EC, 80% out of the 200 MW DG capacity to be integrated into distribution grids by 2030 according to the Ghana Renewable Energy Master Plan report are located in the northern part of the country because of the high solar irradiance values [16]. This potentially will reduce power transfer from the south to the north, resulting in an improved voltage profile in the northern part during the solar hour period. Additionally, power losses on the grid are also minimized.

Notwithstanding, the introduction of PV in the Ghana grid introduces another challenge, which can cause severe overvoltage during the peak generation period, technically termed as voltage rise phenomenon. This is because, the peak solar generation period of the PV which normally starts from the 10^{th} to 14^{th} hour on a typical day, coincides with the low demand period as seen in figure 1.6, describing the typical Ghanaian demand (load) and PV profile [22]. Thus, during the peak solar generation time, there is a rise in the amount of reverse power flows from the PV back to the grid, leading to a voltage rise at the PCC. This situation is further worsened by the fact that the northern part of the country which will account for 80% of the total expected PV integration on the grid is only 10% of the total national load (demand) [23]. Hence, additional reactive power compensation devices are needed to effectively regulate the voltage. Alternatively, DGs are integrated into the grid through their inverter interface which equips them with reactive power capability. Therefore, this can be exploited and utilised for reactive power compensation on the distribution grid.

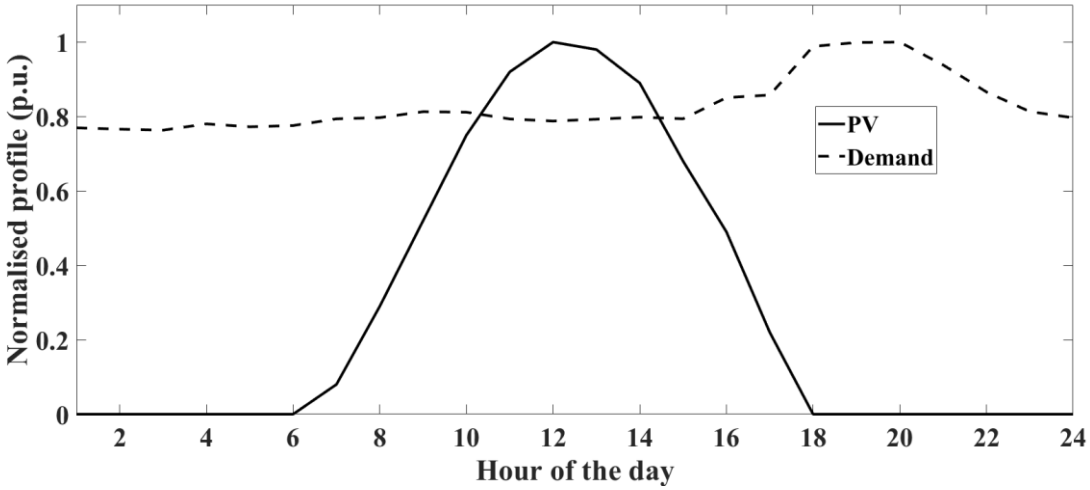

Figure 1.6 Normalized demand (load) and solar PV output in Ghana [22]

The Ghana renewable grid code for distribution networks allows for active participation of DGs in voltage control by providing reactive power compensation [24]. Different local voltage control methods of DGs exist in the national electricity grid code, with each impacting differently on grid operations. These methods include $Q(U)$ control, fixed power factor, and $cos\varphi(P)$. In the $Q(U)$ control, the reactive power compensation provided by the DG solely depends on the voltage at the PCC, whereas the amount of reactive power compensation is changed by adjusting the power factor of the DG as determined by operating active power output of the DG in the $cos\varphi(P)$ control. Under the fixed power factor control, the DG provides reactive power compensation to maintain the power factor at a value specified by the network operator.

The challenge with local voltage or reactive power control methods is how to identify the control settings for optimal performance since they are dependent on prevailing load and generation conditions [25]. Thus, these settings should be adapted to changing grid conditions which are easily achievable through a central voltage control scheme using communication facilities to achieve real-time control. With these facilities, it is easier for the central voltage control to monitor the conditions on the grid and subsequently adapt the settings of the local voltage control. However, distribution grids in Ghana have limited communication facilities on the network like most developing countries. Thus, the implementation of real-time central voltage control to adapt the settings is not possible, as most voltage regulating devices operate based on local measurements. Further research work on how the settings of the local voltage control methods can be adapted to the varying grid conditions without the requirement for communication facilities in the distribution grid is needed. Also important is how to fully utilize DG's reactive power to improve the low voltage experienced on the grid during peak demand period and overcome possible

voltage rise phenomenon during peak solar hours in order to enhance the overall voltage stability in distribution networks in Ghana. These salient points are addressed in this thesis.

1.3 Research Questions and Objectives

The efficient use of the reactive power resources of DGs to enhance voltage regulation in distribution grids is achievable if they are planned and properly coordinated. To properly incorporate this into the planning of distribution grids in Ghana, a proper assessment of the local reactive power control methods and a detailed approach to how the performance of these local control can be adapted to the changing grid conditions are needed.

Given the research problem explained above, this thesis seeks to answer the following research questions.

- How do the various local voltage control methods of DG allowable under the Ghana grid code affect the operation of the MV distribution grid?
- How can the settings of the local control be adapted to the changing grid conditions without the need for communication facilities?
- How the performance of the local control can attain performance comparable to a centralised control which uses communication facilities?

To answer the above research questions, the objectives of this thesis are as follows.

- To provide performance assessment of the different methods of local reactive power voltage control, since each control impacts grid performance differently. In enhancing the accuracy of the results, probabilistic models of load and DGs are developed and used to account for the variability and uncertain nature of loads and DGs in distribution grids in Ghana.
- To develop an approach or concept to adapt the reactive power compensation or control settings of the local reactive power voltage control methods to the changing load and generation conditions in the grid. This approach during implementation operates in a decentralised mode, thus relying solely on measured variables obtained at the point of common coupling (PCC).
- To demonstrate the robustness of this concept in dealing with disturbances on the grid such as changes in generation and load, R/X ratio, and the disconnection of DGs. Also, compare the performance of this concept or

approach to a fully centralised scheme that uses communication facilities to function and a local control method with fixed settings.

1.4 Contribution of Research

The scientific contributions of this thesis are enumerated as follows.

- Developed probabilistic planning models for loads and DGs for Ghana to be used in assessing the performance of distribution networks in Ghana.
- Proposed a novel autonomous adaptive $Q(U)$ control for MV distribution grids that dynamically changes the reactive power compensation provided by the DG with changing or varying grid conditions. This novel approach incorporates a sensitivity fitting function that uniquely determines the amount of reactive power compensation needed at a bus and a voltage stability block that ensures that the amount of reactive power supplied by the DG improves the voltage stability of the PCC bus. Unlike most work in literature which uses central control units to dispatch the DG, this novel idea only uses locally measured variables at the PCC. It is therefore implementable in developing countries where there are limited or no communication facilities like Ghana. This proposed scheme achieved better voltage control performance as compared to when the $Q(U)$ control operates with fixed control settings such as the one proposed by Mueller et al for German distribution networks.
- Proposed a two-stage offline approach to design $Q(U)$ control that adapts the control settings with changing grid conditions. The novelty of this approach is that it combines genetic algorithm (GA) with artificial neural network (ANN). Whiles the GA identifies the optimal control parameters and their corresponding impedance, the ANN develops a fitting function relating the Thevenin impedance to the control parameters. This fitting function is used by the $Q(U)$ to adapt the control settings with changing grid conditions. This is a fully decentralised scheme that does not require communication facilities and can be easily coordinated with other existing voltage regulating devices on the grid.

1.5 Research Scope

The main scope of the thesis is as follows.

- There is no universal definition for DG as different definitions exist in the literature [26]. However, the one that is adopted in this thesis is the definition by Ackermann et al, they define DG based on the integration point or location and not in terms of the technology, rating, or ownership [17]. The DG is thus defined as a power generation source integrated directly into the distribution network [17]. This definition is used because both the Ghana grid code for distribution networks and the renewable energy master plan do not explicitly define DG in detail but use the term embedded or distributed generation to refer to any variable renewable power plant connected to the distribution network.
- The DG in this thesis is a PV generator. The basis of this assumption is that all the licenses issued by the EC for DG owners in the northern parts of the country where voltage regulation challenges persist are all PV generators [27].
- The performance of the local reactive power voltage control methods is analysed through study cases implemented on an MV distribution network. This is because the current renewable energy sub-code for distribution networks covers only MV networks. There are currently no guidelines for DG integrations on low voltage distribution networks.
- Developing algorithms using measurement variables at the PCC to enhance the performance of local reactive power methods on MV distribution networks.
- The MV network used in this thesis is a 16-bus United Kingdom generic 33 kV distribution grid obtained from [28]. It is a radial network, supplied from a bulk supply point (BSP) through a 30 MVA 132/33 kV OLTC between buses 1 and 2. The range of voltage regulation of the OLTC is from +5% to -15% in steps of 1%, making a total of 21 steps. Also, there is a VR located between buses 8 and 9. This network is selected to represent a typical distribution feeder in Ghana because of characteristics such as; a long feeder with an average transmission line length of 13.5 km and the installation of a VR along the feeder to improve the voltage profiles. Further modifications are done to this selected network by setting tap positions per unit nominal values of the VR and OLTC to 0.97 p.u. and 0.92 p.u. respectively. This is to make under voltage profiles at the ends of the feeder, i.e. 0.935 p.u. and 0.950 p.u. for buses 11 and 12

respectively. Also, the length of each distribution feeder is increased by a factor of 1.1 to represent the long distribution lines in Ghana. The network parameters, including line resistance, line reactance, and loads are also obtained from [28] and shown in Appendix A.

1.6 Thesis Outline

This thesis is made up of six chapters and is structured as follows.

Chapter 1 provides the introduction to this thesis by highlighting the status of renewable energy development in Ghana and the research background. Subsequently, the research questions and objectives are also identified.

Chapter 2 explains the impact of DGs on distribution grids and the various types of voltage control schemes being implemented in distribution grids. The chapter concludes by examining the various literature works done on distribution grids in Ghana.

In chapter 3, the performance of the various local reactive power control methods applicable under the Ghana grid code and in various kinds of literature is assessed. The performance indicators are losses, voltage profile index, and the number of tap movements of voltage regulating devices. Also, the optimization algorithm which is used for this performance assessment is explained.

In Chapter 4, the significance of voltage sensitivity to active and reactive power and the methods used in calculating these voltage sensitivity values are discussed. Also, in this chapter, $Q(U)$ control is presented in detail and a strategy to dynamically change the reactive power compensation provided by this control in response to changing load and generation is proposed. The major components of this strategy, namely, voltage sensitivity and voltage stability block are explained. Test cases and simulation results are subsequently discussed.

The concept of artificial neural networks is explained in chapter 5. Subsequently, the procedure of a two-stage design approach for an adaptive $Q(U)$ control is presented. The optimization parameters used in the first stage are also enumerated together with the second (artificial neural network) stage. Various test cases used to determine the efficacy and robustness of this proposed control are also highlighted.

Chapter 6 concludes the thesis by highlighting the major contributions of this thesis and then discusses these contributions and how they can improve the performance of distribution grids in Ghana and other developing countries. It ends by providing an outlook on future related works in this field.

Chapter 2 General Aspects of Voltage Control in Distribution Networks

Extensive research on the impact of DG in distribution networks has revealed its potential benefits in power loss minimization, voltage profile enhancement, and electricity reliability improvement. However, at high penetration levels, the possibility of reverse power flow from DGs poses a challenge to distribution network operators as they significantly impact the grid voltage. This chapter provides an overview of various voltage control methods in distribution grids with DGs. It begins by first providing an assessment of the impact of DGs on distribution networks with an emphasis on the voltage rise phenomenon. The analytical formulation of this phenomenon and why it is a critical issue for distribution network engineers are also explained. Secondly, the impact of DGs on voltage regulation devices (VRD) like on-load tap changers (OLTC) and voltage regulators (VR) are illustrated. Lastly, various voltage control methods used to mitigate these challenges are discussed, together with a review of current literature works, the advantage, and the disadvantage of each method.

2.1 Impact of Distribution Generation on Distribution Networks

The distribution network, mostly owned by a distribution network operator (DNO), is made up of electric lines and substation equipment for transmitting power to end users of electricity. These end users can either be commercial, residential, or industrial customers. The DNOs ensure the following objectives main objectives [29]:

- The delivered power must be within the voltage range limit as specified by the grid code.
- The amount of delivered power must be sufficient to meet the demands of the consumers.
- The delivered power must be reliable at all times without any disturbance or disruption.

In achieving this target, adequate planning measures are required in the design of the network and its components. These measures include forecasting the load growth to determine the needed amount of power generation to meet this demand, reinforcing distribution lines to reduce voltage drop, etc. But, the emergence of new devices such as electric vehicles and DGs introduce some complexities in the planning of distribution networks.

DG, a power generation source connected directly to either the distribution network or the customer side of the meter [17], can be renewable like wind, PV, etc., or non-renewable energy like combined cycle gas turbines. DGs enhance the reliability of electricity supply. A typical example is in [30], where DGs (wind and PV) are included in distribution network planning for a comprehensive reliability assessment. Simulation results from this assessment show the advantages of DG integration on reliability performance indices like improving the average interruption index as compared to the case where there were no DGs in the grid. Other advantages of DG integration include power loss minimization as demonstrated by the authors in [31]. Nevertheless, at a high penetration level, the reverse power flow from DGs increases the voltage at the PCC which can create voltage instability situations [32], if adequate operational and planning voltage control measures are not put in place.

To illustrate the rise in voltage at the PCC where a DG is connected, consider a two-bus network shown in figure 2.1 with a DG integrated at bus 2 which is the load bus.

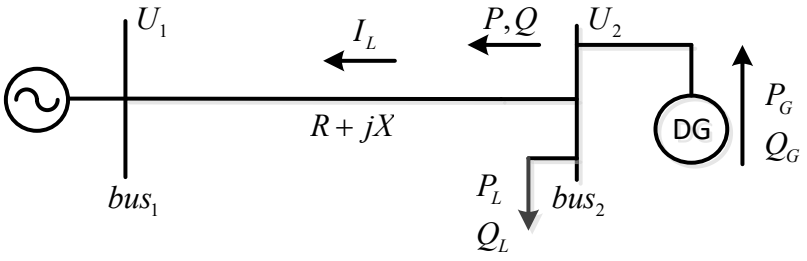

Figure 2.1 Two-bus radial network [33]

$\underline{U_1}$ and $\underline{U_2}$ are the complex voltage at the substation ($bus\ 1$) and load bus ($bus\ 2$) respectively. R and X are the respective distribution line resistance and reactance. P_L and Q_L are the active and reactive power loads at $bus\ 2$ respectively. P_G and Q_G are the active and reactive power generation from the DG respectively. P and Q are the active and reactive power injections from $bus\ 2$ respectively. P and Q are the difference between power generation and the load at $bus\ 2$.

When P_G becomes more than P_L, the current through the distribution line ($\underline{I_L}$) is calculated in p.u. as;

$$\underline{I_L} = \left(\frac{P - jQ}{U_2}\right) \tag{2.1}$$

The change in the voltage ($\Delta\underline{U}$) between bus 1 and bus 2 is also expressed as;

$$\Delta\underline{U} = \underline{U_2} - \underline{U_1} = \underline{I_L}\,(R + jX) \tag{2.2}$$

Substituting (2.1) into (2.2) results in

$$\Delta\underline{U} = \underline{U_2} - \underline{U_1} = \frac{PR + QX}{U_2} + j\,\frac{PX - QR}{U_2} \tag{2.3}$$

In distribution systems the real part of the voltage is far greater than the imaginary part [34], thus, the change in voltage can be approximated as;

$$\Delta\underline{U} = \underline{U_2} - \underline{U_1} \simeq \frac{PR + QX}{U_2} \tag{2.4}$$

It can be inferred from (2.4) that during active power injection from the DG i.e. when the active power output of the DG is more than the load at bus 2 (PCC bus), $\Delta\underline{U}$ will increase as $\underline{U_2}$ increases. This is because the PR term in the equation features more prominently since line resistance in distribution networks is not negligible or small as compared to transmission networks where $X \gg R$. Thus, making R/X ratio in distribution networks larger than that in transmission networks. This steady state rise in voltage above the maximum allowable voltage limit at the bus where a DG is connected is termed the voltage rise phenomenon. The voltage rise phenomenon is thus a major problem in distribution networks with significant penetration of DG units as the active power output of DGs will increase the voltage at the PCC bus. Mitigating the voltage rise phenomenon will require appropriate voltage control measures. These measures include the use of reactive power.

2.2 Reactive Power Capability of DGs

One approach to achieving voltage regulation in distribution grids is by controlling the flow of reactive power, usually at the entry point or beginning of the feeder. At the beginning of the feeder, the control set point is predetermined such that the drop in voltage at the tail end of the feeder is still within the voltage regulatory limit. However, for long distribution feeders which have poor voltage regulation, reactive power compensation devices are integrated along the feeder to improve the voltage. The use of reactive power is more effective in

overhead lines than in underground cables because the latter has more line resistance which makes the voltage more sensitive to the injection of active power than reactive power. About 95% of the MV distribution networks in Ghana are overhead lines [35], thus, justifying the use of reactive power.

Traditionally, voltage control on MV grids is achieved by using an OLTC transformer, capacitor bank (CB) and voltage regulator (VR), etc. The OLTC and VR are equipped with a tap changing mechanism, which is either operated automatically or manually on the principle of increasing or decreasing the voltage at the feeder point where it is connected (mostly at the beginning of the feeder) to compensate for the voltage drop along the feeder in such a way that the voltage at the end of the feeder is still within the regulatory limit. The reverse flow from DGs significantly impacts the operation of the OLTC or VR; the intermittent nature of the DG output potentially increases the number of tap operations of the VR and OLTC, resulting in a reduced life span of these devices [36]. A potential solution to this problem is the active participation of DGs in voltage control by exploiting the reactive power capabilities of DGs.

Figure 2.2 depicts the reactive power potential of DGs [37], where a semi-circle with radius S (apparent power of the inverter) shows the full capability range of the inverter in the PQ space.

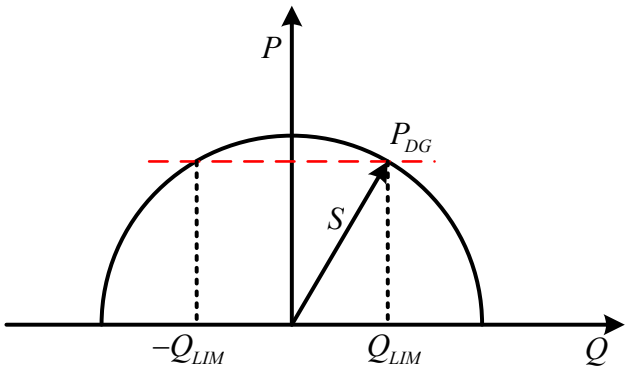

Figure 2.2 DG inverter's reactive power capability [17],[18]

If the inverter is operating at an active power output of P_{DG}, then where the red dashed line intersects the semi-circle becomes the feasible reactive power range of the inverter from Q_{LIM} (supplying reactive power) to $-Q_{LIM}$ (absorbing reactive power). An active power output P_{DG} of zero implies the full utilization of the entire semi-circle for reactive power compensation. The main determinants of the reactive power capability of an inverter are therefore the operating active power and apparent power rating of the inverter described mathematically as in 2.8.

$$Q_{max} = \sqrt{S^2 - P_{DG}} \quad 2.8$$

It can also be deduced that if the DG's output power, P_{DG} is equal to the rating of the inverter, then there is no room for reactive power compensation. In this case, the inverter has to be oversized, in other words by selecting the apparent rating to be more than the peak active power output [38] to guarantee reactive power compensation at all times at the expense of the increased cost of the DG system. Authors of [39], however, propose an apparent power rating of 1.1 times the peak active power to be enough to reduce losses and enhance voltage regulation on the grid. The sizing of the apparent power rating based on [39] is adopted in this thesis.

DG inverters have a fast response as compared to OLTC and VR as they can operate from milliseconds to microseconds [37]. They are therefore used to mitigate fast voltage disturbances on the network. Although the utilization of reactive power resources of DGs for voltage support on the grid is beneficial, they must be properly dispatched in the appropriate voltage control method.

2.3 Voltage control methods on Distribution networks with DGs

Literature reviews about voltage control techniques in future distribution grids with high penetration of DGs are broadly classified into communication-based and autonomous or local control [40]–[42]. Communication-based control can be further classified into centralised and decentralised coordinated control. These classifications are subsequently explained in the next section.

2.3.1 Centralised Voltage Control

In this control, a centralised control unit (CCU) obtains the required measurements data from the distribution network through a remote terminal unit (RTU) and/or smart meter, processes the data, and issues a signal (voltage set-points) to the required VRD such as DGs, OLTC, VR, etc. The schematic of the centralised control is shown in figure 2.3 with the blue broken lines indicating the communication links on the MV distribution network. The voltage ratings in the figure for both the transmission network and MV network are based on the Ghana grid code [43].

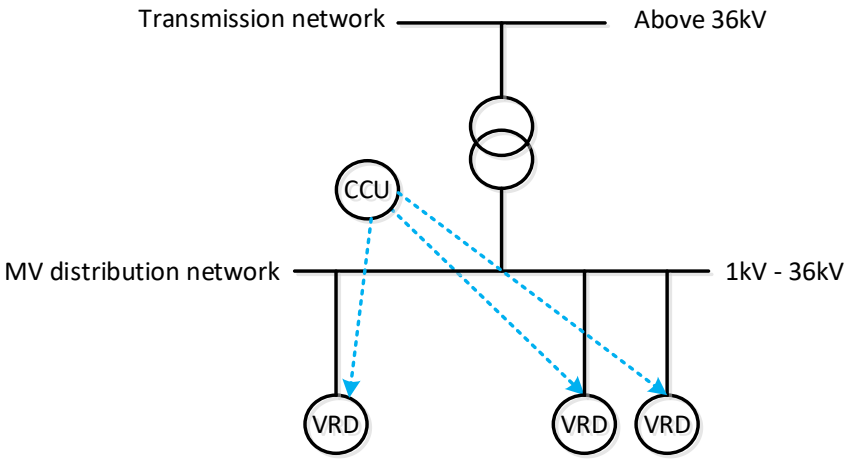

Figure 2.3 Schematic for central voltage control [40]

Two approaches used in literature to achieve centralised voltage control are rule-based and model-driven systems [44][45]. In the rule-based centralised voltage control system, the CCUs make control decisions after receiving real-time voltage measurement information or data from the RTU, which sometimes has the CCU embedded in it or in constant communication with it. The control decisions are based on a set of programmed rules embedded in the CCU which aims to optimize the performance of the feeder in terms of minimizing power losses, minimizing energy consumption, or a combination of both. RTU makes it possible for the CCUs to monitor and control the voltage at the substation and across the network by establishing a communication interface via Supervisory Control and Data Acquisition (SCADA) with the VRDs. SCADA is a control architecture that links several communications devices in the network and provides a graphic user interface for remote monitoring of control devices. Subsequently, the control decisions are communicated to the VRDs through the SCADA interface. An example of a rule-based system is shown in figure 2.4.

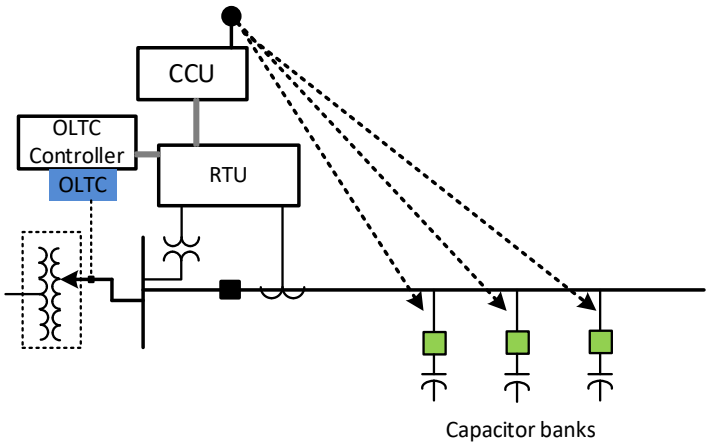

Figure 2.4 Rule-based Central voltage control scheme [44]

The CCU through the RTU controls the up and down tap movements of the OLTC at the substation and also sends control signals to the CBs along the feeder to switch them ON or OFF, based on the set of programmed rules determined by the network or utility operator. Each of these VRDs has its local control, which is overridden when the CCU is activated.

The model-driven centralised voltage control system uses distribution management systems (DMS) for its operation. DMS is an active management system that obtains measurements data from the substation and along the feeder, analyses the data and makes the necessary control decisions for planning and operating the distribution grid, using tools such as SCADA, geographic information system (GIS), customer information system and advanced metering infrastructure [44]. GIS is very essential when determining the output of RE sources like wind and PV since it captures and analyses geographical data of an area. Thus, the combination of all these tools provides a more comprehensive approach to making control decisions since a holistic view of the distribution network is provided. CCUs are embedded within the DMS and hence able to access all the information in the DMS. Functions performed by the DMS include load forecasting, network reconfiguration, power flow calculations, short circuit calculation, fault diagnosis, and management and state estimation [46]. For voltage control, the DMS performs online power flow using real-time voltage measurements obtained from the network via SCADA. Based on the load flow results, the optimal reactive power dispatch among the VRDs is determined, i.e. the tap settings of the OLTC, VR, or the amount of reactive power compensation needed from the shunt capacitor, DG, etc.

Several examples of centralised control have been discussed in the literature. A model predictive control (MPC) based centralised control was used to achieve centralised voltage control scheme using OLTC and DGs [47]. The objective of the scheme was to correct voltages that are outside the regulatory limit on the grid using three control actions; the active and reactive power of the DG and the tap settings of the OLTC. The selection of a particular control is dependent on the cost of the control action. Using the DG reactive power output and the tap settings of the OLTC were considered cheap options while using the active power control is an expensive option according to this research paper. Based on this knowledge, appropriate weights were assigned to each control action. The MPC control classified the power system network into normal, undesirable, and emergency states. This classification is based on the magnitude voltage values determined by the network operator. During the emergency state, all three control actions are used to bring the power system into the undesirable state. In

the normal and undesirable states, only cheap control actions were used. During each state, the MPC control uses the voltage sensitivity matrix, the real-time and previous voltage measurements to calculate the change required in the active and reactive power output of each DG unit, and the OLTC settings to keep the voltage of the monitored buses within the regulatory limits. This control scheme was implemented on an 11 kV MV distribution grid with 75 buses to show its effectiveness in controlling the voltages of all buses within the regulatory limits especially when there were as high as 22 DG units on the grid.

A similar centralised control called system voltage optimisation (SVO) was implemented in [48] as shown in figure 2.5, for both 11 kV and 33 kV networks.

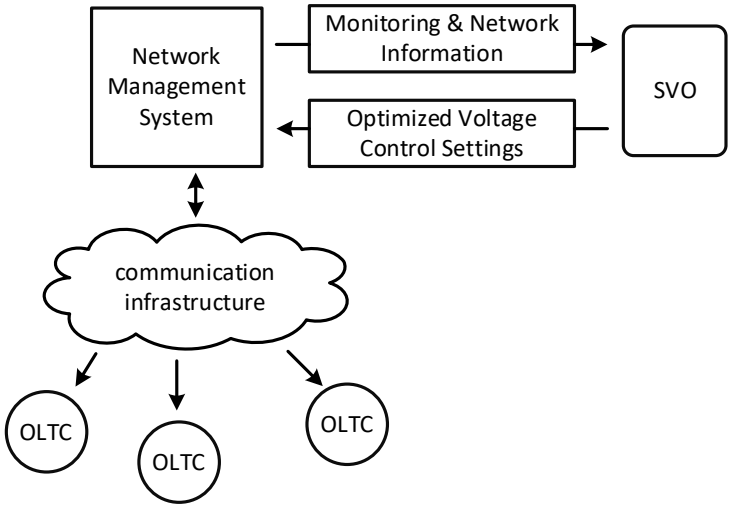

Figure 2.5 SVO System Architecture [48]

The SVO is an external control that works in conjunction with the network management system (NMS) of the network operator to obtain real-time information (power flows, voltage, and current measurements) to determine the optimal settings of the OLTC at the various substations on the network. SVO starts by performing a state estimation of the entire network using measurement information obtained from the NMS. Optimization calculations are then performed by the SVO after the detailed assessment of the network is known through state estimation. The optimization determines the control set points of the various OLTC on the grid which are subsequently sent to the NMS for onward transfer to the control unit of each OLTC. Results from the simulation show the effectiveness of the SVO in increasing the capacity of the network to allow more DGs to be integrated. The challenge however with centralised control like SVO is the slower response time in dealing with fast occurring disturbances on the grid such as electrical faults as compared to local operation of VRDs [18],[19]. For centralised control, the measurement information must

be sent to the CCU before a control action can be taken while the local control will act immediately to respond to the disturbance. Thus, combining both central and local controls as seen in [49]–[51] is beneficial in terms of enhancing the response time in dealing with disturbances.

A combined centralised and local voltage control scheme was implemented in [49] involving OLTC, static var compensators (SVC), and CBs. The control scheme consists of centralised normal and local transient control loops, with the selection of a particular control determined by the state of the network. During steady state conditions, the centralised normal control loop operates by dispatching the OLTC, SVCs, and CBs in a coordinated manner on an hourly basis to regulate the voltages on the grid. But, during disturbances like rapid changes in PV output, the transient loop activates the local control of the SVC and CB to respond to the disturbance. This is coordinated in such a way that the SVCs act first, if the performance is not satisfactory, then CB acts. When this scheme was implemented on IEEE 123 bus distribution network, the power loss and the number of voltage violations on the grid during very cloudy days were minimized. Reactive power resources of PVs were however not considered by this research paper.

Reactive power resources of DGs and OLTC were used in a central voltage control scheme termed as the master-slave scheme by the authors of [50] as shown in figure 2.6.

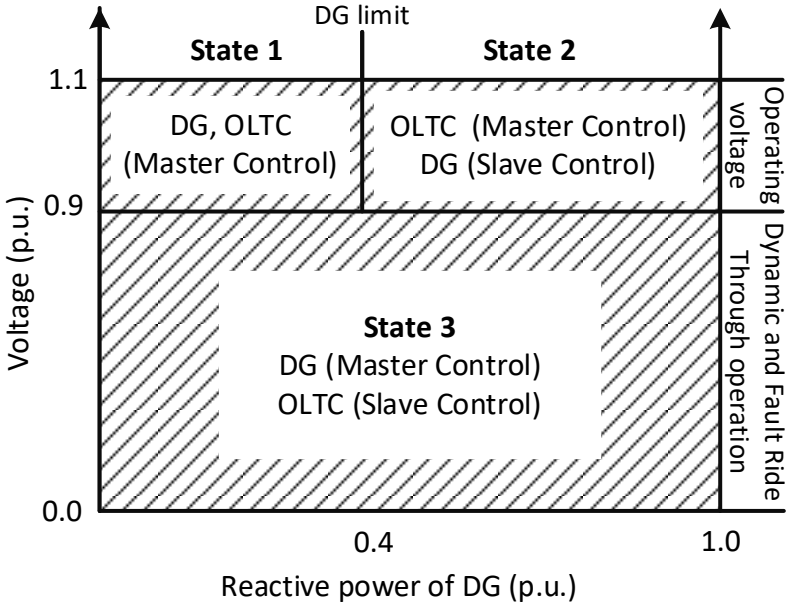

Figure 2.6 Master/slave voltage control operation [50]

The master-slave scheme divides the power system into three states; normal operating state 1, normal operating state 2, and dynamic state. Normal operating state 1 is when the voltages within the network are within the allowed regulatory limit (specified as between 0.9 p.u. and 1.1 p.u. in the paper) and the reactive power output of the DGs are below their maximum limit, the normal operating state 2 is when the reactive power output of the DGs hits their maximum limit and the dynamic state is when there are fast occurring disturbances like three-phase faults on the grid which keep the voltages on the bus outside their regulatory limit. During normal operating state 1, the OLTC and DGs both act as master control, i.e., each device actively takes part in voltage regulation. However, during state 2, when the DGs hit their reactive power limit, the OLTC acts as the master control with the DGs acting as the slave. In the dynamic state, the DGs operate as the master while the OLTC acts as the slave due to the faster response times of the DGs. The master-slave scheme was implemented on a radial distribution network and validated for both steady state and dynamic conditions, resulting in an improved voltage profile during the steady state when there was a gradual change in load. Furthermore, the proposed control enhanced the voltage stability margin when the network was subjected to a three-phase short circuit fault. This master-slave scheme when implemented on a 25 kV MV grid resulted in an improved fault-ride through capability and enhanced transient voltage stability margin using the reactive power resources of the DG. However, during the dynamic state, the DGs were not coordinated as they all acted autonomously. This can potentially increase the power losses on the grid in instances where there is unnecessary and excessive reactive power compensation from the DGs.

To ensure coordination among the DGs, a time delay allocation based on graph theory was used to prioritise reactive power allocation among DGs in the centralised control scheme proposed in [51]. In this scheme, the CCU determines the time delay, unique for every DG, based on the DG location and voltage at the PCC at every time instant determined by the network operator. This is to avoid unnecessary reactive power compensation from DG units that will increase the losses on the grid. In achieving this, only the DG unit located at or close to the voltage violation point will provide compensation. While the reactive power compensation of the remaining DG units is put on standby by the time delay set by the CCU. Afterward, based on the voltage measurements obtained from the grid, the CCU determines the tap position of the OLTC at the substation. Thus, the DGs were combined with OLTC to achieve a centralised voltage control. The performance of this scheme when implemented on a 20 kV

MV grid through a time series and time domain simulation did minimize the power losses on the grid and also ensured efficient utilization of the DG reactive power resources.

The major challenge with a centralised voltage control scheme is the required investment in measurement devices and sensors to establish the communication medium between the CCU and the VRDs [23],[24]. This investment is capital intensive, especially for developing countries like Ghana where there are limited financial resources. Furthermore, the complexity of the voltage control increases with large networks with a high number of DG integrations, resulting in a large computational burden, making it not effective in dealing with fast occurring disturbances on the grid.

2.3.2 Decentralised Coordinated Control

Under this control, VRDs communicate with each other instead of a central controller. This communication results in the VRDs exchanging sensitive information about their current operating states and intended control actions, leading to a collective decision on how the VRDs should respond to grid disturbances to achieve a global approach [41]. Thus, the decentralised voltage control schemes reduce the communication burden associated with centralised control schemes by decomposing the global voltage control problem into sub-parts. Furthermore, the decentralised control enhances the chances of achieving a faster response since the control tasks are distributed as opposed to the centralised control which makes use of a single CCU [40].

To facilitate the communications among VRDs, multi-agent system (MAS) technology has been used for voltage regulation in [53]–[57]. The MAS consists of two or more coordinated agents as used in [57], where the authors coordinated OLTC and VRs on the distribution grid. Each OLTC or VR controls a portion (zone) of the network, with the help of a local agent, which acts autonomously and makes its own decisions based on prevailing conditions in the environment. As shown in figure 2.7, each agent was made up of an interface, knowledge base, and sub-optimization. The interface is responsible for exchanging information with the black board and also sending control signals to the OLTC or VR.

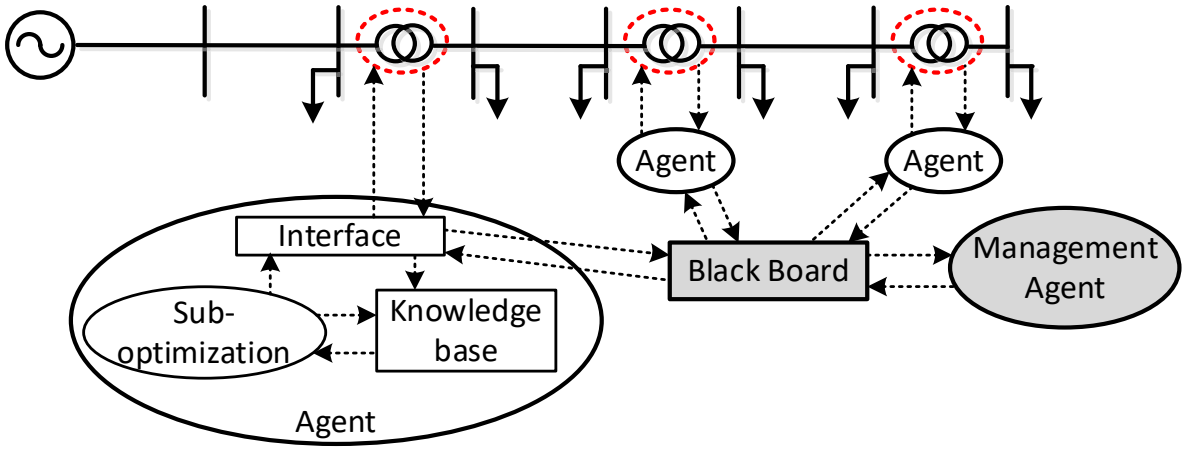

Figure 2.7 Multi-agent decentralised voltage scheme [57]

The knowledge base stores information collected from the interface and optimization. The sub-optimization is responsible for computing the optimization involving the minimization of voltage deviation for the buses in each control zone by determining the tap position of the OLTC and VR. The management agent however performs only monitoring functions. The blackboard provides the platform for knowledge sharing among the agents, helping each agent to know what pertains to other zones. Results from the numerical simulations demonstrated the effectiveness of this MAS decentralised-based control in achieving optimal control performance as the voltage fluctuations caused by the DG output were successfully mitigated when implemented on a 6.6 kV MV distribution grid. This shows that decentralised MAS can achieve both autonomy and optimality at the same time.

Another decentralised MAS scheme was implemented on a combined MV and LV network in [54], [55]. This scheme regulates the voltage of buses on the network using OLTC, active and reactive power resources of DG, and energy storage (ES) devices present on both the LV network operating as a microgrid and an MV network. Each network constitutes a sub-system that is controlled by an agent termed a grid agent. While each DG, OLTC, and ES are controlled by their agent called a resource agent (RA). The communication among these agents is hierarchal. The grid agent for the LV grid shares information about the status of the grid with the grid agent for the MV grid. Based on this received information and the status of its network, the grid agent for the MV grid determines the control set points and communicates them to the grid agent of the LV network. Subsequently, these control set points are shared with the resource agents of the OLTC, DG, and ES devices for them to adjust their control settings to follow desired settings as determined by the grid agent. This process is repeated every 100 ms which is enough to capture the fast occurring

disturbances on the grid. Simulation results show the effectiveness of this agent-based scheme in minimizing curtailment of DG active power and enhancing the voltage stability on the grid during peak renewable generation. This performance is comparable with a fully centralised scheme, though this comparison was not demonstrated in this particular research paper.

The performance of a decentralised voltage control scheme is compared to a fully centralised scheme in [58]. This decentralised control adjusts the active and reactive power set points of DG units to overcome overvoltages occurring on the network. The mode of operation of each DG unit is determined by the status of the voltage across the network. When there are no overvoltages occurring on the grid, DG units act independently using their respective local control to adjust the reactive power output in such a way as to prevent the occurrence of overvoltage at the PCC. The control unit however gives priority to active power during this period. When overvoltages occur, the DG units in each feeder coordinate their reactive power compensation through their respective local controller using the limited communication facilities on the feeder. Thus, every feeder represents a decentralised control zone on the network. However, if the overvoltage situation persists, then active power curtailment is activated among the DG units. This control was compared with fully centralised control and the results reveal that both control methods successfully overcame overvoltages on the grid, but, the decentralised control had a higher amount of active power curtailment of the DGs as compared to the centralised control.

Even though the decentralised voltage control scheme provides an advantage over centralised schemes in terms of the communication requirements on the grid, it still requires some limited communication for effective implementation. Currently, in Ghana, communications facilities exist on a few MV feeders and are limited to the main substations, making it impossible for DGs located along the feeder to communicate with each other. The suitable alternative is that the local voltage control of DGs should be able to operate intelligently, adapting to the changing conditions on the grid.

2.3.3 Local Voltage Control

Local voltage control strategies make their control decisions based on measurements at the PCC. Compared to centralised and decentralised control, local control has the advantage of high reliability and computational efficiency [59], provision of faster response to deal with voltage disturbances [60], and requires no communication facilities for its operation. An example of a local control strategy is active power curtailment, which involves limiting the DG's

active power output to control the rising voltage at the PCC and on the grid. Thus, this voltage control strategy is activated when the voltage at a given bus is above a threshold pre-defined by the network operator. Though active power curtailment seeks to prevent overvoltage conditions on the grid, the control of the active power is a disincentive to DG owners as they are unable to sell power without restrictions, thereby resulting in financial losses [22]. This control is therefore mostly used as a last resort strategy when all other control methods have failed to effectively keep the voltages on the network within the specified regulatory limits. This was the case in the research of [61] where energy storage devices (batteries) were used to control overvoltage conditions on the grid by storing the excess power from several rooftop PVs. In instances where the storage capacity of the batteries is full, active power curtailment is activated.

Other local voltage control strategies include droop-based inverter control such as $Q(U)$, $Q(P)$, and $cos\varphi(P)$. In $Q(U)$ and $Q(P)$ control, the amount of reactive power supplied by the DG is determined by the voltage at the PCC and the active power output of the DG respectively, while for $cos\varphi(P)$, the power factor of the DG is changed depending on the active power output of the DG. The selection of the type of droop-based local control depends on the grid code.

The major challenge of local voltage control is how to tune or adapt the control parameters to the changing generation and load conditions on the grid [62],[25]. This has been addressed in a lot of literary works and has been classified into real-time or offline strategies. These strategies are further explained as follows.

2.3.3.1 Real-Time Tuning Strategies for Local Control

These are operational strategies that mostly used centralised control mechanisms like MPC to tune the characteristic curves or control settings of local controllers. An example of this strategy is found in [36], where a CCU uses MPC to slide or adjust the characteristic curve of a local $Q(U)$ control to keep the voltage of all the buses within the regulatory limit and reduce the number of tap movements of the OLTC. This research also highlights the deficiency of using local controllers when operated with fixed control settings using time series simulation for 24 hours, as several buses exceeded their regulatory limits. The MPC control on the other hand can continuously modify the characteristic of the $Q(U)$ control based on prevailing conditions to keep the voltages within targeted limits. Notwithstanding, there were instances where there was no dead band in the $Q(U)$ control, resulting in excessive demand for reactive power compensation from the DG inverters. This excessive compensation will lead to an increase in the power losses on the grid.

A more robust approach to deal with the uncertainties associated with DG and load generation is adopted by the authors of [63] using robust constrained MPC. The authors introduce an approach called the direct method to estimate the boundaries of nodal voltages on the network using the worst scenarios combination of DG and loads. This method replaced the Monte-Carlo method which is computationally intensive. The estimated nodal voltages are used by the MPC control to optimize the tap setting of the OLTC and also dispatch the set points to the DGs, which are subsequently used to adjust the characteristic curve or settings of the $Q(U)$ control. This scheme efficiently regulated the voltage within the target limit when implemented. However, the coordination between OLTC and DG was achieved in a single timescale. Since the conventional switching mechanism of OLTC is mechanical and hence it has a slower time response as compared to the $Q(U)$ control of the DG [64], it is, therefore more practical and desirable to coordinate them in different time scales.

A two-level control scheme architecture combining central and local control was proposed in [65], using different time scales. The basis of this combination was to harness the advantages of both layers of control. Local voltage control has the advantage of providing a fast response in dealing with disturbances such as faults while central control provides a more optimized approach to achieving voltage regulation. In this scheme, an MPC-based central controller coordinates all the DG units on the network and uses voltage measurements from the network at steady state conditions, together with voltage sensitivity matrices of buses and the reactive power reserve margin of each DG unit on the network to generate a correction signal. The controller generates this signal every ten seconds interval. This signal is sent to each DG unit to be subsequently used to adjust the $Q(U)$ control curve or settings. The local $Q(U)$ then acts in seconds to deal with disturbances on the grid. Results from the simulation reveal that the performance of the local control is enhanced by adjustment of its characteristic curve with the changing grid conditions using a correction signal received from the MPC-based central control. For large networks with several DG units, the generation of the correction signal at every ten seconds interval will require high communication bandwidth.

2.3.3.2 Off-line Tuning Strategies for Local Control

Off-line or planning-based strategies are favourable to networks with limited or no communication facilities as they are developed using offline techniques. They are categorised into coordinated and decentralised schemes.

Coordinated schemes use an offline centralised power flow or optimization algorithm to determine the settings or characteristic curves of the local voltage control, either to be implemented on a day-ahead dispatch or for a reasonable period of planning horizon before it is updated. These schemes use either historical or forecasted load and DG profiles in the power flow or optimization algorithm.

A coordinated planning-based strategy was implemented in [66], where the authors implemented an offline OPF to derive the characteristics curve of each local $Q(U)$ control of DGs on the grid using forecasted load and DG profiles. The objective of the OPF was to minimize the following; power losses, active power curtailment, and the use of reactive power resources of DGs. Based on the solution (bus voltages and the desired reactive power compensation) from the optimization, the settings of the local control are derived. This local setting is subsequently used for real-time operation. The performance of this strategy was accessed through a 24-hour time series simulation and compared with two other methods; the DG units on the grid operate at a unity power factor and the settings of the local $Q(U)$ control for each DG unit are based on the German grid code. The performance indicators used for the assessment are losses, maximum and minimum voltages on the grid, and the amount of active power curtailment. Simulation results indicate that the tuned local control $Q(U)$ in real-time operation recorded marginal voltage violations and less power loss as compared to the other two methods where there were a high number of voltage violations. These results demonstrate that the usage of an effective planning approach to tune local control of DG units will enhance the performance of the network during real-time implementation, thus bridging the gap between the planning and operation stages of the network. Furthermore, the research concludes that the utilization of local controls presents a cheaper alternative to overcoming overvoltage on the network with a high percentage of DGs as compared to the conventional planning approach of network reinforcement.

A more generic planning framework to determine the control curves for local control was proposed in [67] as shown in figure 2.8.

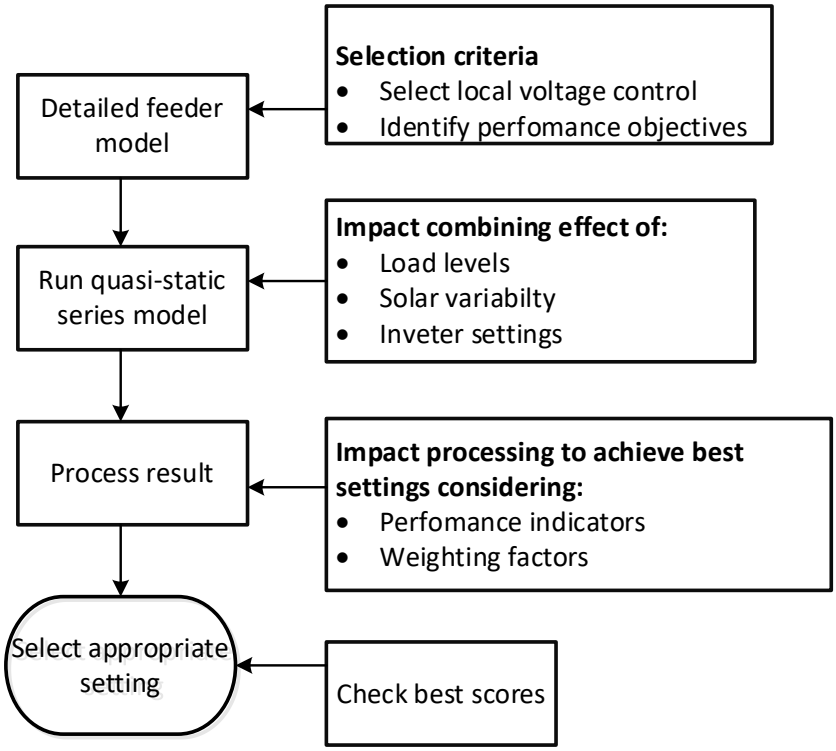

Figure 2.8 Framework for tuning local control setting [67]

In this framework, the authors proposed further categorization of the historical load and DG profiles, because the effectiveness of the local control settings is dependent on the prevailing grid load and generation conditions. The load profiles are thus categorized into peak and off-peak days, while the DG (PV) is categorised into clear, variable, and overcast days. This is used to convert the profiles of a year into six sample days by creating different combinations among the DG and load categorization. Depending on how often a combination occurs within the year, an appropriate weighting factor is assigned to it by the network operator. These are fed into a quasi-dynamic simulation algorithm using different settings of $Q(U)$, $cos\varphi$ (P), and power factor control. To determine the best control settings, key performance indicators such as distribution system losses, ANSI (American National Standards Institute) voltage violation limit, and voltage variability index are used to assess each control setting. Even though this planning framework is very flexible as it provides an opportunity for the planning engineer to modify it to suit the requirements of the network, it is a very laborious process.

On the other hand, a day ahead schedule optimization to determine the optimal control settings or characteristic curves of local voltage control and other conventional voltage control devices like OLTC was implemented in [25] to

minimize power loss, active power curtailment of DGs and voltage deviation. The schematic of this offline method is shown in figure 2.9.

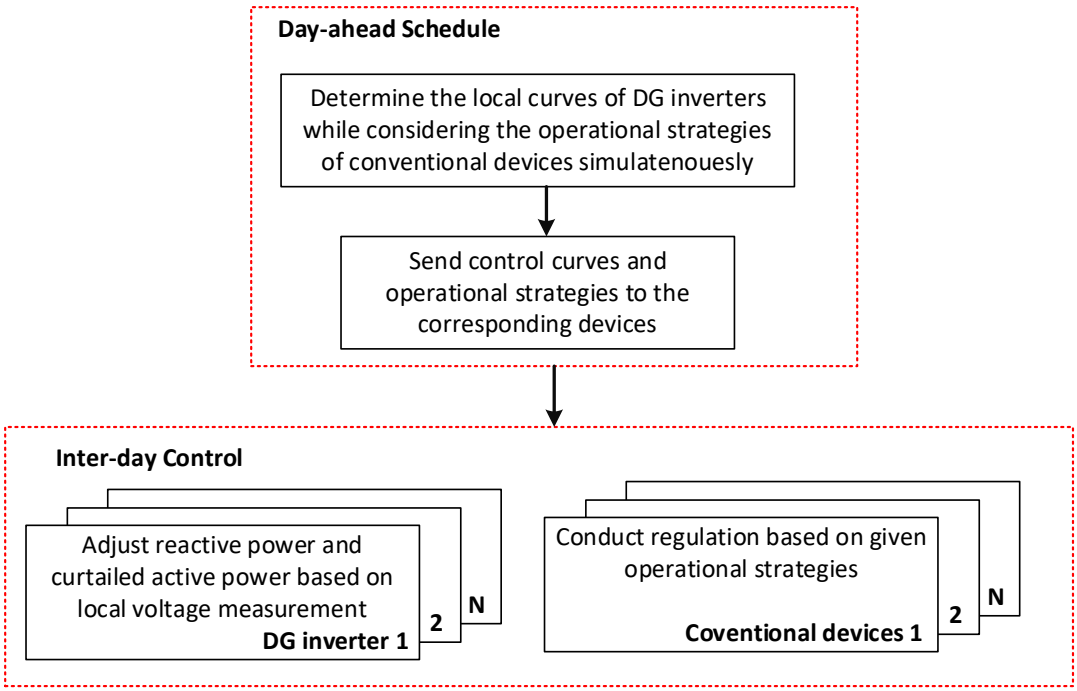

Figure 2.9 Schematic of the offline tuning method [25]

The parameters of the local control are the decision or control variables and are incorporated into the optimization as a piece-wise function which together with the AC power flow constraints makes the optimization a mixed integer nonlinear problem with high non-convexity. Subsequently, this high non-convexity optimization problem was converted into a mixed integer second-order cone programming model for an easy solution. The optimization determines the optimal control settings for each DG unit on the grid. These settings are subsequently used for real-time operation in the next 24-hour period. Simulation results indicate that this method of tuning local voltage control resulted in efficient utilization of reactive power resources as it mitigated over and under voltage conditions on the grid and also did minimize power losses when implemented on a 69-node distribution network. These results were comparable to the results obtained when a fully centralised voltage control scheme that relies on communication facilities was also implemented. Thus, the research concludes that proper tuning of local voltage control in the day-ahead scheme will make power system networks more accommodating toward a higher penetration of DGs without the need for communication facilities. It must be stated that the complexities of this nonlinear optimization increase with large networks.

Similar work was implemented in [68] where the authors proposed a novel concept to reduce the nonlinear complexities in the optimization algorithm in [25] by using Kriging Metamodel. This is a purely stochastic method that employs an interpolation approach in providing precise predictions of extremely nonlinear problems using statistical theory. The Metamodel is thus a simplified model of the actual extremely nonlinear optimization problem and it is built using local voltage and power measurement variables as input to predict the value of reactive power compensation of each DG unit for the next sampling time. The prediction was done using the Kriging method which estimates the output value of a given function at a point using the weighted mean value of known output values of the function around that particular point. Based on this predicted value of the desired reactive power compensation, the characteristic curve of the local $Q(U)$ control is determined. Simulation results indicates the high accuracy of the Metamodel to represent the complex nonlinear optimization algorithm as this proposed method effectively regulated the voltages and minimized power losses on both the IEEE 33 and IEEE 123 distribution networks.

The use of historical or forecasted load and generation profiles by coordinated schemes introduces a challenge; during implementation, if there is a substantial difference between the forecasted values and the actual values, the effectiveness of the local controller will reduce since the local curves cannot adapt to the prevailing conditions.

Decentralised scheme on the other hand relies solely on local measurements available at the PCC to adjust the characteristic curve of the local control with the prevailing grid conditions. For instance, in [69], the authors proposed a location-dependent adaptive local control based on the fuzzy inference method to adjust the characteristic curve of the local control as shown in figure 2.10. The active power output of the DG (P) and the voltage at the PCC (U) are inputs to the fuzzy inference method, which are categorised depending on their values. Different combinations of the categorised input values are created to generate a set of fuzzy rules. The output signal (δ) from the fuzzy rules is used to adjust the curve of the local voltage control. This adjustment is done in such a way that inverters at the tail ends of the feeders absorb less amount of reactive power as compared to those closer to the transformer. However, the identification and categorization of the fuzzy rules are very challenging as prerequisite knowledge about the network is required.

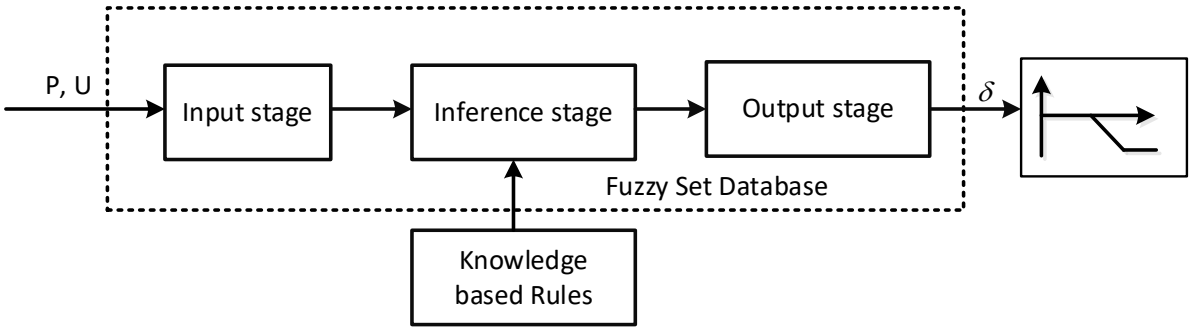

Figure 2.10 Fuzzy-based adaptive Q(U) control [69]

To overcome the challenge of fuzzy classification, the authors of [60] replaced the fuzzy reference method in [69] with a droop function that operates using voltage sensitivity analysis. The sensitivity analysis revealed that voltage sensitivity to active and reactive power injections of a bus increases as the distance of the bus from the substation transformer increases. Based on this knowledge, $cos\varphi(P,U)$ droop voltage control is developed to combine the inherent attributes of both $Q(U)$ and $cos\varphi(P)$ control for effective voltage coordination on the grid. $Cos\varphi(P)$ control is location independent as the control generates the same amount of reactive power irrespective of the location on the DG. $Q(U)$ control on the other hand depends on the location of the DG as the amount of reactive power compensation is determined by the voltage sensitivity of the bus. For instance, during peak solar irradiance, a DG (PV) inverter located at a bus closer to the substation transformer which normally will not take part in voltage regulation when operated in the $Q(U)$ mode as the voltage of this bus is likely to be within the dead band region of the standard $Q(U)$ control and also less sensitive to active power injections. Nonetheless, with $cos\varphi(P,U)$ this particular DG will participate in voltage regulation because reactive power compensation by the DG depends on both voltage (U) and active power (P). This automatically reduces the reactive power compensation requirement of the DG at the tail end of the feeder, thus achieving coordination of reactive power. This scheme proved its effectiveness in minimizing losses on the grid and improving voltage violations when implemented on a Danish distribution feeder. But the authors did not provide a detailed methodology on how to determine the parameters of this droop function as they used the same settings for every DG local control.

A more mathematical approach was adopted in [70] to develop an adaptive droop control for voltage regulation in distribution grids. In this scheme, the characteristic curve of the droop control is varied to change the active and reactive power outputs of the DG based on the prevailing voltage conditions at

the PCC. The control of each inverter operates autonomously from the other and thus no communication facilities are required on the grid for implementation. The objective of the control was to improve voltage regulations within the regulatory limit and also ensure voltage stability. This adaptive control relied on already calculated impedances between the bus of interest and the slack bus to determine the characteristic of the local droop control. However, impedance is dependent on atmospheric conditions and as such could lead to computation errors during implementation, thereby reducing the effectiveness of this approach.

Table 2.1 below summarizes the advantages and disadvantages of the various voltage control strategies discussed in this thesis.

Table 2.1 Comparison of the different voltage control methods

Method	Advantage(s)	Disadvantage(s)
Central	Ensures efficient utilization of network resources Ensure optimal voltage control decisions	Requires communication facilities The complexity of the scheme increases with large networks
Decentralized control	Reduced communication burden as compared to centralized	Results in sub-optimal solutions
Local control	Fast control response Relies solely on measured variables at the PCC	Challenge of tuning the control parameters with changing grid conditions

2.4 Voltage Regulation in Ghanaian Distribution Grids with Distributed Generation

Voltage regulation in Ghanaian distribution networks is achieved with OLTC, VR, and CB. The expected emergence of DG on power grids will impact the operations of these VRDs. On the other hand, it also presents an opportunity to utilize the reactive power resources of DGs to augment the performance of these VRDs.

One such work is [71], where an impact assessment of DG (PV) was carried out on low voltage distribution grids in Ghana. The objective of the research was to

investigate the maximum penetration level of DGs on the feeder with respect to specific performance indicators, namely, voltage profile and total harmonic distortion. The research concluded that even though the DG improved the voltage profile on the power grid, voltage limits were the main limiting barrier in maximizing the penetration level of DGs as compared to total harmonic distortion. The optimal location of DGs in MV distribution grids in Ghana was further investigated in [72]. In this research, the locations of the DGs were varied in an attempt to identify their impact voltage profiles and power losses. The authors concluded that the impact assessment of DGs on an MV grid is dependent on both the location and penetration level of the DG. Furthermore, the analysis reveals that it is more desirable to integrate DGs along the MV feeder than to integrate them at the bulk supply point in order to minimize power loss and enhance the voltage profile. Despite, the DGs were operated at unity power factor without considering the potential of the DG's reactive power capability. To further understand the challenges of DG integration in Ghanaian MV grids, a post-impact assessment of a 20 MW DG located at Gomoa Onyadze in the central region of Ghana on the 33 kV distribution feeder was carried out by the authors of [73]. This DG operated at a power factor of 0.99. The assessment reveals that the DGs will worsen the voltage profile and the utility power factor across the network, especially during the peak solar period. A potential solution is to allow the active participation of DGs in voltage control.

The work in [74] considered the reactive power resources of DGs. The authors of this paper investigated the optimal power factor for operating DG in MV grids in Ghana to reduce power losses. The methodology adopted in the paper was to vary the power factor of the DG located at a specific bus to determine the corresponding power loss on the grid and the voltage violation limits. This was rather a simplistic approach as there could be several DGs connected on the MV grid with each having its characteristic or impact.

2.5 Summary

This chapter discussed several voltage control methods as proposed in the literature, classified into three main groups; centralised, decentralised, and local voltage control. It was revealed that even though centralised control methods ensure optimal and efficient utilisation of reactive power resources on the grid, they require communication facilities to be available on the grid. This requirement leads to significant financial investment in measurement devices

and sensors, creating a challenge for developing countries like Ghana, where there are limited financial resources. Whereas the decentralised control methods reduce the communication burden by dividing the network into zones. On the other hand, local voltage control methods rely solely on measured variables at the PCC, thus there is no requirement for communication facilities.

The key findings about the implementation of local voltage control from this chapter are summarized as follows.

- The major challenge of local voltage control is how to adapt its characteristic curve or control settings with changing grid conditions to guarantee optimal performance. Some research works focused on real-time strategies involving centralised control schemes to adapt or tune the control settings. Unfortunately, it requires communication facilities.
- On the other hand, other researchers implemented planning-based approaches, which use offline tools like optimization algorithms and power flows to tune or adapt the local control curves. This is easily implementable in distribution grids that lack communication facilities. Thus, this thesis works focuses on planning-based approaches, which are grouped into coordinated and decentralised schemes.
- In the coordinated-based approaches, forecasted or historical loading and generation profiles are incorporated into the OPF and used to determine the optimal curves for the local control. However, these curves are unable to adapt to errors encountered if there are significant differences between the actual values during implementation and the forecasted values.
- Decentralised schemes rely on measured values at the PCC to adjust the control settings or curves. Furthermore, very few works exist that have investigated the potential of using the reactive resources of DGs to enhance the performance of MV grids in Ghana. Existing research so far is limited to only power factor control, without investigating the impacts of other local voltage control methods.

Based on these findings, this thesis focuses on local voltage control for distribution networks in Ghana and other developing countries where there are limited or no communication facilities. The Ghana grid code allows for different types of local voltage control methods with each having a different impact on the performance of the grid. There is therefore a need to assess the performance of each local voltage control method and how the settings of these methods are

adapted to the changing grid conditions without the need for communication facilities to enhance control performance.

This thesis starts by assessing the performance of the different local voltage control methods specified by the Ghana grid code for distribution networks.

Chapter 3 Comparative Study of Local Voltage Control Methods

The national electricity grid code of Ghana allows for active participation of DGs in voltage control in distribution networks through the use of different reactive power control methods, which have varied impacts on network performance. A performance assessment of the various local voltage control methods is therefore needed to serve as a guide in the planning and operating of distribution networks. In this chapter, a comparative study among these local voltage control methods is performed to ascertain their respective impact on grid losses, voltage profile, and tap movements of the voltage regulator (VR) and on-load tap changer (OLTC). The chapter begins by explaining the requirements of voltage regulation as underlined in the grid code, followed by a description of the probabilistic models used in modelling uncertainties associated with loads and generations in the grid. Subsequently, the optimal power flow incorporating these developed models used in carrying out the comparative assessment is explained.

3.1 Reactive Power Capability under the Ghanaian National Grid Code

A distribution network is defined in the national electricity grid code as "a system of electric lines and associated equipment (at nominal voltage levels up to 36 kV), which that Distribution Utility is licensed to use to distribute electricity for supply under its distribution license excluding public lighting assets''. They are classified into LV and MV according to the levels shown in table 3.1 [43].

Table 3.1 Voltage classification of distribution networks in Ghana [43]

Definition	**Voltage range**
Low voltage (LV)	Up to 1 kV
Medium voltage (MV)	1 kV to 36 kV

The renewable energy code for distribution networks, a sub-code under the national electricity grid code, allows for reactive power participation from DGs. Under this code, DGs can operate within a power factor (PF) range from 0.95 lagging to 0.95 leading, measured at the point of common coupling (PCC) [24]. Furthermore, DGs that operate at maximum active power are required to have the capability to constantly vary the PF within this entire stipulated range if the voltage at the PCC is within the ±5% of nominal voltage. Thus, there is the need for the apparent power rating of the inverter to be greater than the maximum active power output to make room for reactive power compensation during peak active power generation. When the active power output is within 5 to 100% of the rated power output of the DG, the DG is free to operate within the stipulated PF range, from under-excited (lagging) to over-excited (leading) region, as shown in figure 3.1. However, when the power output is below 5% there is no reactive power requirement from the DG, but the DG can still provide compensation within the range of +/- 5% of the nominal power (P_n), indicated in figure 3.1 as the shaded region of ABCD.

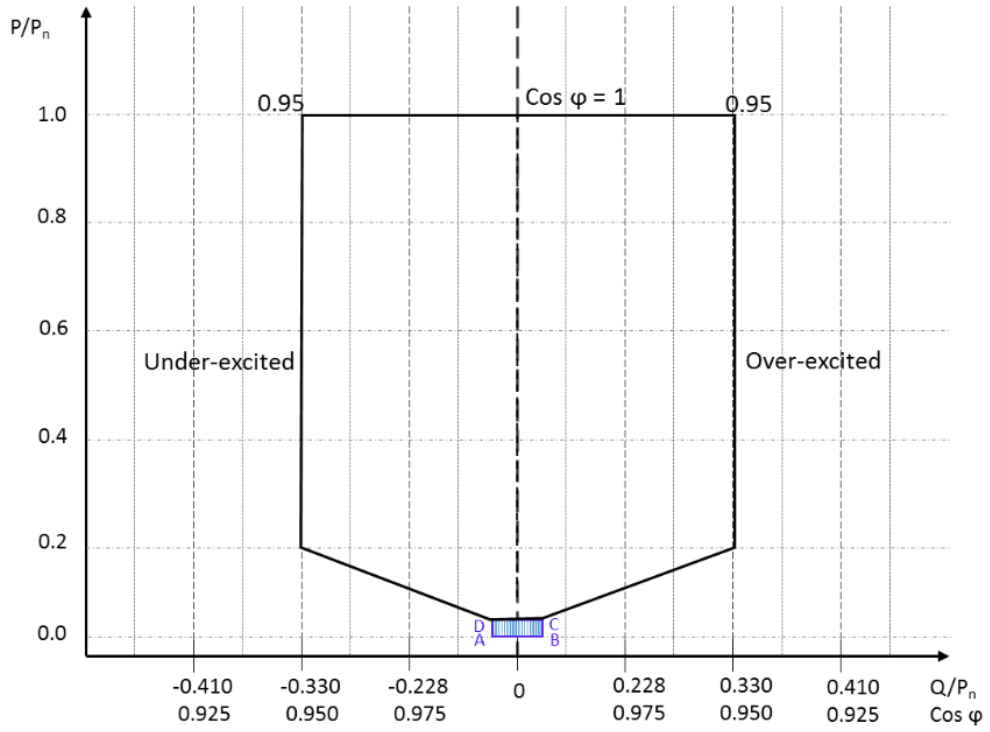

Figure 3.1 Requirements of reactive power under Ghana grid code [24]

3.2 Methods of Reactive Power-based Local Voltage Control

Several methods of reactive power-based local voltage control have been proposed in the literature. However, only two control methods, the $Q(U)$ and $cos\varphi(P)$ control allowed under the national renewable sub-code for distribution and transmission networks [24], [75], will be discussed in the next sub-sections.

3.2.1 Cosφ(P) Control Method

The schematic for this control is shown in figure 3.2. The operating PF of the DG is determined by the active power output (P) at which the DG operates. Based on the schematic in figure 3.2, the DG operates at unity PF until the active power from the DG is equal to a set value P_0. If the active power value is above P_0, the DG begins to provide reactive power compensation by changing its PF until it gets to another set value P_1, where it provides maximum reactive power compensation (PF_{MAX}). The values P_0 and P_1 are determined by the distribution network operator.

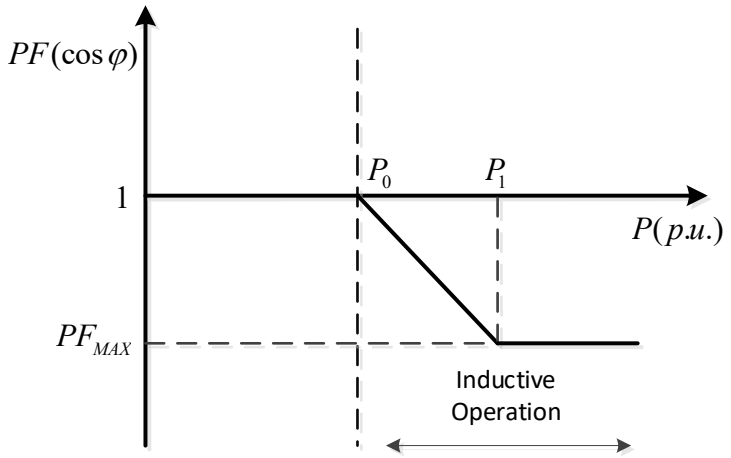

Figure 3.2 Characteristic curve of $cos\varphi(P)$ [76]

The power factor control is mathematically expressed as in (3.1).

$$cos\varphi = \begin{cases} 0 & P < P_0 \\ \dfrac{PF_{MAX}}{P_1 - P_0}\,(P - P_0) & P_0 \le P \le P_1 \\ PF_{MAX} & P > P_1 \end{cases} \qquad 3.1$$

3.2.2 Q(U) Control Method

The characteristic curve of $Q(U)$ control is shown in figure 3.3. The inverter can either operates in the capacitive or inductive region depending on the voltage (U) at the PCC. There is however no reactive power compensation from the inverter during the dead band region (between U_2 and U_3). The amount of reactive power compensation provided either in the capacitive or inductive region is determined by the slope of the curve, with Q_{max} being the maximum reactive power compensation.

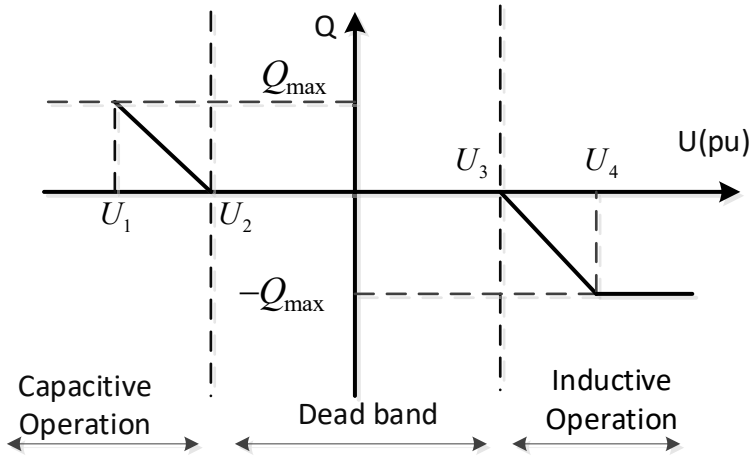

Figure 3.3 Characteristic curve of Q(U) control [76]

The $Q(U)$ control is mathematically expressed as;

$$Q(U) = \begin{cases} Q_{max,} & U < U_1 \\ \dfrac{Q_{max}}{U_1 - U_2}(U - U_1) + Q_{max}, & U_1 \leq U \leq U_2 \\ 0, & U_2 < U \leq U_3 \\ \dfrac{Q_{max}}{U_3 - U_4}(U + U_3), & U_3 < U \leq U_4 \\ -Q_{max,} & U > U_4 \end{cases} \quad 3.2$$

The values of U_1,U_2,U_3 and U_4, are determined are to be determined by the distribution network operator.

3.3 Modelling of Loads and PVs

Loads and PVs are subject to seasonal and daily variations which makes them stochastic. These variations introduce some level of uncertainty in the planning and operation process of power system networks. The use of deterministic approaches is insufficient to account for these uncertainties. For instance, if the values of loads and generation used during the planning stage are different from the measured values during the time of operation or implementation, then the performance and efficiency of network devices will be negatively affected. To account for these uncertainties, mathematical methods such as probabilistic, possibilistic, information gap decision theory, and robust optimization approaches are used to model PVs and loads when planning power system networks [77].

The possibilistic approach was originally introduced by authors of [78] to model the uncertainty of a parameter using a fuzzy approach. It is called possibilistic because each uncertainty parameter is assigned a possible degree of an occurrence described by a membership function (MF) within a set of fuzzy boundaries. There are various MFs whose selections depend on the prior knowledge of the nature of the uncertainty variable i.e. an expert's opinion is required. To illustrate this approach, a function $y = f(X)$ is assumed where y is the output variable and X is the vector of the uncertain parameters $X = [x_i, \dots, x_m]$. If the MF of X is selected or known, the MF of y is determined by the α -cut method as was the case in [79], where it was used to describe the PV's active power output. To illustrate the α -cut method, a trapezoidal MF shown in figure 3.4, proposed by authors of [77], is assumed using a set of fuzzy A, with notations a_{MIN}, a_L, a_V and a_{MAX}.

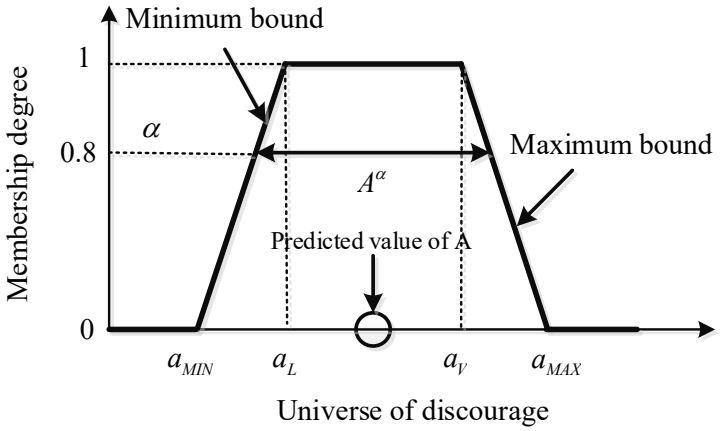

Figure 3.4 Fuzzy trapezoidal membership function [77]

The α-cut of X (A^{α}) is expressed as;

$$A^{\alpha} = \{x \in U \mid \mu_A(x) \geq \alpha\} \quad 3.3$$

$$A^{\alpha} = \left(\underline{A}^{\alpha}, \overline{A}^{\alpha}\right) \quad 3.4$$

Where $\mu_A(x)$ is the MF as defined for each uncertain parameter, U is the range of all possible values of X, $\underline{A}^{\alpha}$ and $\overline{A}^{\alpha}$ are the lower and upper bound values of A^{α} respectively. The α-cut of y is thus calculated as follows [80];

$$y^{\alpha} = \left(\underline{y}^{\alpha}, \overline{y}^{\alpha}\right) \quad 3.5$$

$$\underline{y}^{\alpha} = \min f(X^{a}) \quad 3.6$$

$$\overline{y}^{\alpha} = \max f(X^{a}) \quad 3.7$$

$$X^{\alpha} = \left(\underline{X}^{\alpha}, \overline{X}^{\alpha}\right) \quad 3.8$$

Where the upper bound ($\overline{y}^{\alpha}$) of y is obtained by maximization and the lower bound ($\underline{y}^{\alpha}$) is obtained by minimization.

Probabilistic methods using probability density function (PDF) provide an alternative method to model uncertainties [77]. The PDFs are developed using historical data of the uncertainty parameters. Suppose a function $y = f(Z)$, where Z is an input vector of random variables z_i to z_m with known PDFs and y is the output variable. To model the uncertainty of y, the Monte Carlo method is used, which generates a sample z_i^e from the PDF of each input parameter z_i. The corresponding output of each generated sample is calculated using $y^e = f(Z^e)$, where $Z^e = [z_i^e, \ldots, z_m^e]$. After a predetermined set of iterations, the outcome of y is determined using statistical methods such as mean, histogram, etc. Developing MF for possibilistic method is complex and requires an extensive knowledge about the uncertainty variables [77], [81]. The probabilistic method on the other hand as compared to the possibilistic method is easier to implement and more accurate in representing the uncertainty because the PDFs are developed using historical data of the uncertainty variables. Thus, probabilistic methods are adopted in this thesis to model the uncertainties of PVs and loads.

3.3.1 Probability Density Function

The first step towards the development of the probabilistic models is the selection of the appropriate PDF fitting to represent the uncertainty variable. PDFs are mathematical functions used to describe the behaviour and properties of uncertainty or random variables after observing large measurements or experiments [82]. In this thesis, historical values of load and PV generations will be used to develop the PDFs. Different types of PDFs such as normal, weibull,

beta, etc have been used by power system engineers depending on the nature of the variable. The mathematical formulation of these PDFs is explained as follows.

3.3.1.1 Normal probability density function

This is a type of continuous probability distribution for a real-valued random variable. It is also called the Gaussian distribution and is mathematically expressed as;

$$F(x) = \frac{1}{\sigma\sqrt{2\pi}} exp^{-0.5(\frac{x-\mu}{\sigma})}, -\infty < x < \infty \quad 3.9$$

Where μ is the mean and σ is the standard deviation.

3.3.1.2 Weibull probability density function

This is a two-parameter distribution often used to represent wind speed data. The Weibull PDF is mathematically expressed as;

$$F(x) = \frac{k}{c} * \left(\frac{x}{c}\right)^{k-1} * exp^{-\left(\frac{x}{c}\right)^{k}} \quad for\ c > 1;\ \ k > 0 \quad 3.10$$

Where c is the scale factor and k is the shape factor. Equations 3.11 and 3.12 are used to calculate respectively the shape and scale factors.

$$k = (\sigma/\mu)^{-1.086} \quad 3.11$$

$$c = \mu/\Gamma(1 + 1/k) \quad 3.12$$

3.3.1.3 Beta probability density function

This distribution is used to describe the random behaviour of variables that are bounded between two defined limits α and β. It is defined as;

$$F(x) = \begin{cases} \frac{\Gamma(\alpha+\beta)}{\Gamma(\alpha)\Gamma(\beta)} * x^{(\alpha-1)} * (1-x)^{(\beta-1)}, for\ 0 \le x \le 1, \alpha \ge 0, \beta \ge 0 \\ 0, \qquad Otherwise \end{cases} \quad 3.13$$

The parameters of α and β of the distribution are calculated from (3.14) and (3.15)

$$\beta = (1-\mu) * \left(\frac{\mu * (1+\mu)}{\sigma^2} - 1\right) \quad 3.14$$

$$\alpha = \left(\frac{\mu * \beta}{1-\mu}\right) \quad 3.15$$

Where μ is the mean and σ is the standard deviation.

3.3.2 Probabilistic PV Modelling

To model the PV, hourly solar irradiance, and temperature data for Sunyani (a town in northern Ghana) over three years. The basis for selecting this town is because of the high amount of PV integration in the northern part of Ghana and also this town has the highest demand (32%) in that part of the country [35]. The selection of Sunyani thus presents a suitable test case to assess voltage regulation challenges on a typical Ghanaian MV distribution grid since severe voltages occur because of its location and the total load. The values of irradiance and temperature were obtained from [83], and are converted into active power output (P) using (3.16) - (3.19) [84], [85].

$$P = U_{PV} * I_{PV} * FF \tag{3.16}$$

$$U = U_{OP} - K_U * \left[T_{AC} + \frac{S_{RAD}}{S_{STC}} \left(\frac{N_T - 20}{0.8}\right)\right] \tag{3.17}$$

$$I = \frac{S_{RAD}}{S_{STC}} [\, I_{SH} + K_C(\, T_{CT} - 25)] \tag{3.18}$$

$$FF = \frac{U_{MPP} * I_{MPP}}{V_{OP} * I_{SH}} \tag{3.19}$$

Where

U_{PV} The output voltage of the PV;

I_{PV} The output current of the PV;

FF The fill factor of the PV;

U_{OP} The open-circuit voltage of the module in volts;

K_U The voltage temperature coefficient expressed in $V/℃$;

T_{AC} The ambient temperature in ℃;

N_T The nominal operating temperature of the cell in ℃.

S_{RAD} The solar irradiance values for that hour;

S_{STC} The solar irradiance at standard test conditions;

I_{SH} The short-circuit current of the module in amperes;

K_C The current temperature coefficient in $A/℃$;

T_{CT} The cell temperature in ℃ during the hour of operation;

I_{MPP} The current in ampere at maximum power point;

U_{MPP} The voltage in volts at the maximum power point.

The values for these solar module characteristics (I_{MPPT}, U_{MPPT}, I_{SH}, K_C, U_{OP}, K_U *and* N_T) were obtained from [86] and shown in Appendix B. The following describes the steps (procedure) used to develop the probabilistic PV and load models.

- A month is selected to represent each of the three seasons in Ghana because it is expected that the temperature and solar irradiance values will be similar within each season. The selected months are March, August, and December representing the dry, rainy, and harmattan seasons respectively. Each month is 31 days period subdivided into a 24hr time segment. Thus, for the three years (2014, 2015, and 2016) data, each season is represented by three months. In all, there will be 2,232 hourly values representing each season i.e. 31(days) * 3 (months)* 24(hours). These PV profiles are shown in Appendix C.
- The mean (μ) and standard deviation (σ) are calculated for each time segment (hourly) for both the PV and load models.
- Normal, beta, and weibull PDFs are calculated for each time segment (hourly) for both PV and load hourly values.

3.3.3 Assessing the Fitting Distributions

To assess which PDF best describes the load and PV data, goodness-of-fit tests are carried out. A goodness-of-fit test is used in statistics to describe how a set of observations fits a particular PDF. It is carried out by measuring the error between the observed data and the values obtained from the constructed PDF. One such fitness test is the Anderson-Darling test, which is elaborated on in the next sub-section.

3.3.3.1 Anderson-Darling (AnDar) Test

The Anderson-Darling (AnDar) test was developed by T. W. Anderson and D. A. Darling in 1952 and is calculated using (3.20) [10],[12];

$$A^2 = -n - \frac{1}{n}\sum_{i=1}^{n}(2i-1) * (\ln F(x_{(i)}) + \ln(1 - F(x_{(n+1-i)}))), \quad i = 1,2,\dots,n \tag{3.20}$$

Where $F(x)$ is the value of the theoretical distribution function described by the PDF at x, such that $x(1) < \cdots < x(n)$ are arranged from the smallest to the largest element from n data sample size. A^2 represents the error between the

theoretical and empirical distribution function, hence the smaller the value of A^2, the better the fit. The empirical distribution is the observed data.

3.3.3.2 Goodness-of-fit test results

To reduce the computation, specific hours are selected to represent the 24 hours for each of the months. The hours are 8 am, 12 noon and 4 pm. In each hour, a histogram profile is generated to represent the empirical distribution. Based on equations (3.9), (3.10), and (3.13), normal, beta, and weibull PDFs are generated for each of the selected hours for the PV. The AnDar statistic is then calculated for each of the three PDFs.

Figures 3.5 and 3.6 show the histogram representation of the PV output per unit during the rainy season for loads at 8 am and 4 pm respectively with mathematically described curves for the beta (red dashed line), normal (blue line), and weibull (brown dashed line) PDFs. The histogram represents the PV output data. From these figures, it is difficult to identify which PDF best fits or describes the PV output unless the AnDar statistic is used.

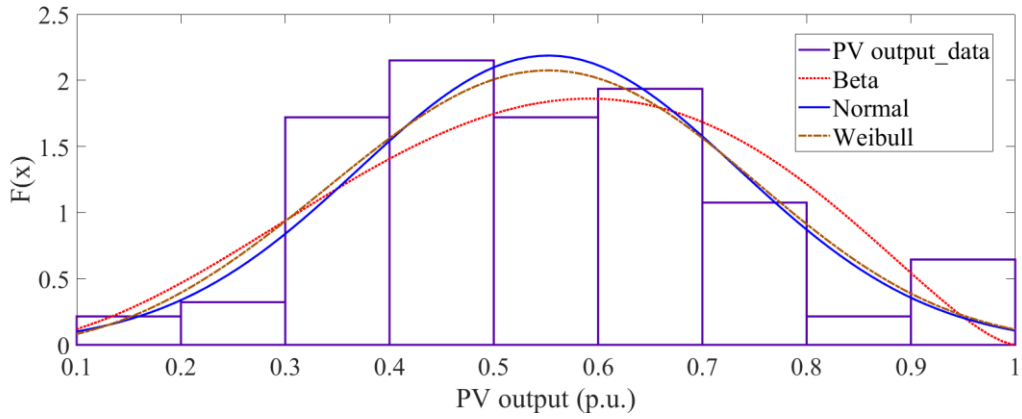

Figure 3.5 Histogram of PV output and distribution fitting for rainy season at 8 AM

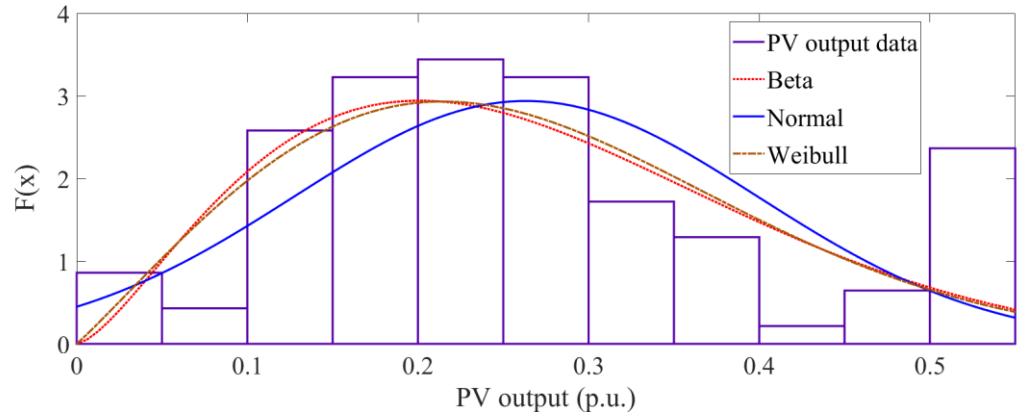

Figure 3.6 Histogram of PV output and distribution fitting for rainy season at 4 PM

In order to determine the PDF that best describes the PV output, table 3.2 summarizes the values of the AnDar statistics for the PV output. At 8 am, during the rainy season, the value of the AnDar statistic for beta distribution was 1.6133 as compared to the normal and weibull where the values were 4.7338 and 7.9215 respectively, thus making beta distribution the best fit for that hour. The trend was similar for 4 pm, however, for 12 pm, the normal PDF fitted the most as it recorded a value of 0.6331, lesser than the values of 1.4745 and 0.7017 obtained for the beta and weibull PDFs respectively. Thus, it is concluded that the beta PDF best fits the PV output for the dry season. For the harmattan season, the normal PDF was also the best fit as it recorded the least AnDar statistic values for both the 8 am and 4 pm as compared to the weibull and beta PDFs. The only exception was at 12 pm where the best fit was the weibull distribution.

Table 3.2 Results of the goodness of fit test

Season		**Distribution**		
		Normal	**Beta**	**Weibull**
		AnDar test		
Rainy	8 am	4.7338	1.6133	7.9215
	12 pm	0.6331	1.4745	9.004
	4 pm	1.7256	0.6563	0.7017
Harmattan	8 am	4.8203	6.3183	5.4649
	12 pm	14.0651	10.3886	8.242
	4 pm	8.6535	10.9884	8.9805
Dry	8 am	2.0981	3.1699	2.8509
	12 pm	9.8069	7.3516	10.701
	4 pm	7.9215	9.0004	9.8283

However, for the dry season, the best fit was the normal distribution since it had the least values for the hours of 8 am and 4 pm with the normal distribution having the least value at 12 pm. The normal distribution, thus, describes best the uncertainty of the PV output for the dry season. In summary, the PV output for the selected site (Sunyani) in Ghana tends to exhibit normal distribution for both

the dry and harmattan seasons, and the rainy season is fitted with the beta distribution. Thus, in this thesis, the normal distribution will be used to model the uncertainty of the PV output as the dry and harmattan seasons account for eight (8) months of the year.

Loads on the other hand are also dependent on climatic conditions and time, mostly assumed to fit normal distribution [89]. Subsequently, authors of [90]–[92] have used normal PDFs to model the uncertainty of loads. Thus, the normal PDF will also be used in this thesis for the loads. The load profiles used are shown in Appendix C.

3.4 Distribution Networks Optimization using Genetic Algorithm

Several optimization algorithms have been used to improve distribution networks' performance in loss minimisation, voltage regulation, etc. The main idea of optimizing distribution networks is to ensure the efficient utilization of network resources and planning to accommodate DGs penetration into the networks. The structure of an optimization algorithm is made up of an objective function that is subject to either equality and/or non-equality constraints. Mathematically this can be expressed as;

$$\text{Minimizing } f(x,u) \tag{3.21}$$

While satisfying

$$g(x,u) = 0 \tag{3.22}$$

$$h(x,u) \leq 0 \tag{3.23}$$

Where $f(x,u)$ is the objective function, $g(x,u)$ is a set of equality constraints, $h(x,u)$ is a set of non-equality constraints, x and u are the vectors of dependent and control variables respectively.

The objective function is a mathematical equation expressed as a function of dependent and control variables and describes the purpose of the optimization. Examples are loss minimization, voltage profile improvements, etc. The control variables are the set of values that are varied by the optimization algorithm to achieve the purpose of the optimization. They can be either discrete or continuous values or both. Examples include tap settings of OLTC, active power output of PV, etc. In power system planning, examples of inequality constraints include lower and upper voltage limits, thermal ratings of transmission lines, the

maximum power output of power plants, etc. Whereas the power flow balanced equation is an example of equality constraints. A selection of an optimization algorithm is dependent on the type of optimization problem, determined by the nature of control or decision variables. In this thesis, both continuous and discrete variables are considered, making it a mixed integer optimization problem. These algorithms are mainly classified into analytical, numerical, and heuristics techniques [93].

Numerical techniques use mathematical approaches like mixed integer linear programming, mixed integer non-linear programming (MINLP), etc. in solving the optimization problem. MINLP is used to solve optimization problems involving both continuous and discrete variables, for instance in [94], where the authors used it to determine the set-points of OLTC as discrete variables and the active and reactive flexible loads as continuous variables for voltage control purposes. Results from MINLP techniques are usually highly accurate, however, the computational complexity increases with large distribution networks, and thus affects the convergence of the optimal solution [95]. On the other hand, heuristic techniques are more robust in handling large networks efficiently [93][96].

Examples of heuristics techniques include particle swarm optimization, genetic algorithm (GA), ant bee colony, etc. GA has an advantage over numerical methods as it adopts a probabilistic approach in its search for the global optimum [97]. The search for the global optimum in the optimization space is done from different random points, unlike the numerical techniques where it is done from a single point using gradient descent methods. As such, it has a higher chance of attaining global optimum and possibly obtaining multiple optimal solutions. Also, GA requires no prior knowledge about the objective function before carrying out the optimization as other numerical methods will require the function to be differentiable. The superior performance of GA in planning power system networks was further demonstrated by the authors of [98]. This was a network expansion problem, formulated as a non-convex, non-linear, mixed-integer optimization problem and successfully solved by the GA. Subsequently, GA is used in this thesis work as the optimization tool.

The concept of GA as an optimization tool was first developed by John Holland [99]. It is an evolutionary algorithm based on the concept of survival of the fittest i.e. individuals with the best features within a population are transferred to the next generations whiles the weaker ones are eliminated. Figure 3.7 further illustrates the GA procedure. The GA begins by generating a random set of initial populations made up of individuals called chromosomes. This population

goes through three GA operators, namely, selection, crossover, and mutation to produce the next population. The operators are explained as follows.

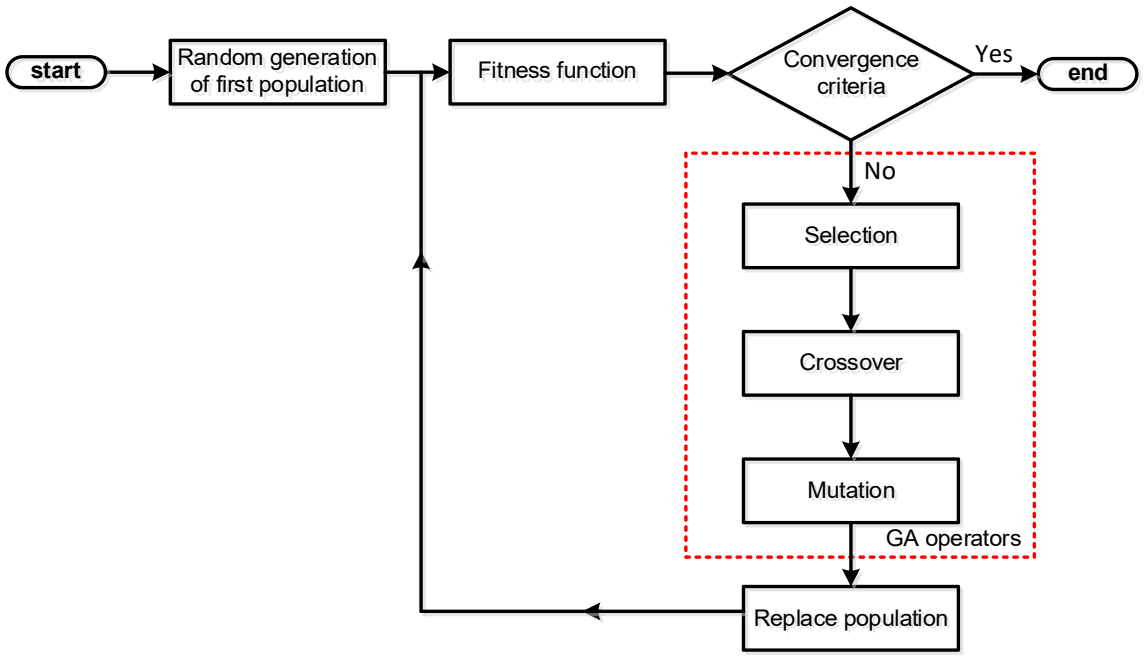

Figure 3.7 Workflow of Genetic Algorithm [100]

Selection: This process selects the best individuals among the population for the next generation. The roulette selection is adopted in this thesis as it computes the fitness value of each individual in the population, thereby discards the weaker chromosomes based on the fitness value and selecting the remaining chromosomes for the generation of the next population.

Crossover: The selected chromosomes are used to create a new population of better chromosomes with higher fitness functions through genetic crossover or recombination. In the crossover, new chromosomes (offspring) are created from two individual chromosomes (called parents) among the selected or existing chromosome population by creating a swapping point in each parent chromosome and subsequently combining each point from each part to create a new one. Thus, it is expected that the offspring will inherit good genetic information from both parents, eventually improving the quality (higher fitness value) of the population to increase the chance of achieving convergence [100].

Mutation: However in mutation, a part of each chromosome is varied to create a new offspring. This introduces diversity in the search space which leads to exploration in new regions and eventually aids the algorithm to avoid local optima solutions [98]. In this thesis, 0.1 is selected as the mutation probability.

The cycle is repeated until the convergence criteria which is the set tolerance level or the maximum number of generation limit is reached. GA is widely used in planning distribution networks [101], for instance, DG allocation such as [102]–[104] and voltage control among voltage regulating devices seen in [105][106].

3.5 Comparative Assessment

3.5.1 Medium voltage distribution network

The network used for implementing the comparative assessment is the 16-bus United Kingdom generic distribution network described earlier in section 1.5 and shown in figure 3.8.

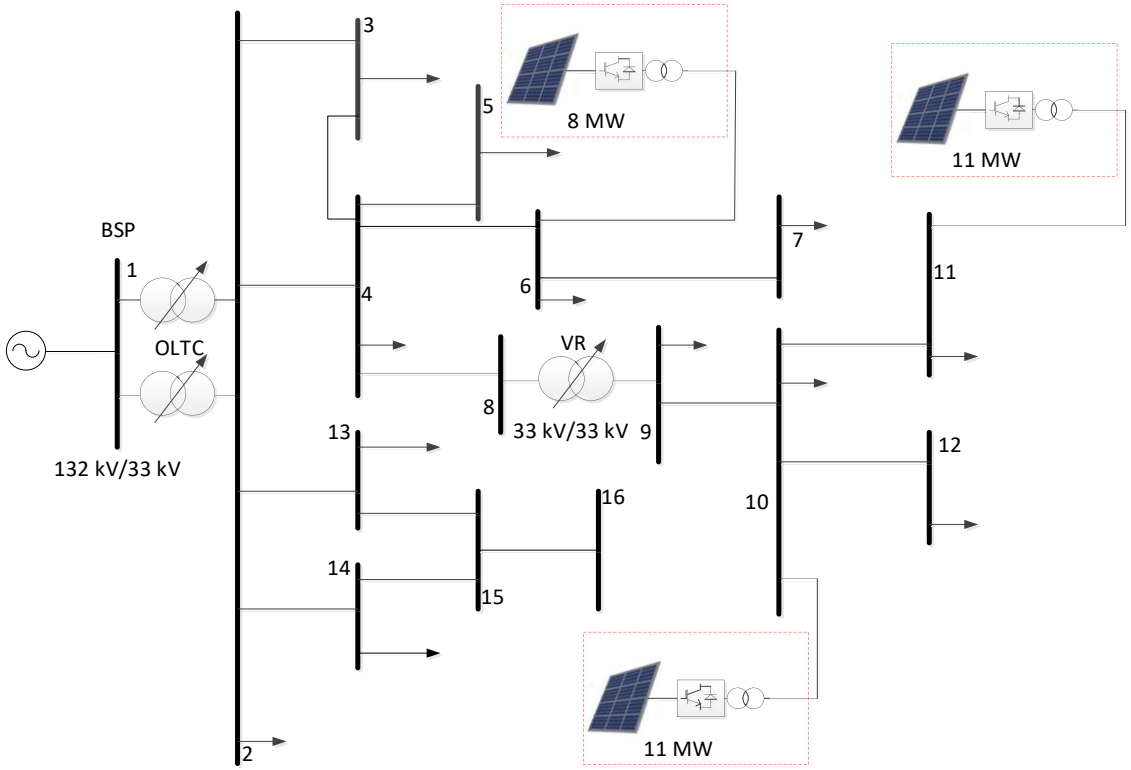

Figure 3.8 16-bus medium voltage distribution grid based on [28]

Buses 6, 11, and 10 are selected as PV locations. Buses 11 and 10 were selected to represent a long feeder in an urban area in the northern part of the country since they are the tail ends of the feeder with low voltages. While bus 6 represents the load center in the network as it is closer to bus 5 which has the heaviest load on the feeder. These PV locations provide the necessary scenarios of voltage rise and voltage drop in MV grids in Ghana. The peak MW ratings of

the PVs are 8 MW, 11 MW, and 11 MW for buses 6, 10, and 11 respectively. The apparent power rating of each inverter is sized 1.1 times the peak MW rating. This size is enough to reduce losses and enhance voltage regulation as determined by the authors of [107].

3.5.2 Algorithm for Comparative Assessment

To carry out the comparative offline assessment of the various methods of local control, a probabilistic optimal power flow is implemented using the Monte Carlo technique. This technique is used to account for the uncertainty of load and PV output by randomly generating values from their respective PDFs to be incorporated into the simulation model. The Monte Carlo technique involves the following steps [108]:

- Step 1) Generate a random value x from the selected PDF
- Step 2) Incorporate the x into the optimal power flow simulation model and determine their respective outputs y after the simulation.
- Step 3) Repeat steps 1 and 2 until the set number of random generations are met.
- Step 4) Analyse the various outputs (y) using statistical tools like histogram, mean, etc.

The optimal power flow is implemented using the GA tool with the parameters shown in Table 3.3 showing the number of generations, population, and crossover function used in the optimization.

Table 3.3 GA parameters

GA parameter	**Value**
No. of Generation	150
Population	40
Crossover function (rate)	0.8
Stall generation limit	100
Tolerance	1×10^{-6}

The integration of PVs in distribution grids will result in an improved profile because part of the load (demand) is supplied by the PV, reducing the voltage drop on the grid. Thus, voltage profile improvement is the objective function of this optimization. Mathematically, the voltage profile improvement index (VP_{INDEX}) is expressed in (3.24) [109].

$$V_{INDEX} = \frac{VP_{W/PV}}{VP_{WO/PV}} \tag{3.24}$$

Where $VP_{W/PV}$ and $VP_{WO/PV}$ are the per unit voltage profile of the busses in the network with PV and without PV respectively. VP, the voltage profile is mathematically defined (per unit) as (3.25);

$$VP = \sum_{i=1}^{N} V_i L_i k_i \tag{3.25}$$

V_i and L_i is the magnitude voltage and load at bus i in per unit respectively. k_i is the weighting factor of bus i which is calculated using (3.26). L_{TD} is the total load on the grid.

$$k_i = \frac{L_i}{L_{TD}} \tag{3.26}$$

The definition of this weighting factor will result in higher values of k_i for buses with high load (demand).

The objective function is subjected to both equality and inequality constraints. These equality constraints are the power flow balanced equations expressed in (3.27) and (3.28).

$$P_{GEN} - P_{DEM} - |U_i| \sum_{j=1}^{N} |U_j| \left(|G_{ij}| cos(\delta_i - \delta_j) + |B_{ij}| sin(\delta_i - \delta_j) \right) = 0 \tag{3.27}$$

$$Q_{GEN} - Q_{DEM} - |U_i| \sum_{j=1}^{N} |U_j| \left(|G_{ij}| sin(\delta_i - \delta_j) - |B_{ij}| cos(\delta_i - \delta_j) \right) = 0 \tag{3.28}$$

Where U_i is the voltage at bus i, P_{DEM} and Q_{DEM} are the active and reactive power load (demand) at bus i respectively, P_{GEN} and Q_{GEN} are the active and reactive power generated at bus i respectively, δ_i is the angle of the voltage at

bus i. G_{ij} and B_{ij} are the conductance and susceptance between bus i and j respectively.

The inequality constraints are expressed in (3.29) and (3.30);

$$U_i^{MIN} \leq U_i \leq U_i^{MAX} \quad 3.29$$

$$S_{LINE} \leq S_{LINE}^{MAX} \quad 3.30$$

Where U_i^{MAX} and U_i^{MIN} are the maximum and minimum voltages at bus i respectively, S_{LINE} is the apparent power flowing through each transmission line.

The decision variables are the tap settings of OLTC and VR and are formulated as discrete variables that are changed in steps of 1. The maximum and minimum values of each of the decision variables are shown in table 3.4. The downward movement of a tap is indicated by the negative sign while the positive values represent the upward movement of the tap.

Table 3.4 Minimum and maximum value of control variables

Control variable	**Minimum value**	**Maximum value**
OLTC	-15	5
VR	-15	5

The objective of this comparative study is to determine how the various local voltage control methods impact the grid in terms of power loss, voltage profiles, and the number of tap movements of the VR and OLTC. As such, each of the local voltage control methods is incorporated into the optimal power flow as the GA tool determines the optimal tap settings of the VR and OLTC for every particular hour. In all, the optimization is run for a total of 72 hours, 24 hours for each season. The mean and standard deviation for each hour that was used to develop the normal PDF for both the load and generation are shown in Appendix D. The algorithm is summarized in figure 3.9.

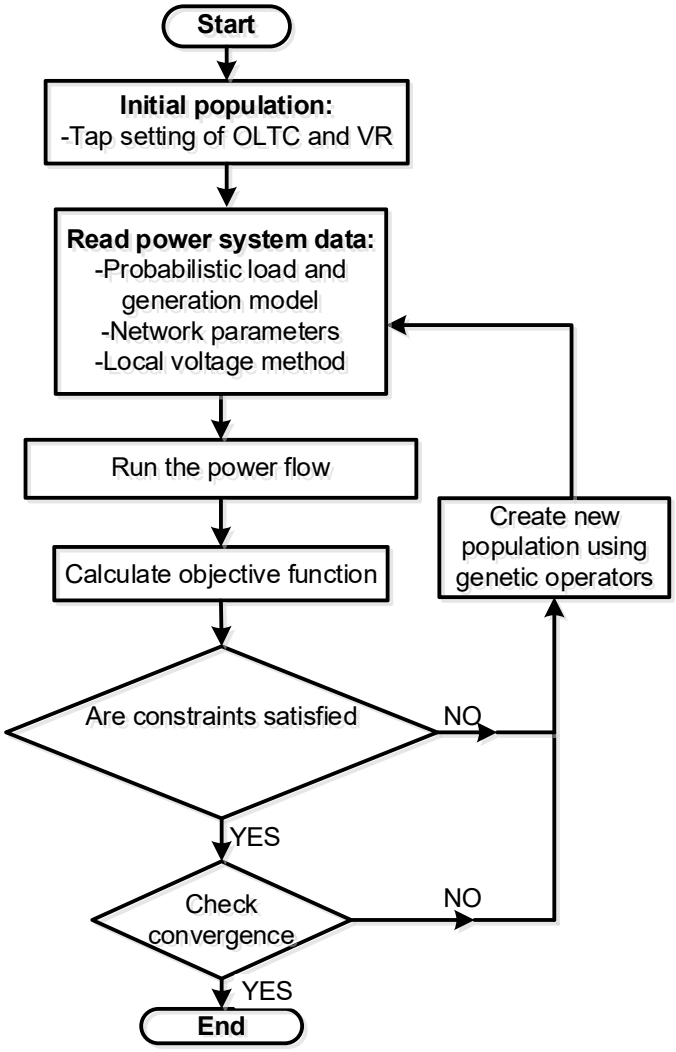

Figure 3.9 Flowchart of comparative study algorithm

Two types of reactive power control methods, $Q(U)$ and $cos\varphi(P)$ are considered, resulting in two scenarios. The parameters of the local control methods are fixed during the entire simulation period of 72 hours. U_1, U_2, U_3 and U_4 of the $Q(U)$ control shown in figure 3.3 are fixed to 0.93 p.u., 0.97 p.u., 1.03 p.u., and 1.07 p.u., respectively based on recommendations of [110] for German distribution networks, while P_0 of the $cos\varphi(P)$ shown in figure 3.2 is fixed to 0.5 p.u [76].

3.5.3 Simulation Results and Discussions

Table 3.4 provides a summary of the performance of the two reactive power control methods. In all three performance indices, the $Q(U)$ control had superior performances as compared to the $cos\varphi(P)$ control. $Cos\varphi(P)$ control recorded a total of 262 tap movements for both OLTC and VR as compared to $Q(U)$ control which was 207. $Cos\varphi(P)$ had this high number of tap movements

because the amount of reactive power compensation is determined by the active power output, which is independent of the voltage at the PCC. Thus, the PV unit operating with $cos\varphi(P)$ will absorb reactive power from the grid once the active power is more than half of the peak value i.e. P_0 value is set to 0.5, even if the voltage at the PCC is within regulatory limits. This leads to unnecessary reactive power flows on the network, resulting in an increased loss of 259.53 MVA and a reduced overall V_{INDEX}. For the $Q(U)$ control, the reactive power compensation is dependent on the voltage at the PCC. Thus, the reactive power compensation was only provided when the PV was outside the dead band region of the control. This resulted in less amount of reactive power compensation being provided with minimum impact on the VR and OLTC tap movements. The reduced reactive power compensation also resulted in low losses (215.42 MVA) and an improved overall V_{INDEX} of 0.972 as compared to $cos\varphi(P)$ control. These results validate earlier works by authors of [76] and [111], who drew a similar conclusion.

Table 3.1 Summarised results of both scenarios

Control method	**No. tap switching (VR and OLTC)**	**Power loss (MVA)**	V_{INDEX}
$Q(U)$	207	215.42	0.972
$Cos\varphi(P)$	262	259.53	0.964

The voltage profiles for both scenarios for the entire simulation period indicating that all the voltages are within the grid code range are shown in Appendix E.

3.6 Summary

The national electricity grid code and the renewable sub-code for distribution networks allow for reactive power participation from PVs to enhance voltage regulation in the grid. PV units can operate within a PF range of 0.95 lagging to 0.95 leading. This participation can be implemented in the form of reactive power local voltage control methods such as the $Q(U)$ and $cos\varphi(P)$ control methods, which have varied impacts on grid performance.

Consequently, a comparative study is needed to ascertain the performance of each control method. Probabilistic modelling is required since the outputs of PV

units and loads are associated with uncertainties, which are modelled using PDFs. PDFs for PV active power output were computed using hourly historical values for the years 2014 to 2016. To reduce the complexity of the computation, each year (12 months) is reduced to three months based on the number of seasons within a year. The months of March, August, and December are selected to represent the dry, rainy, and harmattan seasons. Subsequently, a goodness-of-fit test is conducted among the normal, weibull, and beta PDFs using the Anderson-Darling statistic fitting test. The test concluded that the normal PDF best fit PV unit output, which was also the case for the loads. These probabilistic models for both load and PV units were used in a GA optimization to determine the impact of each control method on grid power loss and V_{INDEX}.

Results from the optimization depict that the $Q(U)$ control achieved better performances as it recorded less power loss and an improved V_{INDEX} compared to the $cos\varphi(P)$ control. Thus, $Q(U)$ control is being adopted in this thesis to be further investigated in the identification of its control parameters. Since the control parameters depend on the load and generation conditions on the grid, the parameters must be adapted to these conditions or an adaptive functionality must be incorporated in the $Q(U)$ control.

Chapter 4 Sensitivity Fitting Function based Adaptive Q(U) Control

The results obtained from the comparative assessment show the efficiency of the $Q(U)$ control as compared to the $cos\varphi(P)$ control method. The performance of the $Q(U)$ control is dependent on the ability to change its reactive power output with the changing or varying grid conditions [25]. This chapter provides an innovative method to achieve this performance by including an adaptive functionality, made up of voltage sensitivity and stability blocks, in the $Q(U)$ control. The voltage sensitivity block generates the amount of reactive power compensation required at the point of common coupling (PCC) using local measurements at the PCC bus. The stability block makes sure that the amount of reactive power enhances the voltage stability of the PCC bus. The chapter begins by first explaining the concept of voltage stability and the stability index used in accessing the distribution grid performance. This is then followed by an explanation of the methods used to determine the voltage sensitivity. Lastly, the proposed method is also illustrated together with the test cases and scenarios used in validating the method.

4.1 Voltage Stability Index

The Institute of Electrical and Electronics Engineers (IEEE) and International Council on Large Electric Systems (CIGRE) joint task force in [112], defined voltage stability as "the ability of a power system to maintain steady voltages at all buses in the system after being subjected to a disturbance from a given initial operating condition". Failure to achieve and maintain steady voltage will result in voltage instability. Voltage instability has been associated with blackouts in the world according to [113], where the authors investigated twelve blackouts and concluded that seven of them were related to voltage instability. The main cause of voltage instability is insufficient reactive power provisioning in the grid [114], resulting from incidents such as changes in load, changes in the output of photovoltaic and wind turbines, generators exceeding their reactive power limit, etc. Thus to avoid instability, there is a need to ensure sufficient reactive power in the grid at all times.

One way to prevent voltage instability or its severe form called voltage collapse is to identify transmission lines or voltage buses in power system networks that are more prone to voltage instability [115][116] using the voltage stability index (VSI). VSI is a mathematical index used both offline and online to determine buses that are more prone to voltage instability and are calculated using measurement information obtained from the grid. Based on the VSI values obtained for both the transmission line and bus, those close to instability point are identified by comparing these values to a threshold value determined by the network operator and mitigating measures are then applied. Measures include increasing reactive compensation to the affected areas by using shunt capacitor, static var compensator, reactive power from the DG, etc.

Several VSIs have been proposed in the literature and are classified into line, bus, and overall indices [117]. Bus VSI provides voltage stability information about buses on the network, whiles line VSI provides stability information regarding transmission lines. Examples of line index include node voltage collapse index [118], voltage stability margin index [119], etc. Overall VSI has no relation to the bus or line but can predict how close the system is to the voltage instability point [117]. The selection of a particular VSI is dependent on the accuracy of predicting voltage stability and simplicity in computation [117]. The authors of [117] concluded that while the line VSI is simple in computation, its accuracy is low compared to the bus and overall VSIs. On the other hand, the overall VSI provides high accuracy in predicting voltage stability but with a complex computation. Bus VSI provides a balance between the line VSI and overall VSI in terms of accuracy and simplicity as illustrated in figure 4.1. The bus VSI is therefore selected for assessing voltage stability in this thesis.

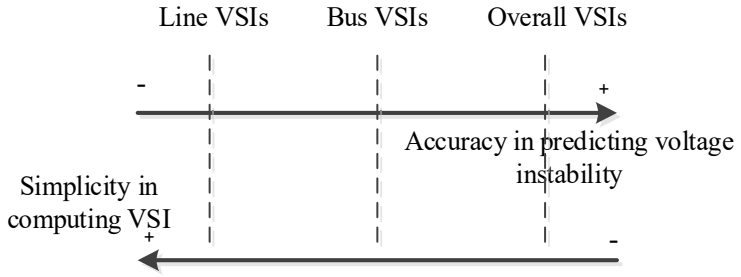

Figure 4.1 Comparison between types of VSI [117]

Different bus VSIs have been proposed in the literature, including the voltage collapse prediction index developed by authors in [120]. This index is derived from the power flow equation using the line impedances of the network. The computation of VSIs that depends on impedances is however associated with errors when used in an offline mode. This is because impedance values are

affected by atmospheric conditions which are difficult to predict during offline analysis. Thus, it is desirable to be used in an online mode where the impedance values are estimated using real-time measurement data, applicable only to networks with communication facilities. Another impedance-based bus VSI is the simplified voltage stability index developed by Perez-Londono et al [121]. Authors of [122] developed a local VSI using Tellegen's Theorem and adjoint networks. This index has the advantage of solely being dependent on locally measured variables at the PCC, thus it can be implemented in distribution networks where communication facilities are lacking. In addition to this, it is independent of power system impedance and can be easily computed without atmospheric effects, making it appropriate for use in this thesis work.

4.2 Voltage Stability Index based on Tellegen's Theorem

This index was developed by Bernard Tellegen and is based on the Tellegen theorem and adjoint network methods. The computation of the index is based on local measurements available at the PCC. Tellegen theorem is a powerful theorem in circuit theory based on Kirchhoff's laws [123]. As long as an electrical network satisfies Kirchhoff's voltage and current laws, the Tellegen theorem can be applied irrespective of the type of circuit be it linear or non-linear, reciprocal or non-reciprocal, time-invariant or time-variant, making it independent of the network elements. This independence makes the theorem a useful tool to describe the behaviour of complex networks like the power system. Tellegen's theorem states that the summation of power at any time for any branch in an electrical network is zero. For any given network, the theorem relates the complex voltages and currents to satisfy Kirchhoff's laws as in (4.1).

$$\sum \underline{U}\,\underline{I} = 0 \tag{4.1}$$

Where $\underline{U}$ is the complex voltage and $\underline{I}$ is the complex current. The basis for (4.1) is explained in Appendix F. This equation is also valid even if the complex voltage and current are for two different networks that have the same topology, i.e. the same incident matrix [122]. The incident matrix is a graphical representation that shows the relationship between the nodes and branches of an electrical network in a matrix form. Thus, the theorem can be extended to analyse and relate complex currents and voltages of two different networks; any given electrical network (base case network) and an adjoint network. An adjoint network is an artificial network that has a similar topology as the base case network but is different in terms of components [124]. The adjoint network

remains the same after disturbances in the base case network since it is decoupled from it [122]. The concept of an adjoint network is very useful in accurately analysing the performance of complex base networks like the power system. For instance in [125], to overcome the complexities of computing the static security of a power system network using the fast decoupled load flow method which involves laborious iterative procedures, the authors developed an adjoint mathematical network model of the power system network with the same topology to evaluate power system contingency analysis. The adjoint network and Tellegen's theorem can therefore be used to simplify the computation of VSI.

For a base network with a complex voltage and a current represented as $\underline{U}_{BC}$ and $\underline{I}_{BC}$ respectively and an adjoint network having a complex voltage $\underline{\hat{U}}$ and current $\underline{\hat{I}}$, then Tellegen's theorem is expressed as (4.2). The hat symbol (∧) is the notation of the adjoint network variables.

$$\underline{U}_{BC}\underline{\hat{I}} = 0 \text{ and } \underline{\hat{U}}\,\underline{I}_{BC} = 0 \tag{4.2}$$

If there is a parameter change in the base network that will automatically result in changes in the complex voltage and current, then the new voltage and current are $\underline{U}_{BC} + \Delta\underline{U}_{BC}$ and $\underline{I}_{BC} + \Delta\underline{I}_{BC}$ respectively. Where $\Delta\underline{U}_{BC}$ and $\Delta\underline{I}_{BC}$ are the changes in complex voltage and current of the base case network respectively.

Substituting these new voltages and current into (4.2) and simplifying results in (4.3).

$$\underline{\hat{I}}\Delta\underline{U}_{BC} - \underline{\hat{U}}\Delta\underline{I}_{BC} = 0 \tag{4.3}$$

Equation (4.3) is called the difference form of Tellegen's theorem [126].

4.2.1 Adjoint Network of a Power System Network

The following procedure, developed by the authors of [122], is used in developing the adjoint network which is a power system network. The power network is made up of buses (slack and other buses) and branches. Equation (4.3) is thus modified to reflect these components resulting in (4.4).

$$\left(\underline{\hat{I}}_S\Delta\underline{U}_S - \underline{\hat{U}}_S\Delta\underline{I}_S\right) + \left(\underline{\hat{I}}_P\Delta\underline{U}_P - \underline{\hat{U}}_P\Delta\underline{I}_P\right) + \left(\underline{\hat{I}}_B\Delta\underline{U}_B - \underline{\hat{U}}_B\Delta\underline{I}_B\right) = 0 \tag{4.4}$$

Where the subscripts S, P, and B represent slack bus, the other remaining buses, and network branches respectively.

The branches and buses of the base case network are always subjected to disturbances and must be taken into consideration. They are network

disturbances on the branches and power disturbances on the buses represented as changes in the network admittance (ΔY) of the networks admittance (Y) and power disturbances modelled as changes in the power (ΔS_M) of a bus from the base value power S_M.

The slack bus is assumed to be invariable in terms of voltage and frequency, and thus it's not affected by any disturbances. This leads to (4.5).

$$\hat{\underline{I}}_S \Delta \underline{U}_S - \hat{\underline{U}}_S \Delta \underline{I}_S = 0 \tag{4.5}$$

ΔY impacts only the branch part of (4.4) and ΔS_M affects the remaining buses (except the slack bus) part of the same equation. The topology of the adjoint network is the same as the base case and as such, remains the same after being subjected to network disturbances. Consequently it can be deduced that,

$$\hat{\underline{I}}_B \Delta \underline{U}_B - \hat{\underline{U}}_B \Delta \underline{I}_B = 0 \tag{4.6}$$

Substituting (4.5) and (4.6) into (4.4) results in (4.6)

$$\hat{\underline{I}}_P \Delta \underline{U}_P - \hat{\underline{U}}_P \Delta \underline{I}_P = 0 \tag{4.7}$$

In [127], it was demonstrated that complex conjugation can be shown as a linear Kirchhoff operator, and thus (4.7) could be written as (4.8) or (4.9).

$$\hat{\underline{I}}_P^* \Delta \underline{U}_P - \hat{\underline{U}}_P \Delta \underline{I}_P^* = 0 \tag{4.8}$$

or

$$\hat{\underline{I}}_P \Delta \underline{U}_P^* - \hat{\underline{U}}_P^* \Delta \underline{I}_P = 0 \tag{4.9}$$

4.2.2 Thevenin's Equivalent of an Adjoint network

For the simple power system network with bus X shown in figure 4.2, where $\underline{U}_X$ $\underline{S}_X$, $\underline{I}_X$ and $\underline{Z}_X$ are the complex voltage, apparent load power, load impedance and load current at bus X respectively.

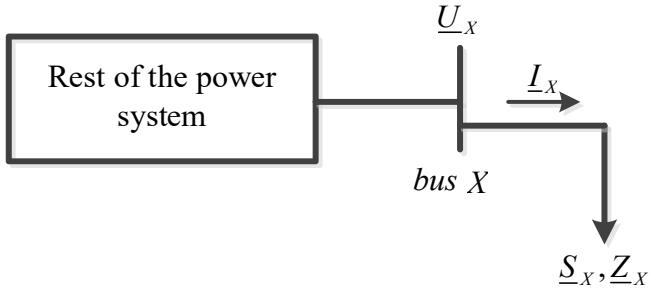

Figure 4.2 Representation of bus X in a power system

The complex load impedance is defined as;

$$\underline{Z}_X = \underline{U}_X / \underline{I}_X \tag{4.10}$$

This network can be represented by equivalent Thevenin impedance seen from the bus X as shown in figure 4.3.

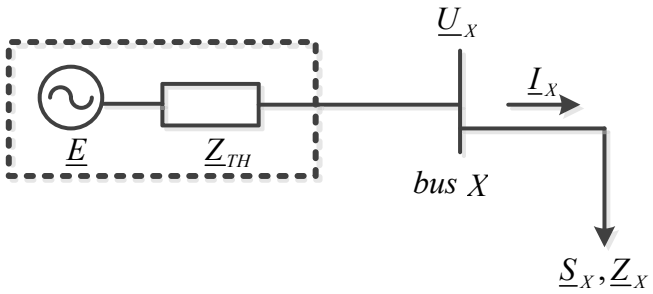

Figure 4.3 Thevenin representation of the power system seen at bus X

Where $\underline{E}$ and $\underline{Z}_{th}$ are the Thevenin voltage and impedance of the network as seen from bus X respectively. The receiving end current is defined as;

$$\underline{I}_X^* = \underline{S}_X / \underline{U}_X = ((\underline{E} - \underline{U}_X)/\underline{Z}_{TH})^* \quad 4.11$$

Equation (4.11) is further simplified as

$$\underline{U}_X(\underline{E} - \underline{U}_X)^* - \underline{S}_X \underline{Z}_{TH}^* = 0 \quad 4.12$$

$$\underline{U}_X^2 - \underline{U}_X \underline{E} + \underline{S}_X \underline{Z}_{TH}^* \quad 4.13$$

In the algebraic expression shown in (4.13), for any given value of $\underline{S}_x$ there will be at least two values of $\underline{U}_x$. For maximum power transfer to occur, (4.14) must hold.

$$\underline{U}_X = (\underline{E} - \underline{U}_X)^* \quad 4.14$$

This is similar to the maximum power transfer theory in circuit theory which occurs when the load impedance becomes equal to the Thevenin impedance as expressed in (4.15).

$$|\underline{Z}_{TH}| = |\underline{Z}_X| \quad 4.15$$

This mathematical analysis carried out in figure 4.3 is extended to an adjoint Thevenin equivalent shown in figure 4.4.

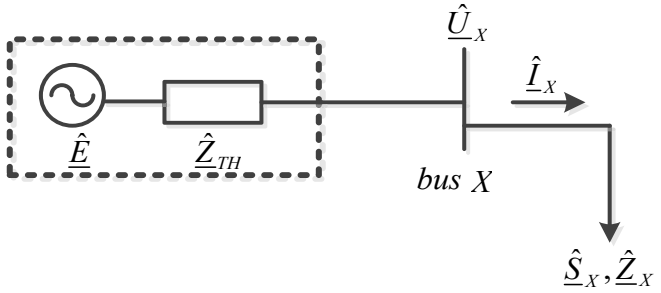

Figure 4.4 Adjoint Thevenin representation of power system seen at bus X

The difference form of Tellegen's theorem expressed in (4.8) or (4.9) is written for figure 4.4 as expressed in (4.16).

$$\hat{\underline{I}}_X^* \Delta \underline{U}_X - \hat{\underline{U}}_X \Delta \underline{I}_X^* = 0 \quad 4.16$$

Where $\Delta \underline{U}_X$ and $\Delta \underline{I}_X^*$ are the respective complex changes in voltage and current after the base case network has been subjected to disturbances at bus X, $\hat{\underline{I}}_X$ and $\hat{\underline{U}}_X$ are the complex current and voltage at the bus X of the adjoint network respectively. The load impedance for the adjoint network is expressed as;

$$\hat{Z}_X = |\hat{\underline{Z}}_X| = |\hat{\underline{U}}_X / \hat{\underline{I}}_X| \quad 4.17$$

Inserting (4.11) into (4.16) results in

$$((\hat{\underline{E}} - \hat{\underline{U}}_X)/\hat{\underline{Z}}_{TH})^* \Delta \underline{U}_X - \hat{\underline{U}}_X \Delta \underline{I}_X^* = 0 \quad 4.18$$

Equation (4.18) is rearranged as shown in (4.19).

$$\hat{\underline{Z}}_{TH}^* = \left(\hat{\underline{E}} - \hat{\underline{U}}_X\right)^* / \left(\hat{\underline{U}}_X \Delta \underline{I}_X^*\right) \Delta \underline{U}_X \quad 4.19$$

Taking into consideration the maximum power that occurs in a Thevenin circuit, an equation similar to (4.14) can be expressed for the adjoint network;

$$\hat{\underline{U}}_X = (\hat{\underline{E}} - \hat{\underline{U}}_X)^* \quad 4.20$$

Substituting the value of $\hat{\underline{U}}_X$ in (4.20) into (4.19) results in (4.21).

$$\hat{\underline{Z}}_{TH}^* = \Delta \underline{U}_X \,/\, \Delta \underline{I}_X^* \quad 4.21$$

Removing the conjugates in (4.21) and replacing them with absolutes values result in (4.22).

$$\hat{Z}_{TH} = |\Delta \underline{U}_X / \Delta \underline{I}_X| \quad 4.22$$

Thus, the Thevenin impedance seen at bus X is calculated from two consecutive samples of changes in voltage and current at that bus. For real-time applications, the measurements are taken from the phasor management unit. It is inferred that this can only be determined only if the operating conditions change at the bus of interest. As such, in instances where there are no changes in the voltage and current, the Thevenin impedance is zero[122].

This can be translated into a VSI expressed as;

$$VSI = (\hat{Z}_X - \hat{Z}_{TH})/\hat{Z}_X \quad 4.23$$

Where

$$\hat{Z}_{TH} = |\Delta \underline{U}_X / \Delta \underline{I}_X| \quad 4.24$$

and

$$\hat{Z}_X = |\underline{U}_X / \underline{I}_X| \quad 4.25$$

In terms of complex notations (4.23) is written as expressed in 4.26.

$$VSI = \frac{|\underline{Z}_X| - |\underline{Z}_{TH}|}{|\underline{Z}_X|} \quad 4.26$$

The load impedance ($\hat{Z}_x$) calculated before the network is subjected to a disturbance, i.e. it is determined using the initial operating conditions. Per circuit theory, maximum power occurs when;

$$|\underline{Z}_{TH}| = |\underline{Z}_X| \quad 4.27$$

Thus, the VSI approaches 1 at normal loading conditions when $\underline{Z}_X \gg \underline{Z}_{TH}$ and approaches 0 at the maximum power point, beyond which voltage instability occurs. Thus, the VSI ranges from 0 to 1.

4.2.3 Voltage Stability Index validation

To validate the concept of using the change in voltage and current to accurately estimate the Thevenin impedance, a two bus network with distribution line parameters of $0.04 + j0.03\ p.u.$ and a load value of $100 + j33\ MVA$ connected at bus 2. The voltage at bus 1 (slack bus) is fixed at $1.0 + j0\ p.u.$ The load is increased in steps of 0.02 p.u. up to a maximum value of 5 p.u with 100 MVA being the base apparent power. At each load step, a power flow simulation is carried out. Then the corresponding increase in voltage and current is used to estimate the Thevenin impedance and the load impedance. Figure 4.5 shows a plot of Thevenin impedance and load impedance at different loading conditions.

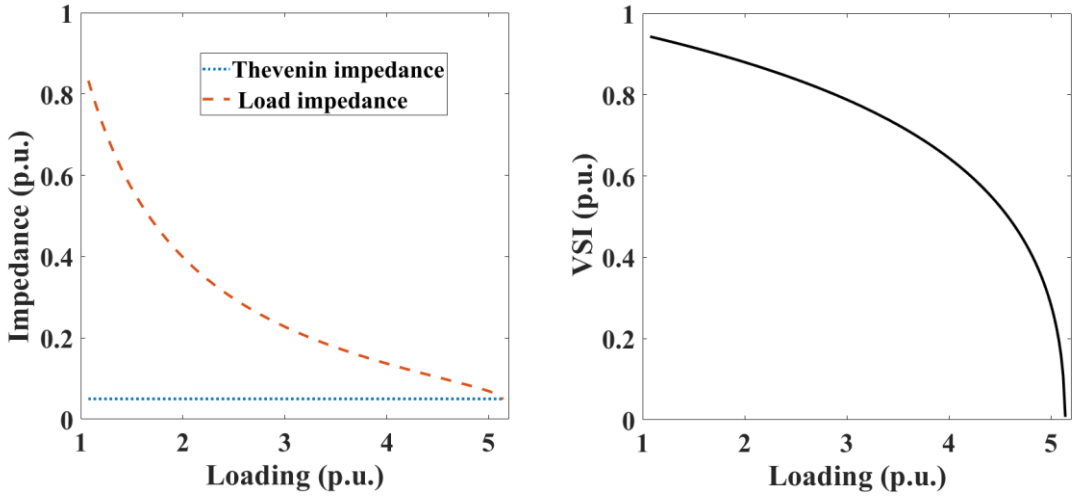

Figure 4.5(a) Load and Thevenin impedances (b) VSI indices for different loading conditions of the two bus network

It can be seen in figure 4.5(a) that the Thevenin impedance was 0.05 p.u. at every load change. These values are equal to the distribution line impedance between bus 1 and bus 2. Thus, this validates the concept of estimating the Thevenin impedance base on Tellgen's adjoint matrix method because the Thevenin impedance of the network seen at bus 2 is analytically equal to the

impedance of the distribution line. Furthermore, figure 4.5(a) reveals that as the load at bus 2 increases, the load impedance reduces and gets closer to the value of the Thevenin impedance. This reduction, therefore, worsens the VSI index as it approaches 0 (close to the voltage instability point) as shown in figure 4.5(b).

4.3 Voltage Sensitivity Fitting Function

Sensitivity analysis is an essential tool in power system network planning and is used to ascertain how power flows across the network and how bus voltages change with the injection of active and reactive power through the use of sensitivity factors such as loss and voltage sensitivity factors. The loss sensitivity factor establishes how the injection of active and reactive power at a bus impacts power losses in the grid. The voltage sensitivity factor on the other hand determines how sensitive bus voltages are to the injection of active and reactive power.

Different approaches have been used in carrying out voltage sensitivity analysis, including the Jacobian matrix method calculated from the power flow balanced equations [47], [128] to the perturb and observe method [129]. In the Jacobian method, the matrix is obtained from the Newton Raphson power flow method. To determine the voltage sensitivity factors, the Jacobian matrix is inverted and evaluated at given initial operating points as shown in (4.28).

$$J^{-1} = \begin{bmatrix} \frac{\partial \theta}{\partial P} & \frac{\partial \theta}{\partial Q} \\ \frac{\partial U}{\partial P} & \frac{\partial U}{\partial Q} \end{bmatrix} \tag{4.28}$$

Where P and Q are respectively the active and reactive power injections at a bus. U and θ are the magnitudes of the complex voltage magnitude and angle respectively. Once the voltage sensitivity factors ($\partial U/\partial P$ and $\partial U/\partial Q$) of a bus are calculated, and it is used to determine the change in voltage that will occur at the bus of interest to the injections of active and reactive power as expressed in (4.29).

$$\Delta U = \frac{\partial U}{\partial P} * \Delta P + \frac{\partial U}{\partial Q} * \Delta Q \tag{4.29}$$

The challenge with this approach is that each time there are changes in load and generation in the grid, the Jacobian matrix must be recalculated using the Newton-Raphson method to obtain new sensitivity factors. This puts a limitation

on its usage in real-time applications for power system networks which lack communication facilities as the recalculation requires real-time information about the grid.

Another method is the Perturb-And-Observe approach proposed in [129], which eliminates the computational burden of using the Jacobian matrix by using two successive power flow results to calculate the voltage sensitivities to active or reactive power. The amount of reactive power injection at the bus of interest and the bus voltage for the first load flow is represented with U and Q respectively. To determine the voltage sensitivity with respective reactive power ($\partial U/\partial Q$), a second load flow is computed with the same load, active and reactive power generation conditions but an increased (by 1 MVAr) amount of reactive power generation. The magnitude of the new voltage (U') obtained from the second load flow is used to determine the voltage sensitivity as expressed in (4.30).

$$\frac{\partial U}{\partial Q} = \frac{(U' - U)}{1\ MVAr/S_{base}} \qquad 4.30$$

The implementation of this approach for real-time applications also requires the distribution network to be equipped with communication facilities.

To overcome the challenge of communication requirements in implementing sensitivity analysis, a new method based on surface fitting techniques is proposed in [130]. This method utilises load flows based on random values of demand and generation profiles to develop a fitting function which is subsequently used to determine the voltage sensitivities to active ($\partial U/\partial P$) and reactive power ($\partial U/\partial Q$).

To illustrate this approach, a two-bus distribution network is considered as shown in figure 4.6. The network has a PV connected to bus 2, which is the PCC bus with a voltage value of U_{PCC}. Bus 1 is the substation bus and has a voltage value of U_S.

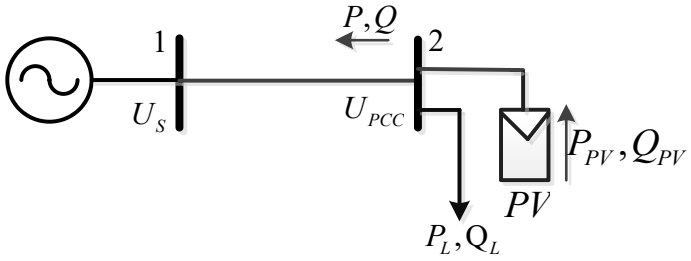

Figure 4.6 Two-bus system

To calculate the voltage sensitivity of bus 2, first, random values of PV generation and load profiles on the grid are used to simulate several load flows.

The results from the power flow are used to develop a fitting function as shown in (4.31).

$$U_{PCC} = f(P, Q) \tag{4.31}$$

Where P, Q are the values of the PV's active and reactive power injection at bus 2 in per unit. U_{PCC} is the voltage value at the PCC. Since the PV is modelled as a negative load, P is the algebraic sum of P_{PV} (PV active power) and P_L (active power) at bus 2, and Q is the algebraic sum of Q_{PV} (PV reactive power) and Q_L (reactive load) at bus 2.

To develop the fitting function, several power flow simulations are carried out involving different values of load and PV's active and reactive power output. The load and active power output of the PV are varied separately from 0 to 1 p.u. of their respective peak value in steps of 0.0067 p.u. These discrete steps will result in 150 values each for the load and active power output of PV. The reactive power output of the PV is varied by adjusting the power factor of the PV from 0.95 to 1 in steps 0.01. Overall, these 150 x 150 x 6 combinations will result in 135,000 power flow simulations.

The surface fitting technique in [131] is employed to develop the fitting function, which is a nonlinear polynomial function expressed in the form of (4.32). A polynomial of the highest degree of two is adopted in this thesis.

$$U_{PCC}(P, Q) = \sum_{x=0}^{2} \sum_{y=0}^{1} A_{xy}\, Q^x\, P^y \tag{4.32}$$

Where A_x is the constant coefficient to be determined by the surface fitting technique through a numerical optimization algorithm. Subsequently, the voltage sensitivities of the bus of interest (bus 2) to active and reactive power are determined using (4.33) and (4.34).

$$\frac{\partial U_{PCC}}{\partial P} = \frac{\partial f(P, Q)}{\partial P} \tag{4.33}$$

$$\frac{\partial U_{PCC}}{\partial Q} = \frac{\partial f(P, Q)}{\partial Q} \tag{4.34}$$

It can be inferred from (4.33) and (4.34) that the sensitivities of any bus are dependent on the power injections at that particular bus and can be subsequently updated with the changing grid conditions such as load and generation profiles. There is thus no need for the remote monitoring of the entire grid since the values of P and Q are determined locally at the PCC.

4.4 Proposed Autonomous Q(U) Control Scheme

The proposed scheme provides an innovative solution to improving voltage regulation challenges in weak MV grids by incorporating an adaptive (AD) functionality into the standard Q(U) control. This AD functionality dynamically changes the compensation being provided by the Q(U) control with the changing or varying grid conditions when the performance of the standard $Q(U)$ control is not satisfactory. The advantage of this scheme is that it depends on locally measured variables at the PCC, making it implementable in grids with limited or no communication facilities, especially in Ghana.

The flowchart of this adaptive autonomous scheme is shown in figure 4.7. It is made up of the $Q(U)$ control explained in section 3.2.2, with an additional AD functionality.

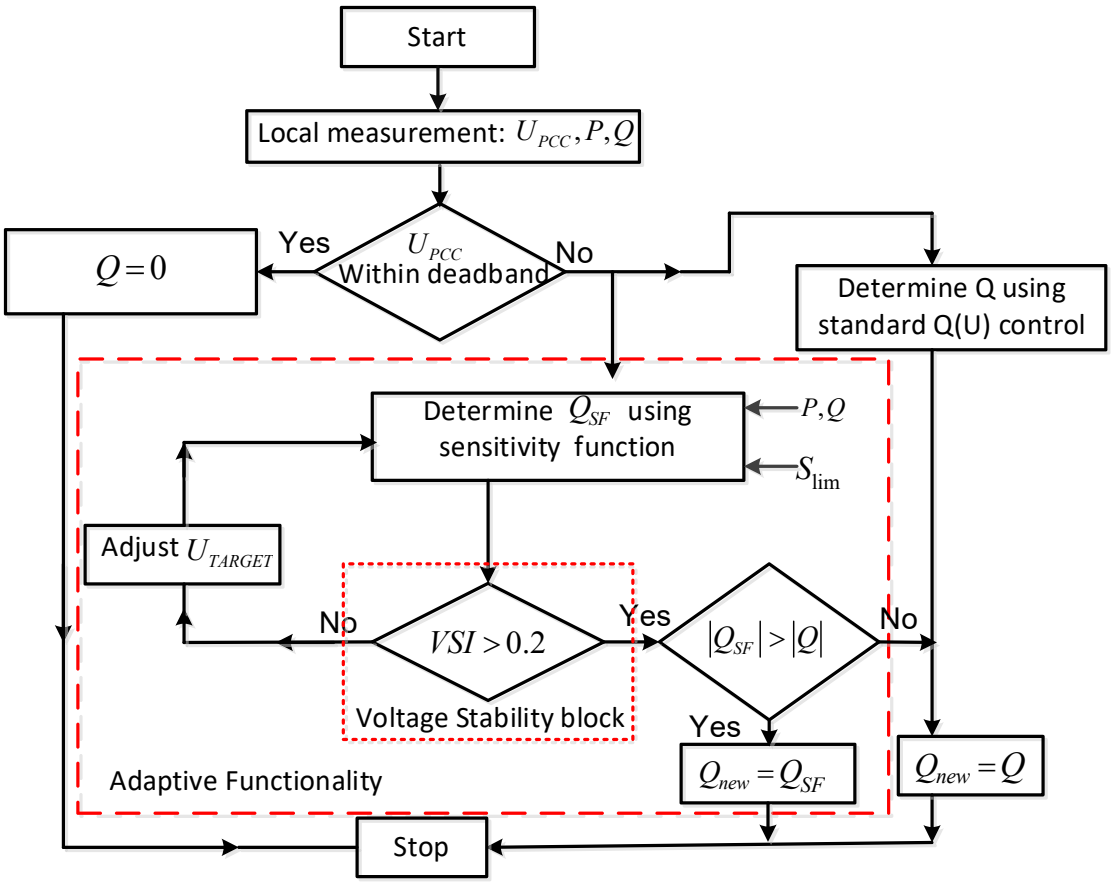

Figure 4.7 Flowchart for the Q(U) with adaptive functionality

This functionality consists of two main blocks, namely, the sensitivity and voltage stability blocks. The sensitivity block which encompasses the voltage sensitivity function determines the reactive power compensation needed at the

PCC to keep the voltage at this bus within the required regulatory limits. The stability block enhances the VSI of the PCC bus through the use of reactive power from the PV inverter.

The scheme starts by locally measuring the PCC bus voltage (U_{PCC}), active (P) and reactive (Q) power injection from the PV inverter. If the value of the U_{PCC} is within the dead band (0.97 p.u. – 1.03 p.u.) of the standard $Q(U)$ control, no reactive compensation is provided. Thus, the AD functionality only works when U_{PCC} is outside the dead band range. For U_{PCC} outside the dead band range, the sensitivity block first calculates $\partial U_{PCC}/\partial Q$ using P and Q as expressed in (4.33) and then determines the required reactive power (Q_{SF}) needed to change the voltage of the PCC bus to the desired voltage using (4.34).

$$Q_{SF} = \frac{U_{TARGET} - U_{PCC}}{\partial U_{PCC}/\partial Q} \tag{4.34}$$

Where U_{TARGET} is the desired voltage at the PCC bus which is set by the distribution network operator. In this work, the value of the U_{TARGET} is set close to the dead band limit, i.e. 0.965 p.u. and 1.035 p.u. for the capacitive and inductive regions respectively. However, any appropriate value within the range of the grid code voltage limits can be chosen for the U_{TARGET}. In this scheme, there is no limitation on the PV's active power as it is given priority. The apparent power rating of the inverter is size as 1.1 times the peak active power of the PV generator based on [39], thus, the PV inverter can still provide reactive power compensation during the period of peak active power generation. To guarantee that the reactive compensation provided by the sensitivity block is not more than the capacity of the inverter, S_{lim}, the apparent power rating of the PV inverter in MVA, is added to the block. If Q_{SF} value is more than the capacity of the inverter, its value it fixed to the maximum allowable reactive power compensation from the PV which is dependent on the inverter capacity and the operating active power output of the PV.

After the sensitivity block is the voltage stability block that enhances the voltage stability of the PCC bus by calculating the VSI as expressed in (4.26). The change in consecutive values of current (ΔI_R) and voltage (ΔU_R) are determined using (4.35) and (4.36).

$$\Delta U_R = |U_{TARGET} - U_{PCC}| \tag{4.35}$$

$$\Delta I_R = \left|\left(S_{AFTER\ Q}/U_{TARGET}\right) - \left(S_{BEFORE\ Q}/U_{PCC}\right)\right| \tag{4.36}$$

Where $S_{AFTER\ Q}$ and $S_{BEFORE\ Q}$ represent the apparent power of the load in MVA after and before the injection of reactive power from the PV. It can be inferred that this VSI is very sensitive to ΔI_R as such in calculating this index;

the minimum threshold of this index is set to 0.015 p.u. The Thevenin impedance (Z_{TH}) is recorded as zero if the ΔI_R is below the set threshold. Also in this work, 0.2 p.u. is selected as the minimum VSI value. This is a very conservative value that can be changed to a higher value to enhance voltage stability as desired by the network operator. The U_{TARGET} is to be adjusted in steps of 0.002 p.u. if the VSI value calculated using (4.25) is less than 0.2. This adjustment is done by increasing the V_{TARGET} value when the $Q(U)$ control is operating in the inductive region or decreasing the value if it is in the capacitive region.

After the stability block, Q_{SF}, the amount of reactive power compensation is provided to the grid. This only happens if the absolute value of Q_{SF} is bigger than the absolute value of compensation provided by the standard $Q(U)$ control termed as Q. The reason is that the AD functionally only acts to compliment the efforts on the $Q(U)$ control when the performance of the latter is not satisfactory and hence can be removed for the $Q(U)$ control to act alone.

4.5 Test Cases, Results and Discussions

Three case studies are created to validate the performance of the proposed scheme. These case studies are implemented on the 16 bus MV grid described in section 3.5.1, using the load and PV output profiles shown in figure 4.8.

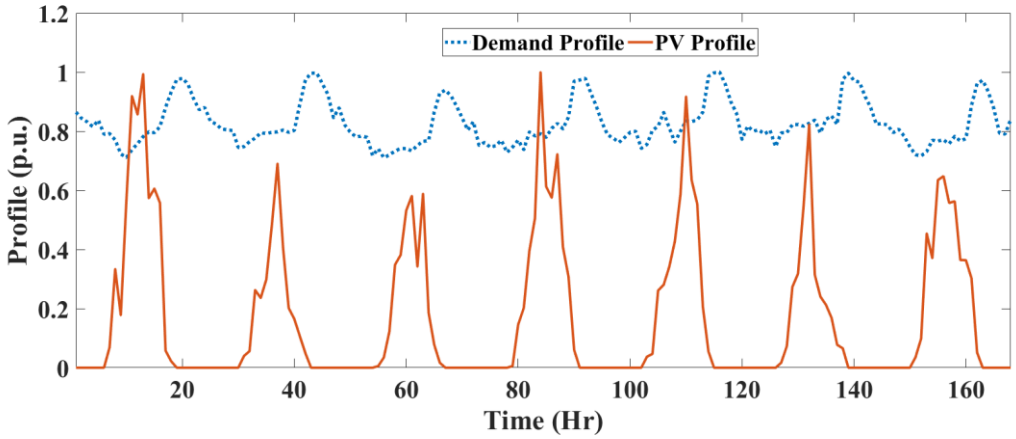

Figure 4.8 Typical Ghanaian demand and PV active power profile

These profiles are hourly values for one week from August 2016 and are normalised against their respective peak values. The load values were obtained from the Ghana Grid company, while the solar irradiance and temperature values that were obtained from [83] are used to generate the PV active power

output profiles using (3.16) and (3.17). In determining the load profile for a particular hour, load values in the test MV grid are multiplied by the corresponding hour value of load (per unit value) in figure 4.8. Similarly, the peak watt value of the PV is multiplied by the hourly value of the PV profile shown in figure 4.8 to determine the PV profile for that particular hour. Furthermore, figure 4.8 reveals that the peak generation of the PV coincides with the low demand period on a typical day, creating the potential voltage rise phenomenon during peak solar hours. The taps position of the OLTC and VR are set to 0.97 p.u. and 0.92 p.u. respectively to create low voltages (below the minimum grid code voltage limit) along the feeder, especially during peak demand periods. The entire simulation is implemented in Matlab with Matpower being used for the power flow simulations.

4.5.1 Case 1: Performance assessment of the autonomous Q(U) control scheme

This case study seeks to validate the proposed autonomous control scheme in section 4.3 in improving voltage regulation challenges in MV grids in Ghana, especially during peak demand periods, and also overcoming voltage rise during peak solar hours. This assessment involves a single PV connected at bus 11, the tail end of the MV feeder, making it more prone to voltage regulation challenges. The PV is rated 8 MW with an inverter capacity of 8.8 MVA. Three scenarios used in the assessment are as follows.

- Scenario 1: There is no PV integrated into the grid.
- Scenario 2: The PV operates with fixed $Q(U)$ control parameters, denoted as $Q(U)_{\mathrm{FIX}}$. The parameters used are 0.93 p.u., 0.97 p.u., 1.03 p.u. and 1.07 p.u. for U_1, U_2, U_3 and U_4 respectively [110] for the $Q(U)$ schematic shown in figure 3.3. The power factor is set to 0.95 based on the Ghanaian grid code regulation [24]. These settings were recommended by Mueller et al for German distribution networks.
- Scenario 3: The PV operates with the proposed $Q(U)$ control with AD functionality, denoted as $Q(U)_{\mathrm{ADAP}}$.

To develop the sensitivity fitting function for scenario 3, the steps described in section 4.2.1 are followed. This resulted in the three-dimensional surface illustrated in figure 4.9, which shows the active power injection into bus 11 within the ranges from 0 to 8 MW and the reactive power injection within the range of 0 to 3.67 MVAr. The black lines indicate the various power flow

scenarios, with each line representing a particular power factor. There are six black lines because of the six power factor settings (0.95 to 1 in steps of 0.01) used in developing the fitting function. All the black lines start from zero and divulge as the active power of the PV increases because active power is proportional to reactive power when the power factor is fixed and there is no limit to the amount of reactive that can be provided. The only exception was at unity power (the first black line) where the active power was zero for all values. Furthermore, it can be seen that different combinations of active and reactive injections at the bus resulted in the same voltages since the voltages are not only dependent on the injections at the bus but also on the power flows from other buses.

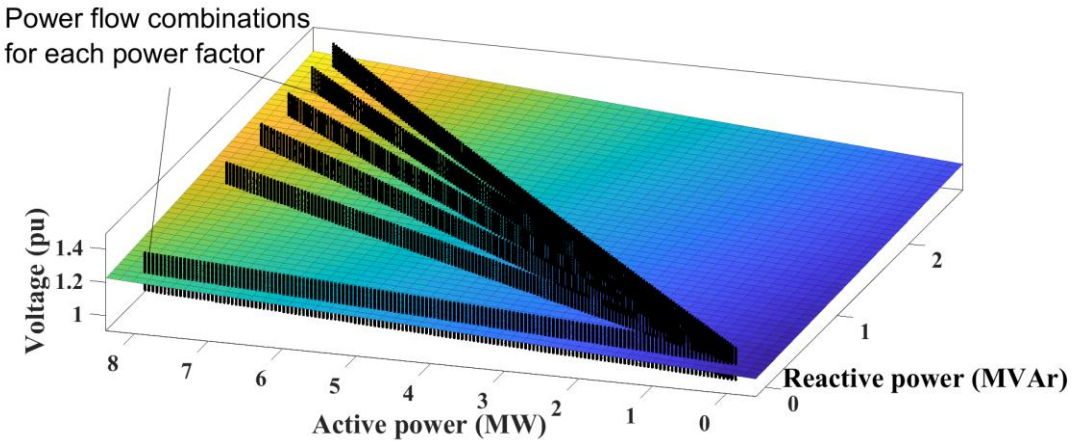

Figure 4.9 Surface fitting for the voltage, active and reactive power for DG at bus 11

From figure 4.9, a non-linear fitting function relating the voltage magnitudes of bus 11 to the corresponding injection of active and reactive power values from the PV inverter at the same bus is expressed in (4.37) using the surface fitting technique in Matlab [132].

$$U_{PCC} = A_{00} + A_{10}Q + A_{01}P + A_{20}Q^2 + A_{11}PQ \qquad 4.37$$

The values of the coefficients (A_{xy}) determined through non-linear regression analysis in Matlab [132] is shown in table 4.1.

Table 4.1 Values of coefficient for the fitting function

Parameters for the fitting function					
Bus No	A_{00}	A_{10}	A_{01}	A_{20}	A_{11}
11	1.028	0.01647	0.02422	0.000522	0.002765

Results of reactive power compensation provided by the PV and voltage profiles for all three scenarios are shown in figures 4.10(a) and (b) respectively. Only the first day (24 hours) results are shown for easy comparison. For scenario 1, the voltage profile was within the grid code range from 0.95 p.u. to 1.05 p.u. except during the peak demand period which starts from the 19th to the 21st hour as shown in figure 4.10(b) where the voltage was below the lower grid code limit. This result shows what exists in parts of Ghana on a typical day during the peak demand period. In scenario 2, the PV operating with fixed $Q(U)$ control parameters sufficiently kept the voltage of bus 11 within the grid code upper and lower voltage limits during the peak demand except for the 11th to the 13th hour (peak solar period), where the voltage was above 1.05 p.u., demonstrating that fixed or general parameterization of the $Q(U)$ control will not always elicit satisfactorily performance.

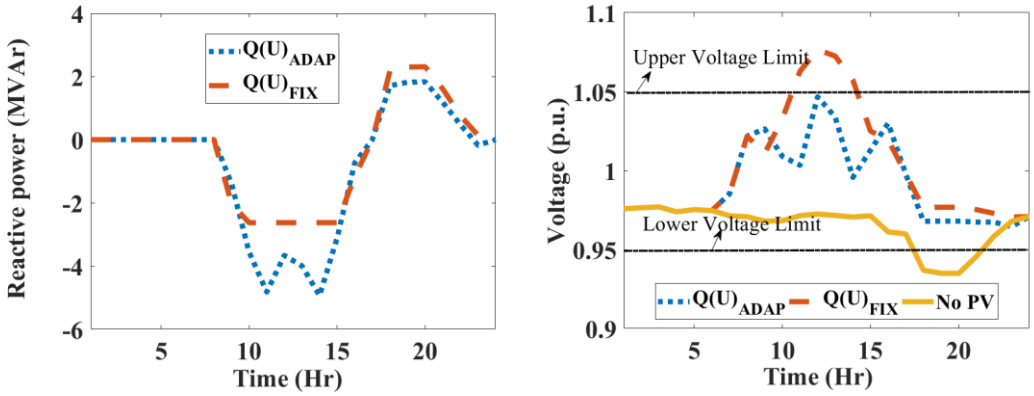

Figure 4.10 Results for the first 24-hour period (a) reactive power compensation by PV and (b) voltage profile for the period at bus 11

The proposed scheme in scenario 3 was able to keep the voltage within the upper and lower grid code voltage limits during the entire period as presented in figure 4.10(b). During the peak solar periods (11th to the 13th hour), the AD functionality was able to adjust the reactive power compensation provided by the $Q(U)$ to absorb more reactive power as presented in figure 4.10(a) to overcome the voltage rise phenomenon. This shows the efficacy of the proposed adaptive scheme in enhancing voltage regulation during both peak solar hours and demand periods.

4.5.2 Case 2: Comparison of the proposed adaptive control scheme with the central voltage control scheme

This case compares the performance of the adaptive control scheme which uses only local variables measured at the PCC with that of centralised voltage control

(CVC) that needs communication facilities. The essence of this comparison is to verify if the adaptive scheme can attain a good performance close to that of a CVC scheme which provides more optimal performance, as it uses communication facilities to obtain an overview of the network before making control decisions. This case involves five PVs connected at buses 7, 10, 11, 13, and 16. Buses 13 and 16 represent areas having low demand with a high potential of experiencing voltage rise if integrated with PVs. Buses 7, 10, and 11 are the ends of the feeders that experience low voltages during the peak demand period. The PVs are rated 5 MW peak value with an inverter capacity of 5.5 MVA. Three scenarios are created under this case study as follows.

- Scenario 1: The PVs operate with the proposed control, i.e. $Q(U)$ control with an AD functionality
- Scenario 2: The PVs operate with fixed $Q(U)$ control parameters same as in case 1.
- Scenario 3: A CVC scheme that uses communication facilities to determine or control the reactive power output of each PV unit using the GA optimization tool explained in section 3.4.1. The CVC based on GA is summarized by the flowchart shown in figure 4.10.

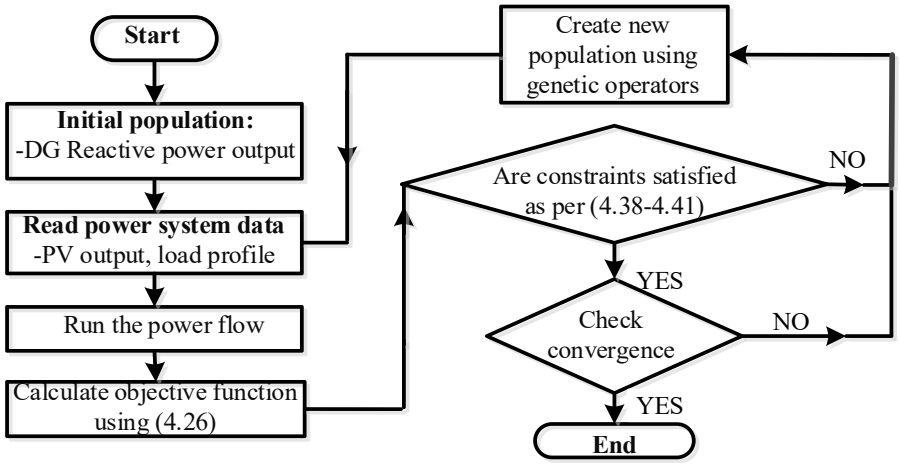

Figure 4.11 Flowchart for the centralised voltage control

From figure 4.11, the CVC starts by determining the initial population of the decision variable (reactive power output of each DG unit), which are continuous variables. The maximum and minimum values of each decision variable are dependent on the operating active power and the apparent power capacity of each inverter. For instance, for peak active power output of 5 MW, the maximum and minimum reactive power output is ± 2.3 MVA, since the apparent power of each DG inverter is 5.5 MVA. Then using the load (demand)

and DG (PV) profiles shown in figure 4.8, a Newton Raphson power flow simulation is out carried to compute the objective function, which is to maximize the overall VSI on the grid as expressed in (4.26). The VSI is subjected to both equality and inequality constraints as expressed in (4.38)-(4.41).

$$P_{GEN} - P_{DEM} - |U_i| \sum_{j=1}^{N} |U_j| \left(|G_{ij}| cos(\delta_i - \delta_j) + |B_{ij}| sin(\delta_i - \delta_j) \right) = 0 \quad 4.38$$

$$Q_{GEN} - Q_{DEM} - |U_i| \sum_{j=1}^{N} |U_j| \left(|G_{ij}| sin(\delta_i - \delta_j) - |B_{ij}| cos(\delta_i - \delta_j) \right) = 0 \quad 4.39$$

$$U_i^{MIN} \leq U_i \leq U_i^{MAX} \quad 4.40$$

$$S_{LINE} \leq S_{LINE}^{MAX} \quad 4.41$$

Where U_i is the voltage at bus i, P_{DEM} and Q_{DEM} are the active and reactive power load at bus i respectively, P_{GEN} and Q_{GEN} are the active and reactive power generated at bus i respectively, δ_i is the angle of the voltage at bus i. G_{ij} and B_{ij} are bus conductance and susceptance between buses i and j respectively. U_i^{MAX} and U_i^{MIN} are maximum and minimum voltages at bus i respectively, S_{line} is the apparent power flowing through each transmission line. The U_i^{max} and U_i^{min} values are set to 1.05 p.u. and 0.95 p.u. respectively based on Ghana's grid code [43].

If the constraint conditions are not met, the GA operators, namely, selection, crossover, and mutation are applied to create a new population of decision variables and the process is repeated. On the contrary, if the constraint conditions are met, then the convergence criterion which is either the tolerance value or the number of generations of the GA is checked to stop the optimization. This optimization is carried out every hour. However, the VSI requires two consecutive values of voltage and current measurements, thus, the optimization starts at the second hour ($t = 2$) using the $t = 1$ and $t = 2$ values of the PV and load from the profiles shown in figure 4.7. The parameters used for the GA are shown in table 4.2. The GA toolbox in Matlab is used for running the optimization.

Table 4.2 Parameters for Genetic Algorithm

GA parameter	**Value**
No. of Generation	100
Population	50
Crossover function (rate)	0.8
Stall generation limit	70
Tolerance	1 x10^{-6}

The coefficients of the fitting functions of scenario 1 for each of the PV units at the bus where they are integrated are shown in table 4.3.

Table 4.3Values of coefficient for the fitting function

Parameters for the fitting function					
Bus No	A_{00}	A_{10}	A_{01}	A_{20}	A_{11}
11	1.028	0.01647	0.02422	0.000522	0.002765
10	1.044	0.03628	0.02869	0.002207	0.004062
13	1.025	0.01237	0.003264	0.00053	-0.0002774
16	1.025	0.01606	0.008906	0.000553	8.62E-06
7	0.9859	0.0208	0.0133	0.00096	0.0006683

Figures 4.12 and 4.13 depict the voltage profiles and reactive power compensation provided by the PVs located at buses 11, 10, 13, 16, and 7 in the 16-bus MV network shown in figure 3.8 respectively for scenario 1 during the entire one-week period (168 hours). During the high solar generation period, which occurs from the 11th to 14th hour every day, the proposed scheme ($Q(U)$ control with AD functionality) sufficiently regulated the voltage within the grid code range of $\pm 5\%$ as shown in figure 4.12 by absorbing sufficient reactive power during this period as shown in figure 4.13. Similarly, during the 17th to 20th hour, representing the peak demand period, the proposed control worked effectively in regulating the bus voltages within the 0.95 p.u to 1.05 p.u. grid code range as presented in figure 4.12 by injecting sufficient reactive power shown in figure 4.13.

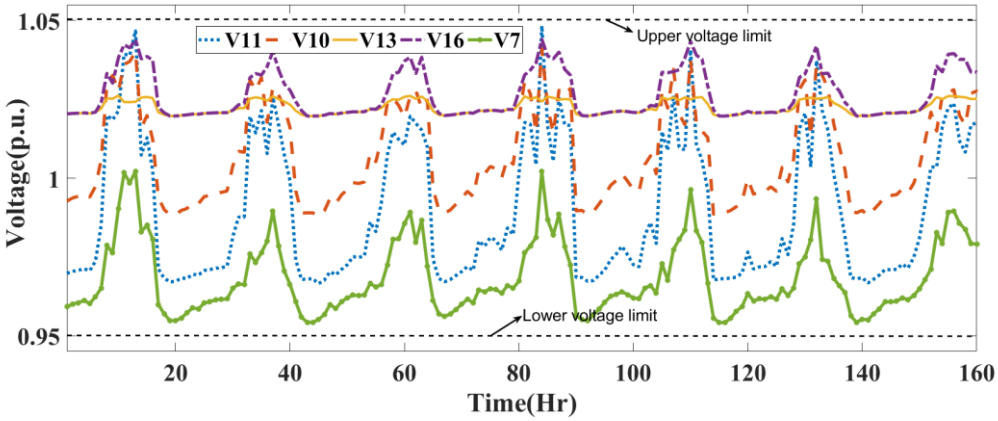

Figure 4.12 Voltage profile of buses 11, 10, 13, 16, and 7 for one week

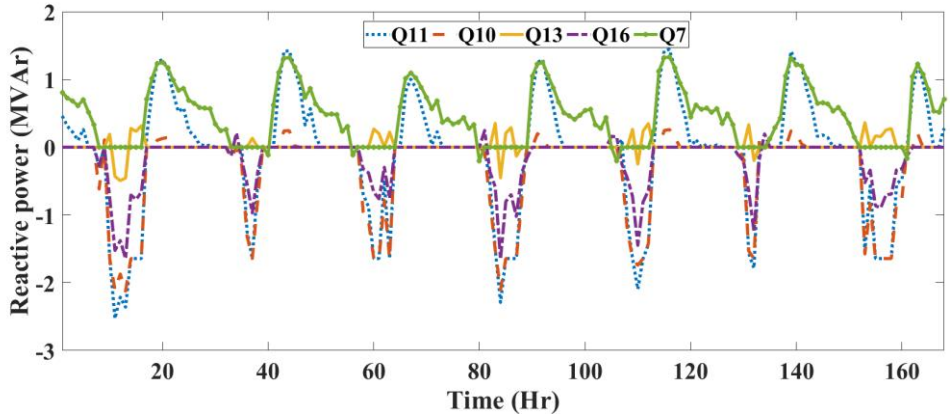

Figure 4.13 Reactive power compensation by inverters for one week at buses 11, 10, 13, 16 and 7

The performance of the $Q(U)$ control with AD functionality (scenario 1) is compared with the $Q(U)$ control with fixed parameters (scenario 2) and the CVC scheme (scenario 3) for the first day of the week as shown in figures 4.14 (a)-(d). Only results of the first day are shown here for easy analysis and also because similar results were obtained for the rest of the six days. Results from scenario 2, denoted as $Q(U)_{\text{FIX}}$, indicate the voltage profiles for buses 10 and 11 exceeded the upper grid code limit of 1.05 p.u. during the period from the 11^{th} hour to the 13^{th} hour. For instance, in figure 4.14(a), the voltages were 1.062 p.u., 1.053 p.u. and 1.064 p.u. on the 11^{th}, 12^{th}, and 13^{th} hour respectively for bus 10, and for bus 11 on figure 4.14(b), the voltages were 1.072 p.u., 1.059 p.u. and 1.076 p.u for the same period.

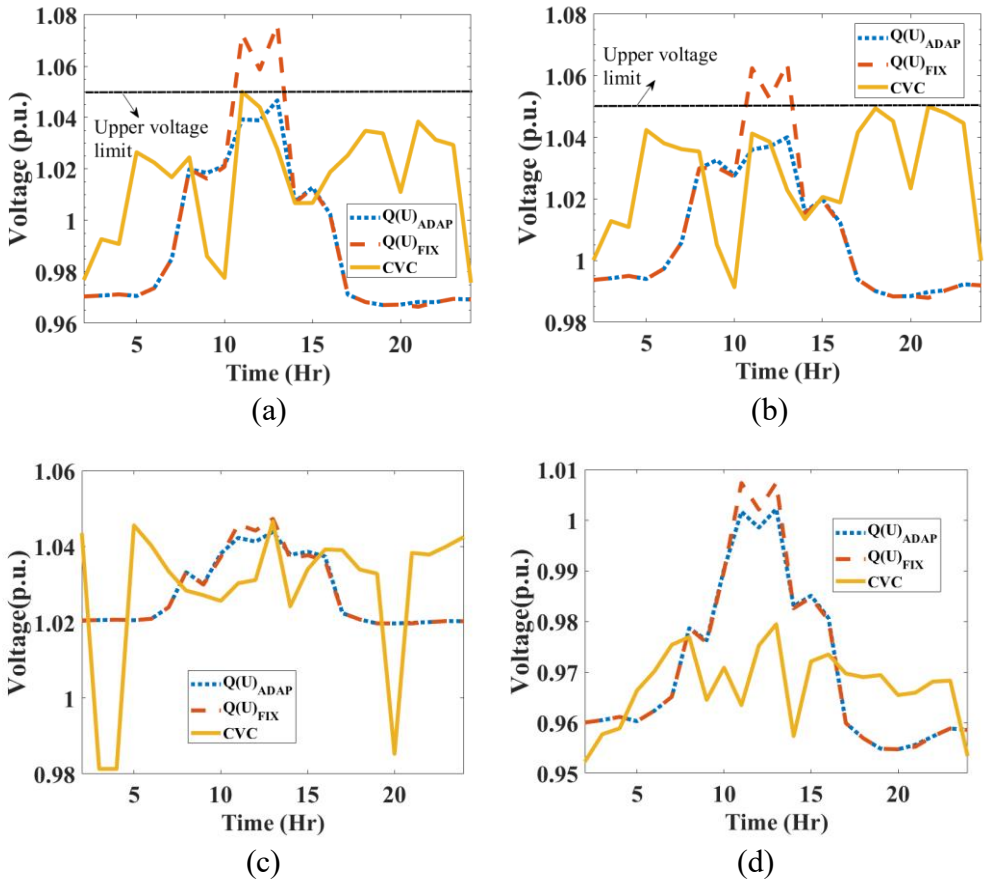

Figure 4.14 Voltage profile for the $Q(U)_{ADAP}$, $Q(U)_{FIX}$ and CVC control methods at (a) bus 11, (b) bus 10, (c) bus 16 and (d) bus 7

Though the $Q(U)_{\mathrm{FIX}}$ absorbed reactive power during this period as seen in figures 4.15 (a) and (b), it was not enough to overcome the voltage rise phenomenon, since the control was not sensitive to the changes in the grid. Thus, satisfactory performance is only guaranteed during peak solar hours for certain circumstances such as for buses 16 and 7 shown in figures 4.14 (c) and (d) respectively where the voltage profiles were within regulatory limits. On the other hand, both $Q(U)_{\mathrm{ADAP}}$ and CVC were able to control the voltage from 0.95 p.u. to 1.05 p.u. during both the peak solar and demand period as shown in figure 4.14 for all the buses with PV connection. This is very significant as the CVC uses communication facilities and the $Q(U)_{\mathrm{ADAP}}$ relies solely on measured variables at the PCC. Thus, making $Q(U)_{\mathrm{ADAP}}$ a cheaper alternative to implement since it is developed through an offline planning procedure as highlighted in section 4.3. This procedure is not challenging even with large networks as the emergence of powerful computers and power flow simulation software reduce the complexity.

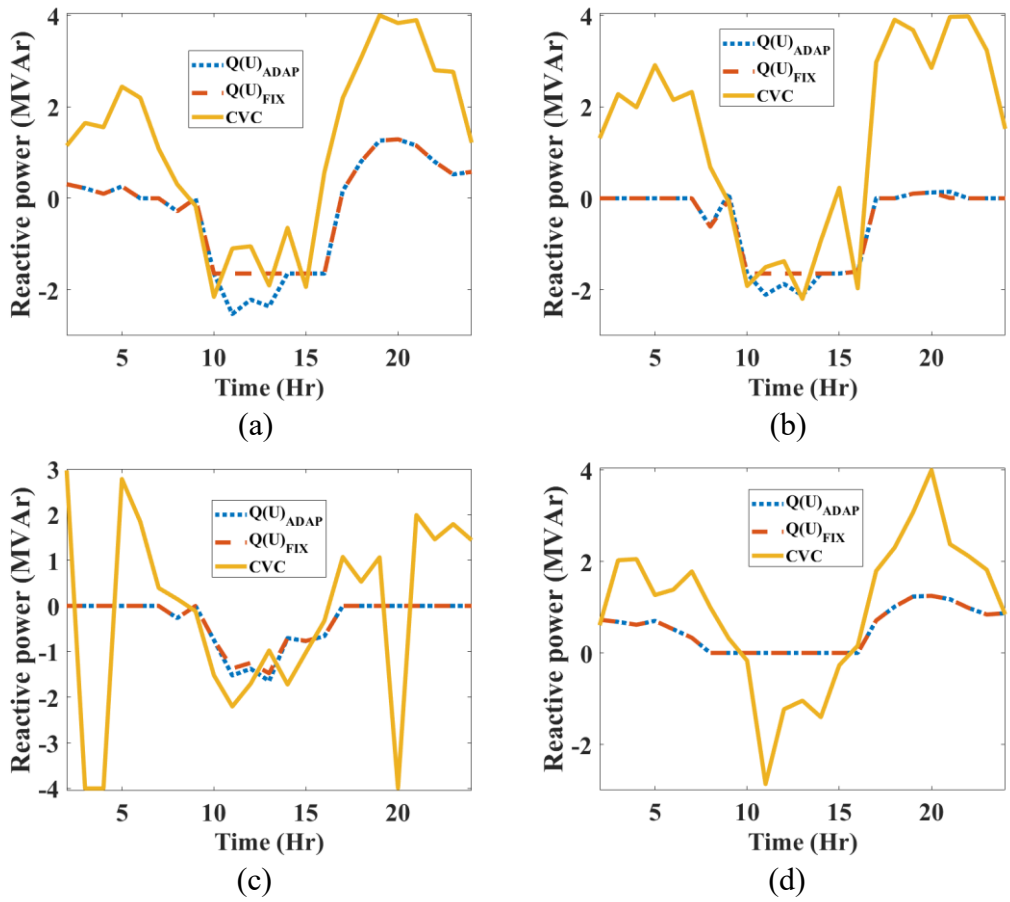

Figure 4.15 Reactive power compensation by DG for $Q(U)_{ADAP}$, $Q(U)_{FIX}$ and CVC at (a) bus 11, (b) bus 10, (c) bus 16 and (d) bus

Further analysis of the three scenarios for the entire MV grid is shown in table 4.4. CVC had the best performance for voltage regulation as the minimum and maximum voltage on the grid for the entire week was 0.95 p.u. and 1.05 p.u. respectively. Thus, there was no violation on the grid as compared to the $Q(U)_{\text{ADAP}}$ and $Q(U)_{\text{FIX}}$ which recorded total voltage violations of 29 and 37 respectively.

Table 4.4 Summary of overall grid performance

Measuring indicator	**$Q(U)_{ADAP}$**	**$Q(U)_{FIX}$**	**CVC**
Max. voltage (p.u.)	1.06	1.08	1.05
Min. voltage (p.u.)	0.94	0.94	0.95
VSI	0.937	0.916	0.876
Net reactive power (MVAr)	-21.49	-22.28	595.91
Total no. of voltage violations	29	37	0

The reason is that CVC obtains measurement information about the entire grid before making a control decision whiles $Q(U)_{\mathrm{ADAP}}$ and $Q(U)_{\mathrm{FIX}}$ act locally based on measurements at the PCC. The violations for $Q(U)_{\mathrm{ADAP}}$ occurred on buses with no PV integration. $Q(U)_{\mathrm{ADAP}}$ had the best VSI index of 0.936 as compared to CVC and $Q(U)_{\mathrm{FIX}}$ which had 0.876 and 0.916 respectively. CVC obtained this low value because of the high amount of reactive power injection to the grid from the PVs totalling 595.91 MVAr to mitigate all the voltage violations on the grid.

4.5.3 Case 3: Robustness of the adaptive scheme

This case has the same PV location, number, and rating as the second case study and thus the same fitting functions. Since the $Q(U)_{\mathrm{ADAP}}$ proposed control is developed through offline simulation using estimated or historical load and generation profiles, the load and generation values during implementation may be substantially different from those used in developing the sensitivity function. The line impedances are also dependent on atmospheric conditions and thus impedance values are not constant. The objective of case 3 is to demonstrate the robustness of the proposed $Q(U)_{\mathrm{ADAP}}$ in dealing with the difference in offline and online load and generation values. Two scenarios created in this case study are as follows.

- Scenario 1: Both loads and PVs are simultaneously increased by 10%.
- Scenario 2: There is an increase of 10% of the line impedance (both resistance and reactance).

The results for the voltage profiles for four out of five PV-connected buses and their respective reactive power compensation are shown in figures 4.16 and 4.17 respectively for scenario 1. During the entire week, the $Q(U)_{\mathrm{ADAP}}$ was able to regulate voltage within the stipulated grid code range at all times including both the peak and solar demand period because the reactive power compensation generated by the sensitivity fitting function was dependent on the load and generation conditions at the PCC. Thus, it was possible for the $Q(U)_{\mathrm{ADAP}}$ to keep up with the change and adapt subsequently. Results from scenario 2 shown in figure 4.18 after a 10% percent increase in line impedance show a similar trend in effective voltage regulation as the voltage profiles were kept within the grid code limits, because of the appropriate compensation provided by the control as shown in figure 4.19. Increasing the line impedance increases the voltage drop across the network, resulting in high voltage sensitivity values at

the ends of the feeder. These values were accurately estimated by the developed sensitivity fitting function, leading to effective voltage regulation.

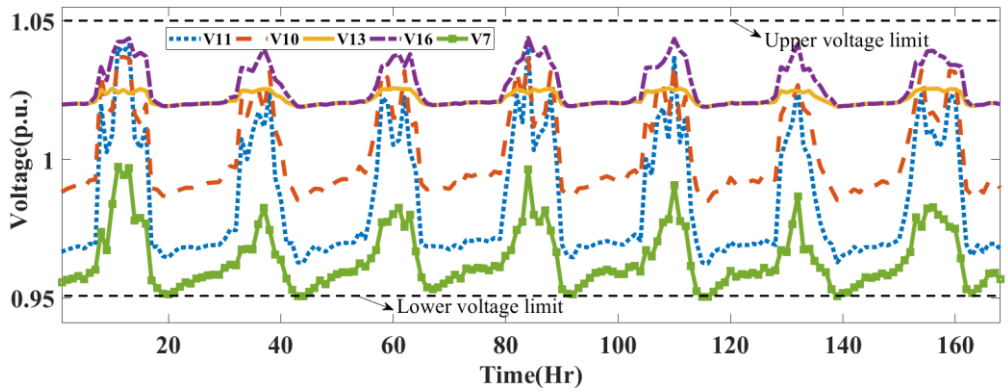

Figure 4.16 Voltage profile of buses 11, 10, 13, 16 and 7 after a 10% increase in load and PV

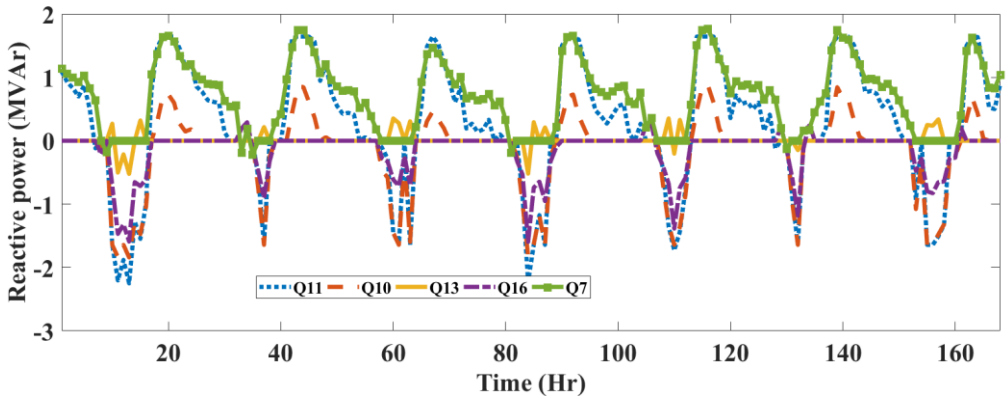

Figure 4.17 Reactive power compensation by inverters for the one week at buses 11, 10, 13, 16 and 7 after a 10% increase in load and PV

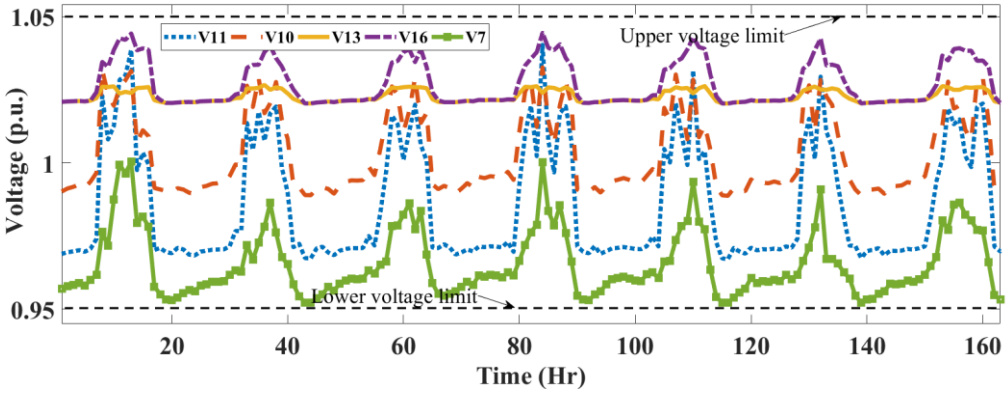

Figure 4.18 Voltage profile of buses 11, 10, 13, 16 and 7 after a 10% increase in line impedance

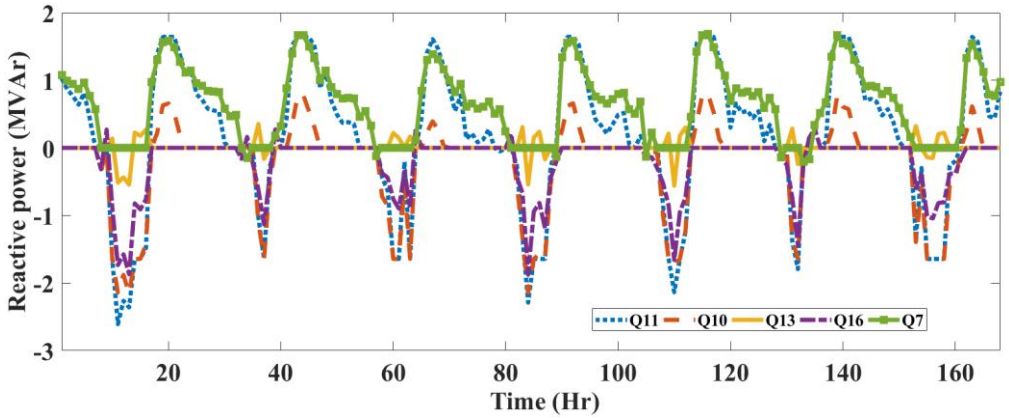

Figure 4.19 Reactive power compensation by inverters for the one week at buses 11, 10, 13, 16 and 7 after a 10% increase in line impedance

In all the study cases the proposed adaptive scheme was able to control the voltages within the lower and upper limits as per the grid code, because of the voltage sensitivity block which encapsulates the sensitivity fitting function, which must be updated or recalculated when major changes occur in the network topology, caused by new loads, substations, etc. Notwithstanding there is enough time to calculate the fitting function since it takes time for such changes to occur [130].

4.6 Summary

In this chapter, a static $Q(U)$ control that uses measured variables at the PCC to dynamically change its reactive power output as the generation and loading conditions change is illustrated. It was achieved by adding an adaptive functionality to the standard $Q(U)$ control. This functionality is made up of a voltage sensitivity block that uniquely determines the required compensation needed to improve the voltage and a voltage stability block that ensures that the reactive power compensation provided improves the voltage stability index of the PCC bus.

Simulation results depict the effectiveness of the adaptive scheme in enhancing voltage regulation on the MV grid by mitigating the voltage rise phenomenon which mostly occurs during peak solar generation and improving the voltage profiles during the peak demand period. In comparison with $Q(U)$ control operating with fixed parameters, the adaptive scheme performed better as there was voltage violation at buses located at the ends of the distribution feeder during the period of peak solar generation. The performance of this proposed control is comparable to the CVC scheme, even though the latter relies on

communication facilities, requiring the need for investment in measurement devices and sensors. The proposed control however operates locally, making it a suitable alternative to MV grids with limited or no communication facilities. This proposed control could be very beneficial to countries like Ghana where there are limited financial resources.

The AD functionality only compensates for the reactive power provisioning from the standard $Q(U)$ control when the $Q(U)$ performance is not satisfactorily in regulating the voltage at the bus without changing the control parameters of the control. The next chapter focuses on changing the control parameters.

Chapter 5 Two-Stage design approach for Adaptive Q(U) Control

This chapter introduces a two-stage approach to adapting the settings of the $Q(U)$ control with changing generation and load conditions. In the first stage, a genetic algorithm (GA) based on optimal power flow determines the optimal control parameters for the $Q(U)$ control of the PV unit, and the results (voltage and current) from the power flow are subsequently used to estimate the Thevenin impedance seen from the point of common coupling (PCC) bus i.e. the bus where a PV is connected. These control parameters, unique for every PV integrated into the grid, are sent to the artificial neural network (ANN) stage to develop a pattern relating the Thevenin impedance values to the optimal control parameter values. The developed pattern is used to adapt the $Q(U)$ control parameters to the changing grid conditions.

The chapter starts by explaining the concept of artificial neural networks and their applications in the power system. This is followed by a detailed description of the methodology used to design the two-stage approach, including how it is implemented on the MV distribution network. The chapter concludes with study cases and scenarios used in validating the two-stage design approach.

5.1 Artificial Neural Networks

ANN is one of the branches of artificial intelligence (AI), which in computer systems is defined as the ability of a machine to carry out tasks that are usually a characteristic of human intelligence [133][134]. Intelligent traits in humans include learning, problem-solving, reasoning, etc. These traits as exhibited by modern computing systems have become a useful tool in technology for finding the relationships between a set of input and output variables and hence used in areas such as pattern recognition, spam filtering, etc. ANN, which is an interconnection of small processing units or nodes called neurons, mimics the human brain in its capacity to acquire knowledge, learn and subsequently store this knowledge in a structure known as weights. These weights are the connections that link individual neurons to one another [135]. As the dataset or information is passed along these neural interconnections, the ANN learns and

recognises patterns from these data through a series of training and testing or validating. The newly recognised patterns are therefore used for predictions or classifications when the ANN is presented with a new set of data.

5.1.1 Structure of ANN

ANNs consist of input and output layers [136][137], which are described as either a single-layer or multi-layer network. The multi-layer network has one or more layers between the output and input layer called the hidden layer. This hidden layer increases the capability of the neural network to learn patterns from a given set of data, thus giving an edge to multi-layer networks to produce better patterns especially for complex problems as compared to the single-layer[137]. The architecture of a neural network refers to the number of neurons in each ANN layer, the number of hidden layers, and how these neurons are interconnected with each another. The architecture affects the transformation process from the input layer to the output layer to generate an output. ANN architecture is classified into feed forward and feedback network.

The feedback architecture is a closed loop architecture where information flows in both directions from the input layer to the output layer and vice versa. Thus, there exist connections from the output to the input neurons, which serve as feedback to the input neurons to improve the performance of the network. This architecture is mostly suitable for time-varying complex problems [138].

The feedforward architecture on the other hand allows information to flow only in one direction from the input layer to the output layer in the forward direction, resulting in a simpler architecture as compared to a feedback network. This architecture is mostly applied in load forecasting and pattern recognition problems [139]. An example of this architecture made up of an input, hidden and output layer is shown in figure 5.1. In each layer are neurons or nodes that are depicted as circles. The linkage between neurons is through connection weights $(w_1, w_2, \dots, w_n)$ which are responsible for storing knowledge from the preceding node. The ANN process must first be presented with a set of input data $(x_1, x_2, \dots, x_n)$ and the corresponding desired (target) output before the start of the process. These data sets are used by ANN to learn and recognise patterns, which are subsequently used for predicting a set of outputs when presented with a new set of data input. The input-output data sets are divided into two groups, one for training and the other for validation [140]. The training data sets account for a higher percentage of the overall data.

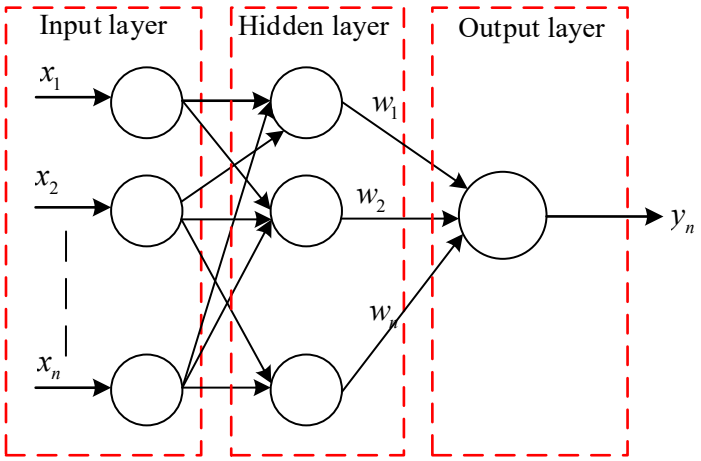

Figure 5.1 Structure of artificial neural network

The ANN starts with the training phase where the network input layer accepts a set of input data, then the network learns a pattern from the input data and generates an output (y_n) to match the desired output as the input data set moves through the neurons from the input layer to the output layer. The generated output is thus constantly being compared with the desired output value to minimize the difference or error between them. This error is minimized by adjusting the connection weights with the aid of an appropriate learning algorithm, which is mostly the back propagation (BP) algorithm [141].

The BP algorithm is a learning algorithm based on the gradient descent method and it changes the weights along its gradient to minimize the error between the network output and the desired output. The adjustment process to the weights is done when the input data sets move from one node to the other. Figure 5.2 summarizes how the input data is processed from one node to the other node.

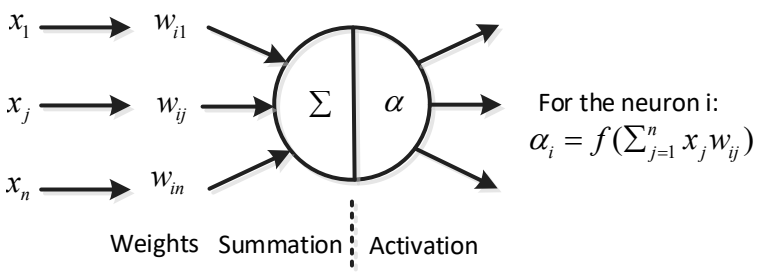

Figure 5.2 Information processing in artificial neural network

Every node through its input connections receives weighted activation, made up of input and weight values from preceding nodes. These weight activations are first summed up and then transferred to an activation function (α) which acts as a medium for transferring the weighted input to the output of the node.

Examples of activation functions include linear, sigmoid function, and logistic functions. The choice of a particular function depends on the nature of the problem and the neural network architecture [137][142]. The steps used in adjusting the weights using on BP algorithm are therefore described in appendix G based on [143], [144].

The BP algorithm determines the modification factors which are subsequently used to adjust the connection weights. Afterward, the training is repeated. If the difference between the network's output and the desired output is more than a set tolerance value, the connection weights are adjusted again to minimize the error. However, when the error margin is within the set tolerance value after some predefined level of training, the connection values for the weights are stored. The ANN then moves to the validation phase where the trained network and connections weights are tested with the remaining set of input and output data. Afterward, these stored data are used to identify patterns and make decisions when new data sets which are different from the trained data are presented.

5.1.2 Selection of ANN parameters

The selection of the input-output data sets affects the efficacy of the ANN's ability to learn and develop relationships used to predict the behaviour of a process or system. Thus, there is a need to select and define the appropriate input and output variables that significantly characterise the entire process or system. There is no scientific approach to determining the appropriate input data. However, a comprehensive analysis that involves plotting how the input parameters impact the output variable can be beneficial in selecting the appropriate input variables [1]. Input variables that have no impact on the output are discarded to simplify the learning process of the ANN.

The selection of the appropriate number of hidden layers also affects the accuracy of the ANN prediction model, especially for the ANN model that uses BP learning algorithms. The number of neurons in the hidden layer depends on the number of neurons in the input and output layers. Although the number of neurons in the hidden layer is mostly determined by trial and error, the authors of [145] provided an empirical formula to estimate it mathematically using (5.1).

$$\begin{aligned} &Number\ of\ hidden\ layer\ neurons \\ &\quad = 0.5 * (\ number\ of\ inputs\ + output\ neurons) \\ &\quad + \sqrt{number\ of\ training\ data\ points} \end{aligned} \tag{5.1}$$

Authors of [146] also provided another thumb rule to estimate the number of hidden layers in the ANN model using (5.2).

$$\begin{aligned} &Number\ of\ hidden\ layer\ neurons \\ &= \frac{2}{3} * number\ of\ elements\ in\ the\ input\ vector \\ &+ number\ of\ elements\ in\ the\ output\ vector \end{aligned} \qquad 5.2$$

Equations (5.1) and (5.2) serve as the starting point in determining the number of neurons used in this thesis.

5.1.3 Application of ANN

The estimation of the power flows and the performance of power networks involve complex nonlinear mathematical equations made up of line impedances, loads, etc. Identifying and using these equations to develop mathematical relationships for example to ascertain the impact of certain control actions of a power system network device like OLTC on network performance in terms of losses, voltage profile, etc. is challenging as it involves solving complex differential equations. This computation problem is further complicated with the emergence of RE sources like PV as their output values are dependent on factors such as weather conditions. Thus, creating another challenge for power system engineers in predicting the output values for RE sources. These challenges have given a boost to the applications of ANN in the power system as ANN avoids these complex differential equations and time-consuming approaches to developing mathematical relationships among a given set of network parameters and also provides an accurate prediction of weather-dependent generation sources. ANN achieves this by adopting a black box approach [147], i.e., ANN requires no detailed information about the power system network but only the input (e.g. control actions of a power system network device) and output (e.g. network performance indicator like voltage profile) data sets to develop patterns and relationships [148].

ANN has been used successfully in a broad range of applications in the planning and operation of power system networks that include load and power generation forecasting, economic dispatch, voltage control, fault diagnosis/fault location, power flow, and harmonics.

In generation forecasting, ANN has been used in predicting power production from renewable-based DGs such as photovoltaic (PV) and wind turbines (WT). This is very essential when planning power networks with significant penetration levels of DGs because of the uncertainties associated with their

outputs. These outputs must be correctly forecasted to make accurate planning decisions, as substantial errors in the forecasted values will affect the performance of the network during implementation. To provide accurate predictions for PV output, the authors of [149] used a 4-input and single output ANN structure. The input parameters were wind speed, solar irradiance, ambient temperature, and relative humidity, with the output parameter being the PV output. In training the ANN, the historical data sets of these parameters for 42 months were grouped into 24 hourly values to represent a typical day. Then, the ANN model was built for each hour to be subsequently used to predict the PV output on an hourly basis. The effectiveness of this approach was verified and assessed using the mean absolute and root mean square errors. In all these assessments, the ANN predicted model showed better performance as compared to other benchmarking learning models.

In voltage control, ANN has been used in areas such as enhancing the control performance of power converters of DGs [150], minimising the non-linear effects of inverters [151], etc. Li et al used ANN in the control architecture of DGs to deal with voltage fluctuations caused by DGs and loads [150]. The control architecture consists of an outer and inner current loop control, with the inner loop being an ANN controller. The voltage measured at the PCC and the active power outputs of the DG serves as input to the outer loop control to generate the reference current for the inner loop ANN current control. A 4-layer architecture had 4-inputs which are the d and q components of the error signal from the outer loop control and their respective error terms. The ANN architecture has two output which are the d and q component of the inverter voltage. These voltage signals are injected into the grid to minimize the voltage fluctuations on the grid. An offline training methodology was used to train the ANN considering different reference values for d and q current signals. Results obtained from both the simulation and laboratory experiment show the advantage of the ANN controller controller in minimising voltage fluctuations as compared to the conventional proportional integral droop control.

ANN is also used as a voltage control algorithm in [151] to minimize the non-linear effects of voltage source inverters (VSCIs). These nonlinear effects, caused by the dead time of the VSCI, distort the voltage by creating harmonics that affect the quality of the power supply. A dead time is normally inserted in the control of VSCIs to avoid conduction overlap that happens during the switching of signals in each phase leg of the inverter. However, the introduction of this dead time creates a disparity between the actual phase and the reference voltages, leading to a voltage mismatch which eventually distorts the phase

currents and voltages. To eliminate this mismatch, an appropriate voltage strategy must be incorporated into the VSCI control to compensate for the mismatch. This compensation is achieved by developing a non-linear complex function relating the current in each phase of the inverter to the dead time compensation voltage (distorted voltage from the VSCI caused by the dead time) using ANN. The input to the ANN structure is phase current in each of the three phases and the output is the distorted dead time compensation voltage. Based on this developed complex function between the phase currents and distorted voltage. An adaptive law is constructed for online implementation such that the distorted output voltage from the ANN structure serves as input to another control architecture (current predictive control) which uses the distorted voltage to generate an output voltage from the VSCI that compensates for the distortions in the voltage, thereby resulting in an output voltage that matches the phase voltages. Experimental results obtained from this strategy depict the effectiveness in accurately reducing the current and voltage distortions.

The successful implementation of ANN in various aspects of voltage control in the power grid and its ability to operate independently of the parameters of the inverters and the grid serves as the basis for its selection in this thesis work to enhance the performance of $Q(U)$ control of DGs in distribution networks.

5.2 Proposed two-stage design

The proposed design used to adapt the control settings of the $Q(U)$ control to the changing load and generation conditions is made up of two stages, namely, the GA optimization and ANN stages. A graphical representation of the proposed design is presented in figure 5.3, which starts with the optimization stage for determining the optimal control settings of the control and their corresponding Thevenin impedance values. These values are subsequently passed on to the ANN stage to develop a function relating the Thevenin impedance to the control parameters. A detailed explanation of the two stages is given as follows.

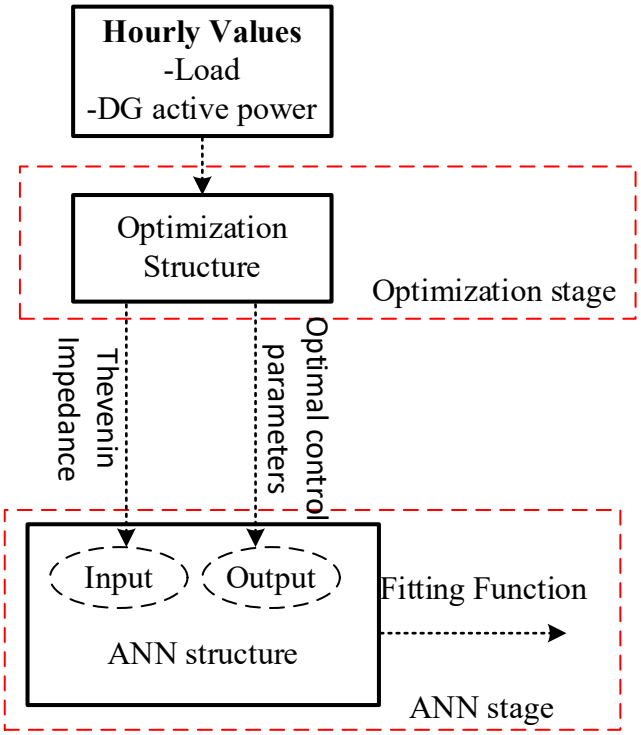

Figure 5.3 Two-stage design approach

5.2.1 Genetic algorithm optimization stage

The objective function of the optimization is the bus voltage stability index (VSI) explained in (4.26) and expressed in (5.3)

$$VSI = \frac{|\underline{Z}_X| - |\underline{Z}_{TH}|}{|\underline{Z}_X|} \quad 5.3$$

Where $\underline{Z}_X$ and $\underline{Z}_{TH}$ are the complex load and Thevenin impedance calculated using (5.4)

$$\underline{Z}_X = {|\underline{U}_r|}/{|\underline{I}_r|}\,, \underline{Z}_{TH} = {|\Delta\underline{U}_r|}/{|\Delta\underline{I}_r|} \quad 5.4$$

Where $\underline{U}_r$ and $\underline{I}_r$ are respectively the complex voltage and current measurements at the bus of interest, $\Delta\underline{U}_r$ and $\Delta\underline{I}_r$ are the change in two consecutive samples of voltage and current measurements at the bus of interest respectively.

This objective function is subjected to both equality and inequality constraints. The equality constraints are expressed in (4.38) and (4.39) and the inequality constraints are expressed in (4.40) and (4.41).

The control parameters of the $Q(U)$ control - $U_{MAX,}\, PF, DB$ and U_{SET} are the decision variables whose maximum and minimum values are provided in Table 5.1. The optimization is a mixed integer optimization problem as PF and U_{SET}

are discrete variables changed in steps of 0.01, DB and U_{MAX} are continuous variables.

Table 5.1 Maximum and minimum value of each decision variable

Control variable	Minimum value	Maximum value
DB	0.02	0.06
U_{MAX}	1.05	1.09
U_{SET}	0.85	1.03
PF	0.90	0.99

Figure 5.4 summarizes the flow chart of the GA optimization algorithm. The optimization starts by randomly initialising the control or decision variables. Next, the algorithm obtains the MV grid parameter and the load and PV output profiles for each hour to be subsequently used in the power flow simulations.

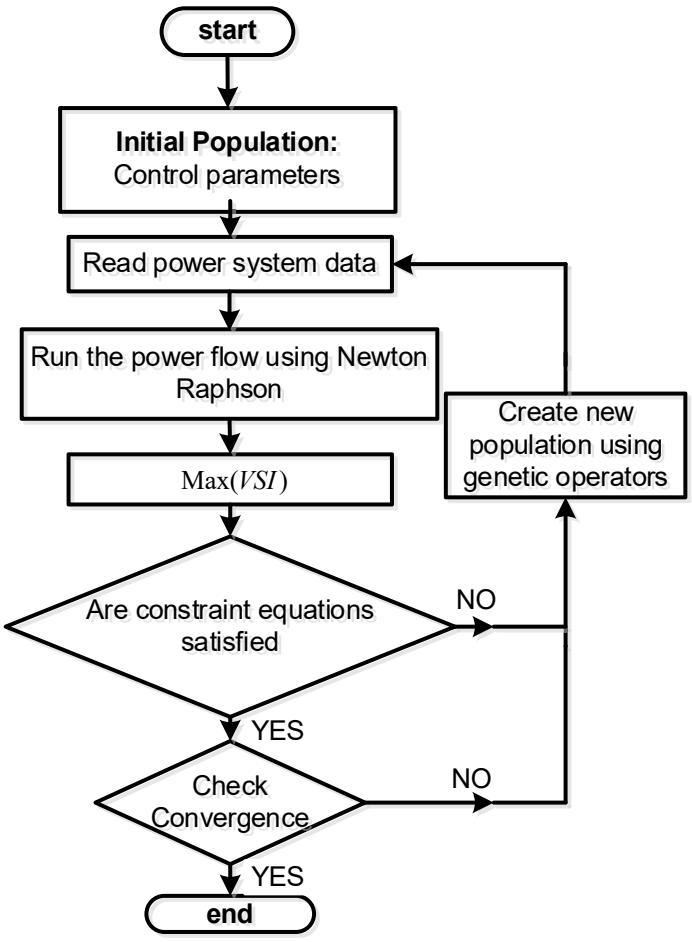

Figure 5.4 Flowchart of genetic algorithm optimization

The MV grid is the 16-bus network described in section 3.5.1 of the thesis. The hourly load profiles are two years (2014 and 2015) of historical data, a total of 17,250 hours, obtained from the Ghana Grid Company, whereas the active power output of PVs was determined using the solar irradiance and temperature values obtained from [83] for Sunyani (a town located northern part of Ghana). These values are converted to MW using (3.16) and (3.17). Both the PV and load profiles are normalised against the respective peak values to obtain the per unit values. These per unit values are multiplied by the base load values from the MV grid and rated peak active power for each PV unit to determine the load value and PV active power output respectively for each hour. In calculating the VSI, two successive samples of voltage and current measurements are needed, which translates into the optimization starting from the second hour ($t = 2$), for instance at $t = 2$, the hourly profiles for $t = 1$ and $t = 2$ are used for the power flow simulations to determine the VSI for that second hour. This GA optimization algorithm determines the optimal control values for each PV unit and their corresponding Thevenin impedance seen at the PCC bus for every hour. These values are subsequently sent to the ANN stage. However, when there is no convergence of the optimization in a particular hour, the results are discarded and not sent to the ANN stage. The parameters of the GA used are shown in table 5.2.

Table 5.2 Genetic algorithm parameters

GA parameter	**Value**
No. of Generation	20
Population	10
Crossover function (rate)	0.8
Stall generation limit	15
Tolerance	1×10^{-6}

5.2.2 Artificial Neural Network Stage

At this stage, a function correlating the optimal $Q(U)$ control settings (U_{MAX}, PF, DB and U_{SET}) and their matching Thevenin impedances (Z_{TH}) for each PV unit is developed. Z_{TH} is used because the impedance is a total representation of the network impedance which includes line impedances, OLTC and VR parameters, etc., seen at the PCC bus. Thus, a good indicator to

be used as input to the ANN stage in predicting control parameters that will improve both the performance of the PCC bus and the grid as a whole. Table 5.3 provides the parameters used in implementing the ANN stage in Matlab.

Table 5.3 Artificial neural network parameters

ANN parameter	Value
No. of Hidden layer	5
Number of neurons in each hidden layer	20
Max. No. iterations	2500
Training ratio	70%
Testing and validation ratio	30%

5.2.3 Implementation of the adaptive Q(U) in the 16 bus medium voltage distribution grid

The flowchart depicting how the proposed adaptive two-stage design approach is implemented is shown in figure 5.5. As the proposed design operates solely on measured variables at the PCC, the first step of the approach is the measurement of the local voltage (U_{PCC}) and the estimation of the Z_{TH}.

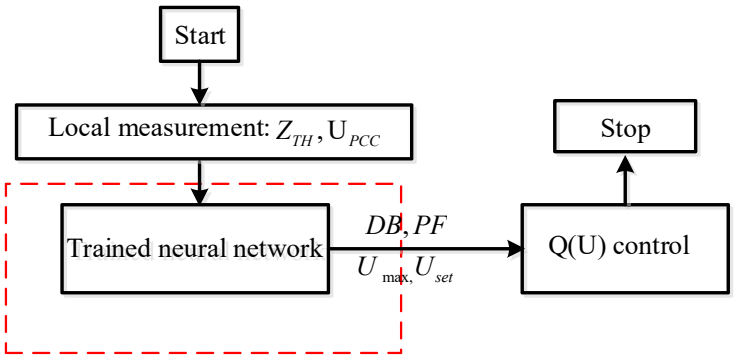

Figure 5.5 Schematic of Adaptive $Q(U)$

The Z_{TH} which serves as input to the trained neural network and is used to predict the control parameters. These parameters together with U_{PCC} are then used to the determine amount of reactive power compensation needed for voltage regulation. According to (4.24), Z_{TH} is calculated from two measured samples of voltage and current, hence the $Q(U)$ control will operate with initial parameters at the first hour. In this thesis, the initial parameters are 1.07 p. u, 0.95, 0.06 p. u. and 1 p. u. for U_{MAX},PF, DB and U_{SET} respectively

based on the work of authors of [110]. Furthermore, if the Z_{TH} is zero for a particular hour, then the control parameters for the previous hour are used.

Time series load flow is used in assessing the performance of the proposed design. The GA was implemented using Distributed Evolutionary Algorithms in Python (DEAP) software interfaced with DigSILENT/ Powerfactory for the power flow simulations. The training of the neural network was done in Matlab using the ANN toolbox. In validating the proposed design, load and PV output profile for the year 2016 was used which is different from the profiles used in the design approach. In simplifying the simulation, a month each is selected to represent each of the three seasons in Ghana - March, August, and December representing the dry, rainy, and harmattan seasons. The profiles for load and PV output for these seasons are shown in figure 5.6.

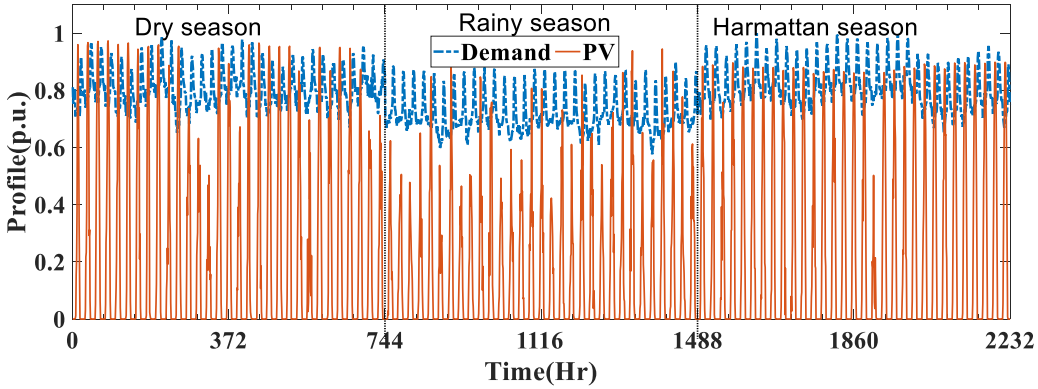

Figure 5.6 Load (demand) and PV profile

The validation of the proposed design is carried out with three PV connections at buses 10, 11, and 16 of the 16-bus MV grid. Each DG unit inverter is rated 5.5MVA with a peak megawatt value of 5MW, which implies that reactive power compensation can still be provided during peak active power generation. Two case studies used in assessing the performance of the scheme are explained as follows.

5.2.3.1 Case study 1: Performance of the proposed scheme

This scenario involves two case studies, in which the PV units are operated with different control methods (schemes).

Scenario 1: Each PV unit is operated with the control $Q(U)$ settings as recommended by the authors of [110]. The settings are $U_{set} = 1.0$ p.u., $PF = 0.95$, $U_{MAX} = 1.07$ p.u. and $DB = 0.06$ p.u. which remained fixed throughout the simulation.

Scenario 2: Each PV unit is operated with the proposed two-stage design approach for $Q(U)$ control.

The results of the neural network training are shown in Appendix H. Voltage profiles of buses 10, 11, and 16 are shown in figures 5.7, 5.8, and 5.9 respectively. The profiles were observed to be within the grid code range from the lower voltage limit of 0.95 p.u. to the upper voltage limit of 1.05 p.u. for the proposed $Q(U)$ control. There were violations exceeding the upper voltage limit for scenario 1 where the PV operates with fixed control parameters.

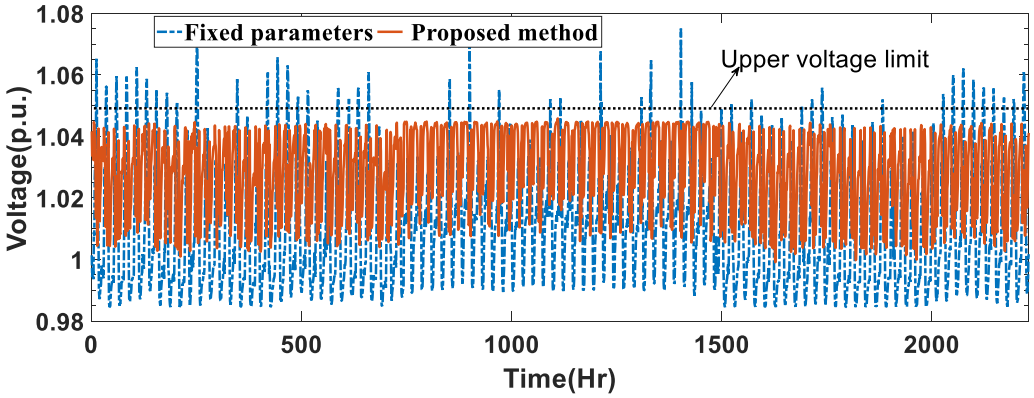

Figure 5.7 Voltage profile for bus 10 for the three months

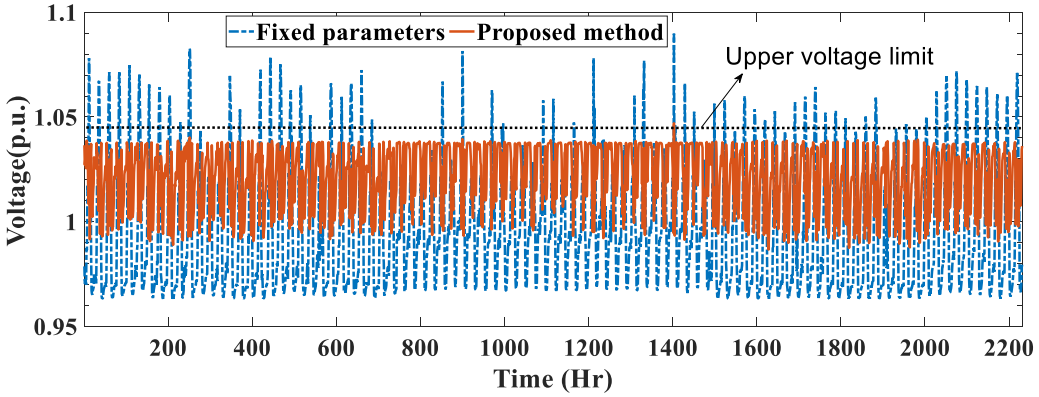

Figure 5.8 Voltage profile for bus 11 for the three months

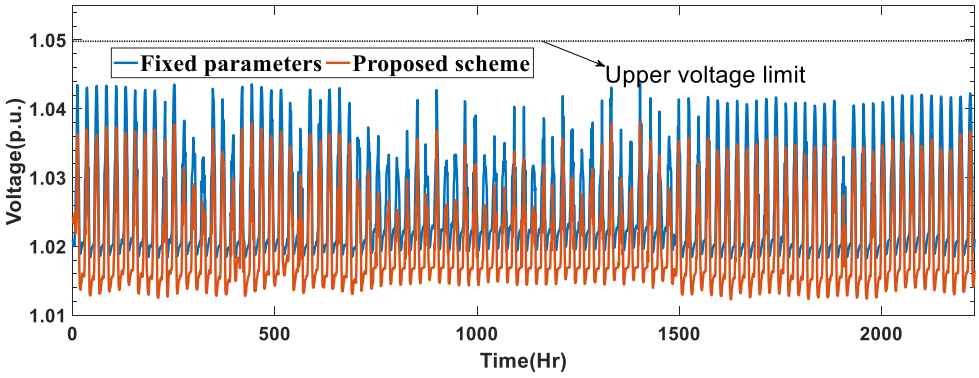

Figure 5.9 Voltage profile for bus 16 for the three months

For a further analysis of these results, figures 5.10 and 5.11 capture the voltage profiles and their corresponding reactive power compensation for the first 24-hour period for buses 10 and 11 respectively.

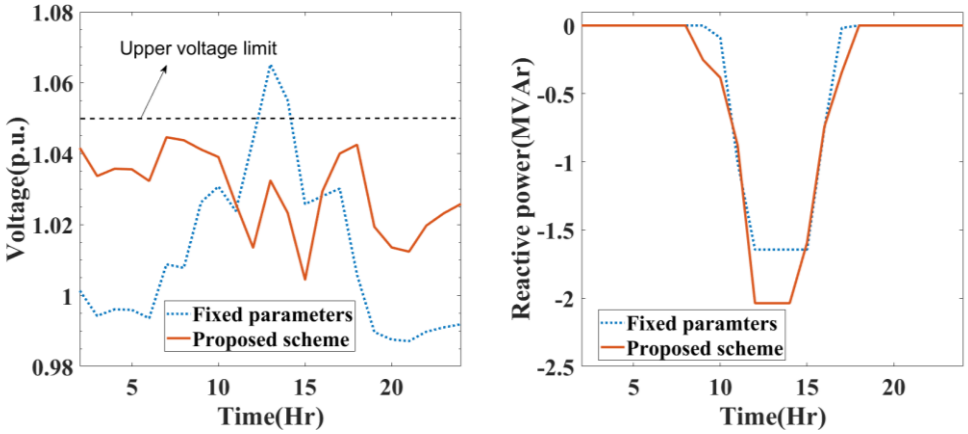

(a) (b)

Figure 5.10(a) Voltage profile (b) reactive power compensation by PV at bus 10 for the first 24-hour period

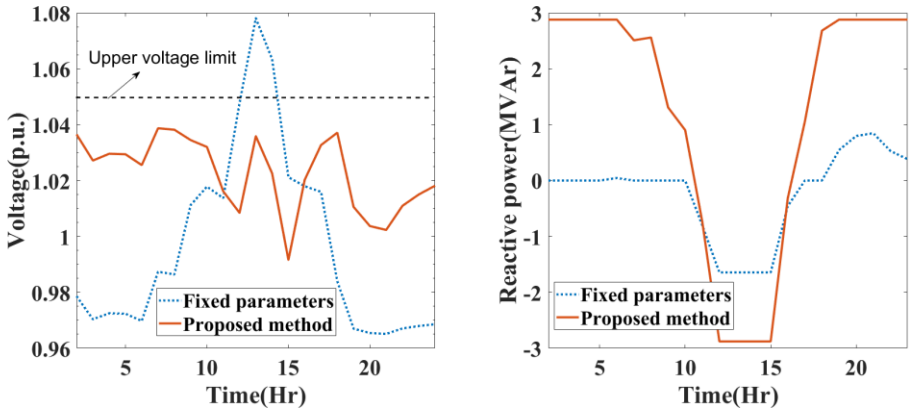

(a) (b)

Figure 5.11(a) Voltage profile (b) reactive power compensation by PV at bus 11 for the first 24-hour period

In figure 5.10 (a), the fixed $Q(U)$ control (scenario 1) was not able to keep the voltages below the upper voltage limit except during the peak solar generation which starts from the 11^{th} to the 13^{th} hour of the day for bus 10. This can be explained that the 1.62 MVAr absorptions of reactive power by the inverter (refer to figure 5.10(b)) was not enough to overcome the voltage rise occurring during these hours. However, for the proposed $Q(U)$ control (scenario 2) the reactive power compensation of 2.85 MVAr as seen in figure 5.10(b) was enough to keep the voltage profile below the upper voltage limit during the peak solar hour shown in figure 5.10(a). Similarly, in figure 5.11(a), the proposed control was able to regulate the voltage within the upper and lower voltage limit for the entire period, while that of the fixed $Q(U)$ control resulted in voltages above the upper limit during the peak solar hours. The total number of voltage violations recorded for the buses with PV connections for both scenarios 1 and 2 are provided in table 5.4. Scenario 2 exhibited a superior performance as it recorded no voltage violations and also had an overall VSI value of 0.994.

Table 5.4 Summary of grid performances

Scenario	VSI	Total number of voltage violations
1	0.992	83
2	0.994	0

5.2.3.2 Case study 2: Robustness of the proposed Q(U) control

In developing the two-stage adaptive $Q(U)$ control, line impedances, historical values of load, and PV output values were used. These values are however dependent on atmospheric conditions, resulting in a possible mismatch between the historical values and those encountered by the control during implementation which must be accounted for during the design of the control. This case study assesses the robustness of the proposed control in dealing with these mismatches. The three scenarios are as follows.

- Scenario 1: The transmission line resistance and reactance are increased by 10% and 5% respectively, resulting in an increase in the average R/X ratio of the MV grid from 1.026 to 1.074.
- Scenario 2: Both the load and PV profiles are increased by 10% to represent unexpected changes or growth of load and/or PV output.

- Scenario 3: One of the PVs (bus 10) is disconnected to assess the impact on the other PVs connected at buses 11 and 16.

Both the voltage profiles and reactive power compensation for the first seven days, representing a total of 168 hours, are shown in figures 5.12 and 5.13 respectively for scenario 1. Results of the voltage profiles in figure 5.12 show the effectiveness of the proposed $Q(U)$ control in keeping the voltage within the upper and lower voltage regulatory limits. The reason is that changing the R/X ratio changes the power flows along feeders, which automatically reflects in the current and voltage measurements at the PCC. These measurements are used to estimate the Thevenin impedance value which serves as input to the trained neural network to predict the appropriate control parameters in providing the required reactive power compensation as shown in figure 5.13.

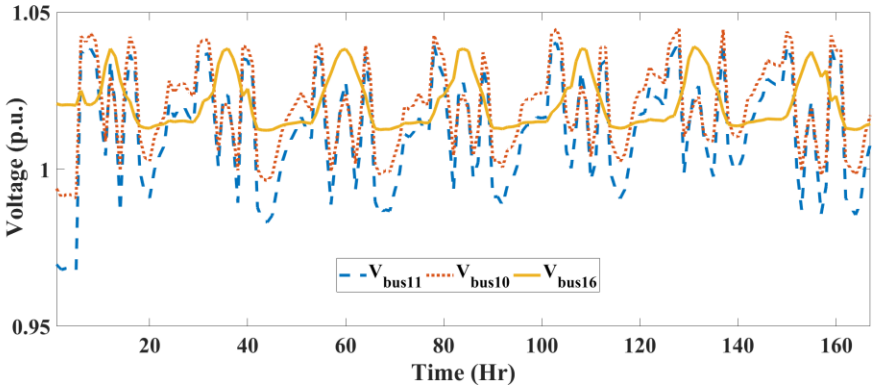

Figure 5.12 Voltage profile of PV-connected buses in Scenario 1

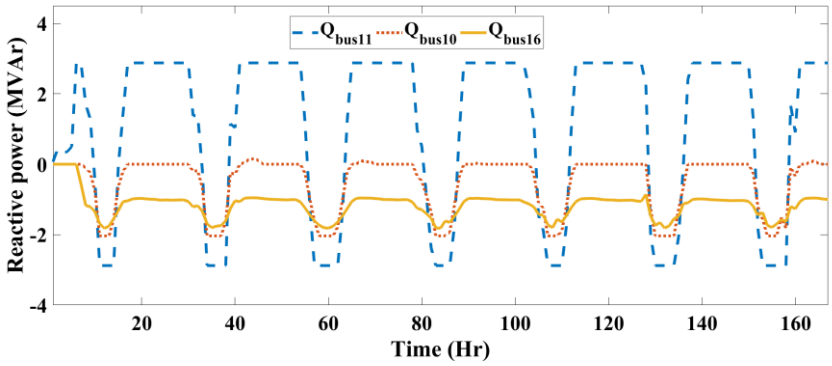

Figure 5.13 Reactive power compensation provided by PVs in Scenario 1

Similarly in scenario 2, the proposed scheme also kept the voltage within the voltage limit as shown in figure 5.14 with the reason being the same as in scenario 1 since the 10% increase in load and PV profiles changed the power flows in the grid which reflected in the voltage and current measurements at the PCC buses.

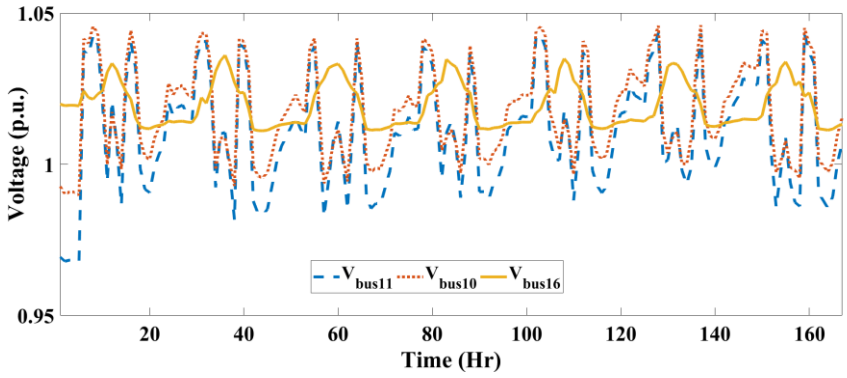

Figure 5.14 Voltage profile of PV-connected buses in Scenario 2

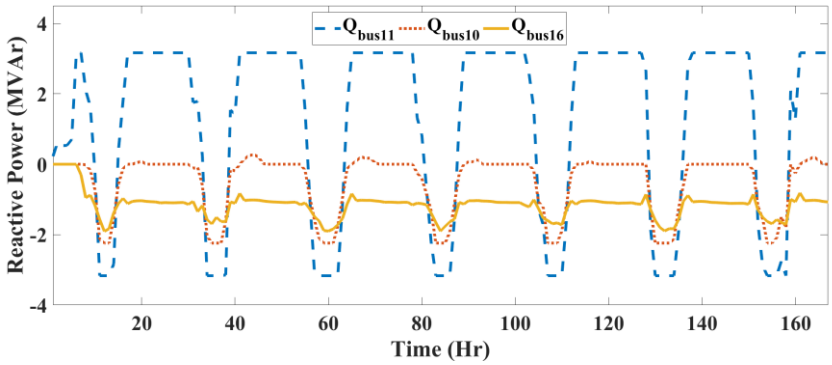

Figure 5.15 Reactive power compensation provided by PVs in Scenario 2

In scenario 3, figure 5.16 shows that the proposed $Q(U)$ control of each PV unit operates independently from the other PVs as the voltages of buses 16 and 10 were kept within the regulatory limit after the disconnection of the PV at bus10 by providing the needed compensation shown in figure 5.17. It is inferred from these results that the trained neural network of each $Q(U)$ control of every PV unit is independent of one another. Hence, when integrating new PVs, there is no need to update the neural network of the existing PVs in the MV grid. The procedure is only repeated for new PVs since the control operates independently relying solely on measured variables (voltage and current) at the PCC. However, when there are significant changes in the network topology and/or configuration resulting in new substations and loads, the fitting function must be updated.

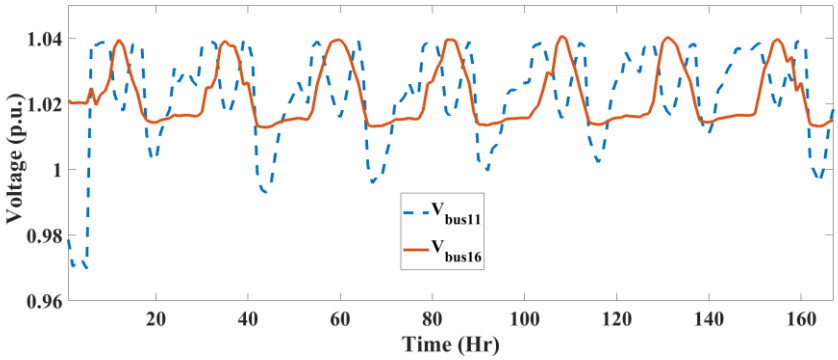

Figure 5.16 Voltage profile of PV-connected buses in Scenario 3

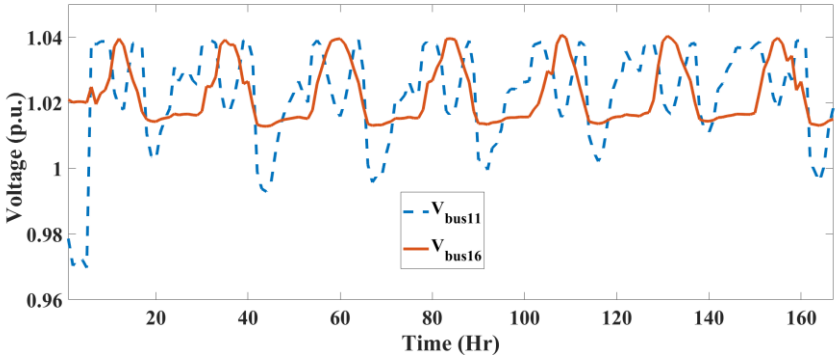

Figure 5.17 Reactive power compensation provided by PVs in Scenario 3

5.3 Summary

The chapter describes an offline methodology used to achieve an adaptive $Q(U)$ control that uses local voltage and current measurements at the PCC and whose control parameters change with the grid load and generation conditions. The proposed methodology involves a two-stage design approach using GA optimization and ANN. At the GA stage, the optimization is run for every hour using hourly load and PV generation profiles for two years (2014 and 2015). In each hour the optimal parameters and their corresponding Thevenin impedance values at the PCC are determined. These parameters and impedance values are then sent to the ANN stage to train the neural network to develop a correlation uniquely for each PV unit. Subsequently, the trained neural network is used to predict the $Q(U)$ control parameters as the grid loading and generation conditions change. During implementation, the estimated Thevenin impedance determined from the local voltage and current measurements at the PCC serves as input to the trained neural network. The trained neural network predicts a set

of control parameters for the $Q(U)$ control which is used to determine the required amount of reactive power compensation.

Two study cases are used to validate the effectiveness of this scheme. In case study 1, a comparison was made between the proposed scheme and the PV with fixed $Q(U)$ control parameters using a time series simulation. The results from the simulation show the effectiveness of the scheme in regulating the voltage profile within the upper and lower regulatory limits during the entire period, demonstrating the effectiveness of the proposed scheme to be able to adapt the control settings to the changing grid conditions. The case was however different for the PV with fixed control parameters as there were voltage violations during the peak solar hours. Case study 2 demonstrated the robustness of the proposed control in dealing with unexpected changes on the grid such as changes in the R/X ratio, a 10% increase in load and PV output, and the disconnection of a PV unit. In all these changes, the proposed control operated successfully without any voltage violations for the entire period. The reason is that this control solely relies on measured variables at the PCC and is thus independent of other external factors on the power grid.

This proposed control is implementable in MV grids with limited or no communication facilities since it relies on locally measured variables and can therefore be utilised by distribution network engineers in Ghana. Although large networks with several PVs increase the complexity of developing this adaptive $Q(U)$ control, the emergence of powerful power flow simulation software and computers creates an opportunity for relatively easy development of the control.

Chapter 6 Conclusion and future outlook

6.1 Conclusion

There is a gradual attempt in Ghana to diversify the energy dependence from thermal and hydropower generation to photovoltaic and wind energy. One basis of this transition is the growing worldwide concerns about the emission of greenhouse gases from the burning of fossil fuels in thermal power generation. Another basis is to enhance the reliability and security of the supply as the output of hydropower is low during the dry season because of the long period of drought which affects the water level in the dam. Additionally, the West Africa Gas Pipeline, a pipeline linking gas generation from Nigeria to the thermal power plants in Ghana, has suffered interruptions in recent years mainly due to inadequate gas supply from Nigeria and a deficit in financial payment on the part of Ghana. To drive this transition, the Government has put in place initiatives to promote the adoption of RE sources including DGs.

Chapter 1 outlines the two main issues facing distribution networks in Ghana. These are summarised as follows.

- Low voltages during peak demand periods especially in the northern parts of Ghana.
- Limited communication facilities on the MV/LV distribution networks.

The expected integrations of DGs will improve the voltage profiles during the solar generation hours but on the other hand, will potentially create another voltage challenge (voltage rise phenomenon) because the peak solar hours coincide with the low demand periods in Ghana. An extensive review of voltage control in distribution networks in chapter 2 revealed that DGs have the potential to provide reactive power compensation to improve these voltage regulation challenges. Already, the national electricity grid code of Ghana allows for reactive power compensation from DGs to take part in voltage control in distribution networks as highlighted in chapter 3. Reactive power compensation in the form of local voltage control is easily implementable in distribution grids in Ghana because it relies solely on measurement variables at the PCC and therefore, requires no communication infrastructure on the grid.

Each local voltage control method has a varied impact on the grid performance. Hence, a comparative study was conducted between $Q(U)$ and $cos\varphi(P)$ local voltage control methods in chapter 3. The study revealed that better loss minimization and improved voltage profile were achieved with $Q(U)$ control than with the $cos\varphi(P)$ control. Thus, the $Q(U)$ control method is highly recommended for distribution networks in Ghana and is also the main focus of this research study. Notwithstanding the potential benefits of $Q(U)$ control, simulation results in chapter 4 revealed that the optimal performance of the $Q(U)$ control is dependent on the control parameters or characteristic curves. This was the case when fixed $Q(U)$ control parameters proposed by Mueller et al for German distribution networks were implemented on the 16-bus MV distribution network resulting in instances where the voltages were above the upper grid code limits, mostly during the peak solar generation hours. Hence, operating local voltage control methods with fixed control parameters will not always result in satisfactory voltage control performance.

To guarantee the optimal performance of the $Q(U)$ control, the reactive power compensation must adapt to the changing load and generation conditions in the grid. Therefore, this thesis proposed a $Q(U)$ control with incorporated adaptive functionality in chapter 4. This functionality is made up of voltage sensitivity and stability blocks. The sensitivity block generates the required amount of reactive power compensation based on voltage measurements and reactive power injection at the PCC. The voltage stability block ensures that the reactive power compensation being provided enhances the voltage stability index of the PCC bus. A detailed performance assessment of this proposed control shows its effectiveness in regulating the bus voltages during both peak demand and DG generation periods within the upper and lower grid code voltage limits. To further demonstrate the robustness of the proposed scheme, the line impedance is increased by 10% in addition to a simultaneous 10% increase in load and DG output. The results show that the proposed scheme was able to keep the voltages at the PCC buses of the DGs within the regulatory limits because the $Q(U)$ control was able to adapt to the changing grid conditions.

A two-stage design control approach to adapt the local control settings to the changing grid conditions was proposed in chapter 5. The first stage involves an optimization stage which determines the optimal parameters of the $Q(U)$ control that will enhance the voltage stability index and their corresponding Thevenin impedance determined by the Newton Raphson load flow method. The next stage involves developing a pattern or relationship between the control parameters and the Thevenin impedance using an artificial neural network.

Performance assessment of this two-stage design also showed its effectiveness in voltage regulation.

Both methods in chapters 4 and 5 achieved voltage regulation performances on the grid which are comparable to a centralised voltage control that uses communication facilities. However, there is a difference in both approaches. The method which incorporates the adaptive functionality of the $Q(U)$ only acts to compensate for the performance of the $Q(U)$ without changing the control parameters, while the two-stage approach on the other hand changes the control parameters of the control with the changing load and generation conditions. The adaptive functionality is easier to implement since it only involves load flow simulations as compared to the two-stage control which involves training of the neural network. However, the two-stage design approach is more robust to the grid conditions as compared to the $Q(U)$ control with adaptive functionality. This is because the latter uses voltage sensitivity which is very sensitive to topology changes in the grid as demonstrated in chapter 5 when a DG was disconnected, but the two-stage design approach was able to keep the voltage profiles within the grid code limits.

Both approaches rely on only measured variables at the PCC, thus it is easily implementable in Ghana where communication infrastructure in MV distribution networks is limited. Therefore, this presents an opportunity for planning engineers to efficiently utilize the reactive power resources of DGs to improve distribution grid performance (voltage regulation).

6.2 Future outlook

This research reveals the effectiveness of proposing an adaptive local voltage control method to regulate the voltages in the grid, especially during both the peak demand and solar hour periods using locally measured variables at the PCC. As each DG unit in this study operated autonomously, future studies should investigate whether the voltage control performance could be enhanced if the DGs are coordinated without using communication facilities and also the control interactions among the various control units. A possible coordination algorithm for the investigation is the use of a decentralised time-delay control. Another issue that arises is how to coordinate the proposed control with the existing voltage regulating devices like the on-load tap changer and voltage regulating devices. This is very essential since these voltage regulating devices must still control the voltages of buses with no DG integration. Lastly, these

works must be carried out and validated in realistic Ghanaian distribution networks.

Currently, in Ghana, there exists no framework or guideline for the planning of distribution networks with high penetration of distributed generation. Future works should investigate the major technical and economic components that must be incorporated into such a framework considering the nature of the Ghanaian power system network. Considering the challenge of insufficient reactive power provision in Ghana's distribution network, there is a need to investigate the possibility of allowing DGs integrated into the LV networks to take part in voltage control. This is because the current renewable energy code is only limited to MV grids. In drafting such a code, the strength of the network and the level of unbalance that pertains to the LV grid must be taken into consideration. This consideration is essential since active power curtailment might be more beneficial than reactive power compensation in weak LV distribution grids. This framework must also consider other emerging new devices such as battery energy storage which has the potential to further improve the voltage profiles, especially in the northern parts of the country.

List of Publications

Articles in international Journals

- D. O. Ampofo and J. M. A. Myrzik, “Autonomous adaptive Q (U) control for distributed generation in weak medium-voltage distribution grids,” IET Energy Syst. Integr., vol. 3, no. 2, pp. 158–171, 2021

Conference contributions, published in full in conference proceedings

- D. O. Ampofo, A. Abdelsamad, J. M. A. Myrzik, and M. W. Asmah, “Adaptive Q(U) Control using combined Genetic Algorithm and Artificial Neural Network,” in EPEC 2020; IEEE Electrical Power and Energy Conference, 2020, pp. 1–6.
- D. O. Ampofo, A. Abdelsamad, M. W. Asmah, and J. M. A. Myrzik, “A Strategy to Parameterize Q (U) Control to Enhance Voltage Stability using a Centralized Based Method,” in NEIS 2020; Conference on Sustainable Energy Supply and Energy Storage Systems, 2020, pp. 1–6.
- D. O. Ampofo and J. M. A. Myrzik, “A comparative study of different local reactive power control methods of distributed generation in Ghana,” in 2019 IEEE PES/IAS PowerAfrica, 2019.

Appendix

Appendix A: Medium Voltage Distribution Network Parameters

The base MVA of this 132/33 kV 16 bus distribution network is 100 MVA

Table A.1 Load data

Bus Number	Bus type	Load values	
		Active power (MW)	Reactive power (MVAr)
1	Slack	0	0
2	PV	5.41	1.09
3	PQ	1.93	0.39
4	PQ	0.06	0.01
5	PQ	18.4	3.74
6	PQ	1.96	0.4
7	PQ	1.9	0.39
8	PQ	0.55	0.11
9	PV	0	0
10	PQ	2.7	0.55
11	PQ	2.85	0.58
12	PQ	0.81	0.16
13	PQ	1.01	0.2
14	PQ	0.58	0.12
15	PQ	0	0
16	PQ	0	0

Table A.2 Transformer parameters

From bus	To bus	Transformer parameters				
		Rating (MVA)	Reactance (p.u.)	Susceptance (p.u.)	Maximum tap position (p.u.)	Minimum tap position (p.u.)
1	2	60	0	0.125	1.05	0.85
8	9	15	0.0728	0.1039	1.05	0.85

Table A.3 Transmission line parameters

From bus	To bus	Line parameters			
		Resistance (p.u.)	**Reactance (p.u.)**	**Susceptance (p.u.)**	**Length (Km)**
2	3	0.198	0.446	0	12.05
2	4	0.187	0.299	0	18.48
3	4	0.216	0.287	0	8.79
4	5	0.0305	0.029	0.0015	2.055
4	6	0.517	0.376	0	10.53
6	7	0.394	0.348	0	10.15
4	8	0.441	0.392	0.007	16.45
9	10	0.538	0.733	0	22.28
10	11	0.944	0.657	0	19.05
10	12	1.59	1.21	0.001	32.79
2	13	0.213	0.284	0	8.69
2	14	0.506	0.532	0.002	17.18
13	15	0.265	0.281	0.001	8.76
15	14	0.4	0.291	0	8.16
15	16	0.401	0.292	0	8.19

Appendix B: Solar module characteristics

Table B.1 Solar module characteristics [86]

Parameter	**Value**	**Unit**
Solar irradiance at STC	1000	w/m^2
Open circuit voltage	2.98	V
Short circuit current	5.32	A
Voltage at maximum power	17.32	V
Current at maximum power	4.76	A
Voltage temperature coefficients	14.4	mV/℃
Current temperature coefficients	1.22	mA/℃
Nominal cell operating temperature	43	℃

Appendix C: PV output profiles for the three seasons

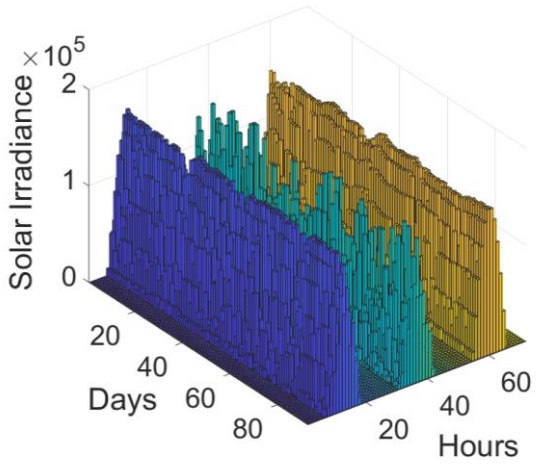

Figure C.1 PV profile for the three seasons (dry, rainy and harmattan). Each season is represented by 31 days, thus making a total of 93 days. The dry, rainy and harmattan seasons are represented as blue, green and yellow respectively.

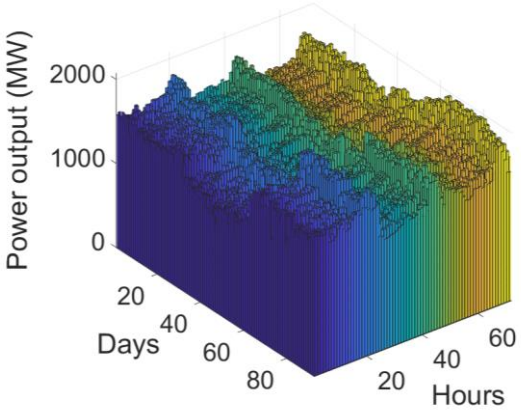

Figure C.2 load profile for the three seasons (dry, rainy and harmattan). Each season is represented by 31 days, thus making a total of 93 days. The dry, rainy and harmattan seasons are represented as blue, green and yellow respectively.

Appendix D: Mean and standard deviation of PV output

Table C.1 Mean and standard deviation of PV output

Hour	Rainy season (August)		Dry season (January)		Harmattan (December)	
	Mean (p.u.)	Standard deviation(p.u.)	Mean (p.u.)	Standard deviation(p.u.)	Mean (p.u.)	Standard deviation(p.u.)
1	0	0	0	0	0	0
2	0	0	0	0	0	0
3	0	0	0	0	0	0
4	0	0	0	0	0	0
5	0	0	0	0	0	0
6	0	0	0	0	0	0
7	0.03738227	0.032006397	0.04327586	0.02460387	0.06643	0.019539278
8	0.11969456	0.073673285	0.18251876	0.086466109	0.226708	0.076786629
9	0.2362109	0.099813404	0.36471592	0.151057316	0.415809	0.110941343
10	0.34998082	0.138592348	0.55836273	0.175293126	0.583372	0.154101813
11	0.43129942	0.165275371	0.73176542	0.192989878	0.747147	0.14112611
12	0.55245931	0.182402533	0.84558012	0.172367919	0.854905	0.109576718
13	0.55613545	0.193883087	0.87082569	0.166879466	0.845197	0.110564329
14	0.45399957	0.191030046	0.78721509	0.187626073	0.751683	0.109689358
15	0.41639926	0.169646229	0.63946995	0.183203916	0.595183	0.099767777
16	0.26323852	0.135773948	0.40842963	0.175305607	0.389401	0.105770725
17	0.15686057	0.102354302	0.21061039	0.101464981	0.178188	0.059748042
18	0.04700098	0.026651355	0.03638312	0.023520697	0.00261	0.005636486
19	0	0	0	0	0	0
20	0	0	0	0	0	0
21	0	0	0	0	0	0
22	0	0	0	0	0	0
23	0	0	0	0	0	0
24	0	0	0	0	0	0

NB: The base value is 166.819 kW

Appendix E: Voltage profiles for Cosφ(P) and Q(U) control

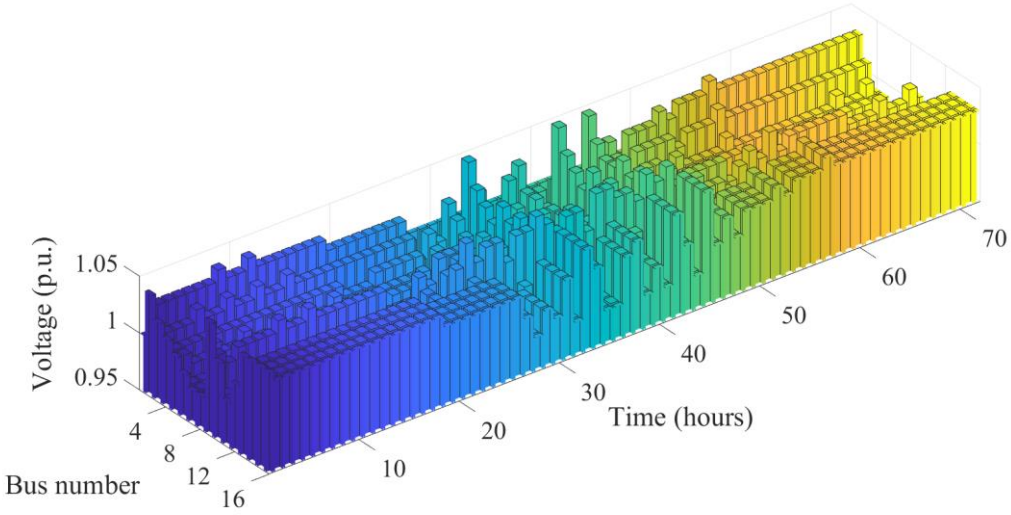

Figure E.1 Voltage profiles for the 16 buses for Q(U) method for the entire 72 hour period

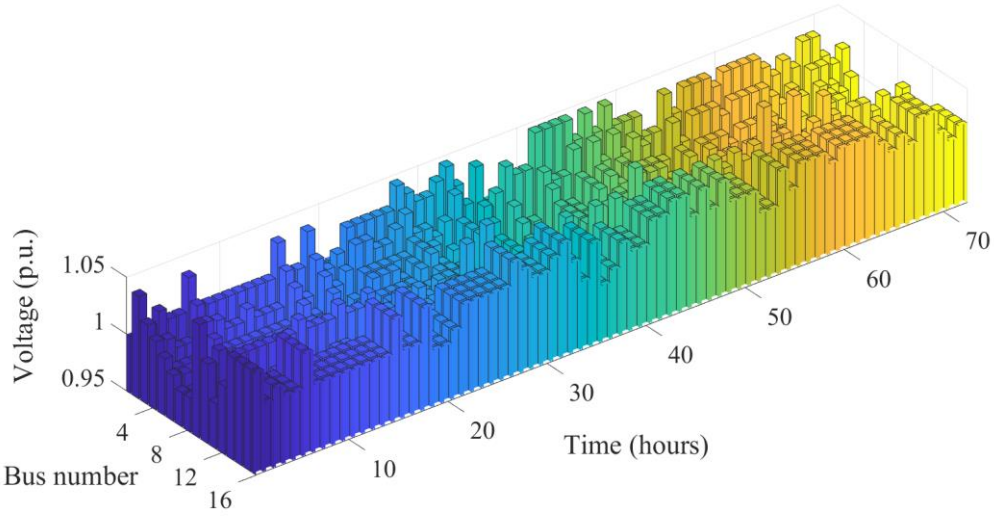

Figure E.2 Voltage profiles for the 16 buses for Cosφ(P) control method for the entire 72 hour period

Appendix F: Validation of Tellegen's theorem

According Tellegen's theorem, the summation of power at any time for any branch in an electrical circuit which is linear or non-linear, reciprocal or non-reciprocal, time invariant or time variant is zero, i.e.

$$\sum_{b=1}^{n} u_b i_b = 0 \qquad \text{F.1}$$

Where u_b and i_b are the instantaneous power voltage and current in each branch for a total of n branches in a circuit.

To explain this theorem, consider the circuit shown in figure below with u_1, u_2 and u_3 being the voltage for node 1, 2 and 3 respectively.

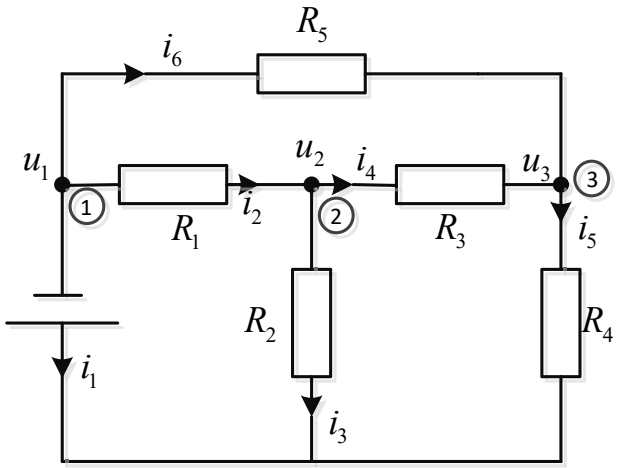

The summation of instantaneous power in the branches is expressed as

$$\sum_{b=1}^{n} u_b i_b = u_1 i_1 + u_{R1} i_2 + u_{R2} i_3 + u_{R3} i_4 + u_{R4} i_5 + u_{R5} i_6 \qquad \text{F.2}$$

Where u_{R1}, u_{R2}, u_{R3}, u_{R4} and u_{R5} are the voltages across R_1, R_2, R_3, R_4 and R_5.

Equation (F.2) can be written and simplified as (F.3) and (F.4);

$$\sum_{b=1}^{n} u_b i_b = u_1 i_1 + (u_1 - u_2) i_2 + u_2 i_3 + (u_2 - u_3) i_4 + u_3 i_5 + (u_1 - u_3) i_6 \qquad \text{F.3}$$

$$\sum_{b=1}^{n} u_b i_b = u_1 (i_1 + i_2 + i_6) + u_2 (-i_2 + i_3 + i_4) + u_3 (i_5 - i_4 - i_6) \qquad \text{F.4}$$

Applying Kirchhoff's current law to node 1, 2 and 3 reveals that $(i_1 + i_2 + i_6) = 0, (-i_2 + i_3 + i_4) = 0$ and $(i_5 - i_4 - i_6)$=0.

Thus equation (F.4) reduces to

$$\sum_{b=1}^{n} u_b i_b = 0 \qquad \text{F.5}$$

Equation (F.5) thus verify the theorem.

Appendix G: Backward propagation algorithm

The backward propagation algorithm which is used in adjusting the weights in neural network are therefore described as follows [143], [144].

Step 1: The algorithm assumes a random number for weights.

Step 2: The network's output vector is represented as $[y_1, y_2, \dots, y_n]$ and input vector is $[x_1, x_2, \dots, x_n]$. To differentiate between the connection weights in the ANN structure, w_{ij} and v_{ij} are the connection weight values between the i^{th} and j^{th} neutron (or node) of the hidden layer and output layer respectively. Therefore, the output of a node in the output layer is expressed mathematically as (E.1).

$$y_i = f\left(\sum_j^n v_{ij} * h_i\right) = f(y_i^{net}) \qquad \text{G. 1}$$

Where h_i is the hidden layer.

The output of the hidden layer (h_i) is expressed in (G.2).

$$h_i = f\left(\sum_j^n w_{ij} * x_i\right) = f(h_i^{net}) \qquad \text{G. 2}$$

Step 3: The root mean square error signal (E) is calculated for the output layer using (G.3).

$$E = 0.5 \sum_i (d_i - y_i)^2 = 0.5 * \sum_i (d_i - f\left(\sum_j^n w_{ij} * h_i\right))^2 \qquad \text{G. 3}$$

Where d is a vector of the desired output. The ideal situation is when the network's output is identical to the desired output, resulting in a E value of zero.

Step 4: Once the network output is determined, the error term is calculated for each node (neuron) using the gradient descent method. For the output layer, the derivative of the error function with respect to the connection weight is given by;

$$\frac{\partial E}{\partial v_{ij}} = \sum_{k=1}^{n} \frac{\partial E}{\partial y_k} * \frac{\partial y_k}{\partial v_{ij}} = \frac{\partial E}{\partial y_i} * \frac{\partial y_i}{\partial v_{ij}} \qquad \text{G. 4}$$

The error E is a function of y_k made up of several y_i, with only one y_i being related to v_{ij}. The individual y_is are independent of one another each other.

Inserting in (E.3) into (E.4) and taking the partial derivative $\partial E/\partial y_i$ results in (G.5).

$$\frac{\partial E}{\partial y_i} = 0.5 \sum_k \left[-2(d_k - y_k) * \frac{\partial y_k}{\partial y_i}\right] = -(d_i - y_i) \quad \text{G.5}$$

Inserting in (5.1) into (5.4) and taking the partial derivative $\partial y_i/\partial v_{ij}$ results in (5.6)

$$\frac{\partial y_i}{\partial v_{ij}} = \frac{\partial y_i}{\partial y_i^{net}} * \frac{\partial y_i^{net}}{\partial v_{ij}} = f'(y_i^{net}) * h_i \quad \text{G.6}$$

Thus,

$$\frac{\partial E}{\partial v_{ij}} = -(d_i - y_i) * f'(y_i^{net}) * h_i \quad \text{G.7}$$

If an error term, δ_i is defined for each node in the output layer as expressed in (G.8).

$$\delta_i = (d_i - y_i) * f'(y_i^{net}) \quad \text{G.8}$$

Then,

$$\frac{\partial E}{\partial v_{lj}} = -\delta_i * h_i \quad \text{G.9}$$

Step 5: Next the derivative of the error function for the hidden layer is calculated. The derivative of the error function is given by,

$$\frac{\partial E}{\partial w_{ij}} = \sum_i \sum_j \frac{\partial E}{\partial y_i} * \frac{\partial y_i}{\partial h_j} * \frac{\partial h_j}{\partial w_{ij}} \quad \text{G.10}$$

The error E is a function made of several y_i for a specific w_{ij}, corresponding to a particular h_i. Taking the partial derivatives $\partial E/\partial y_i$, $\partial y_i/\partial h_j$ and $\partial h_j/\partial w_{ij}$ results in (G.11), (G.12) and (G.13) respectively.

$$\frac{\partial E}{\partial y_i} = 0.5 \sum_k \left[-2(d_k - y_k) * \frac{\partial y_k}{\partial y_i}\right] = -(d_i - y_i) \quad \text{G.11}$$

$$\frac{\partial y_i}{\partial h_j} = f'(y_i^{net}) * v_{ij} \quad \text{G.12}$$

$$\frac{\partial h_j}{\partial w_{ij}} = f'(h_i^{net}) * x_i \quad \text{G.13}$$

Then inserting (G.11), (G.12) and (G.13) into (G.10) results in (G.14).

$$\frac{\partial E}{\partial w_{ij}} = -\sum_i (d_i - y_i) * f'(y_i^{net}) * v_{ij} * f'(h_i^{net}) * x_i \quad \text{G. 14}$$

Substituting (G.8) into (G.14) results in (G.15).

$$\frac{\partial E}{\partial w_{ij}} = -\sum_i \delta_i v_{ij} f'(h_i^{net}) * x_i \quad \text{G. 15}$$

If an error term, δ_i' is defined for each node in the output layer as expressed in (G.16).

$$\delta_i' = f'(h_i^{net}) * \sum_i \delta_l v_{ij} \quad \text{G. 16}$$

Then,

$$\frac{\partial E}{\partial w_{ij}} = -\delta_i' * x_i \quad \text{G. 17}$$

Step 6: The modification factors Δv_{ij} and Δw_{ij} are calculated as expressed in (G.18) and (G.19) for both the hidden and output layer respectively

$$\Delta v_{ij} = -\eta \frac{\partial E}{\partial v_{ij}} = \eta \delta_i * h_i \quad \text{G. 18}$$

$$\Delta w_{ij} = -\eta \frac{\partial E}{\partial w_{ij}} = \eta \delta_i' * x_i \quad \text{G. 19}$$

Where η is learning rate, a constant predefined before stating the ANN process.

Appendix H: Error histogram and regression plots for neural networks training

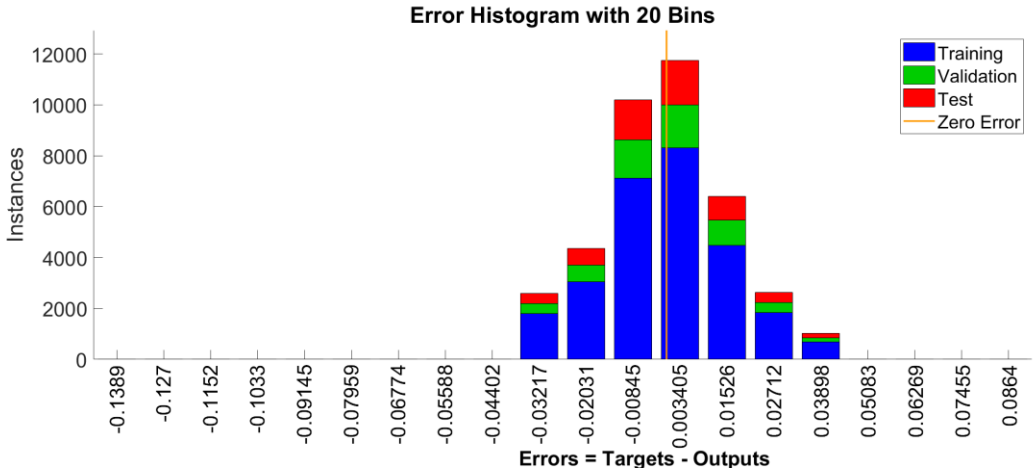

Figure H.1 Error histogram plot for bus Q(U) control at bus 10

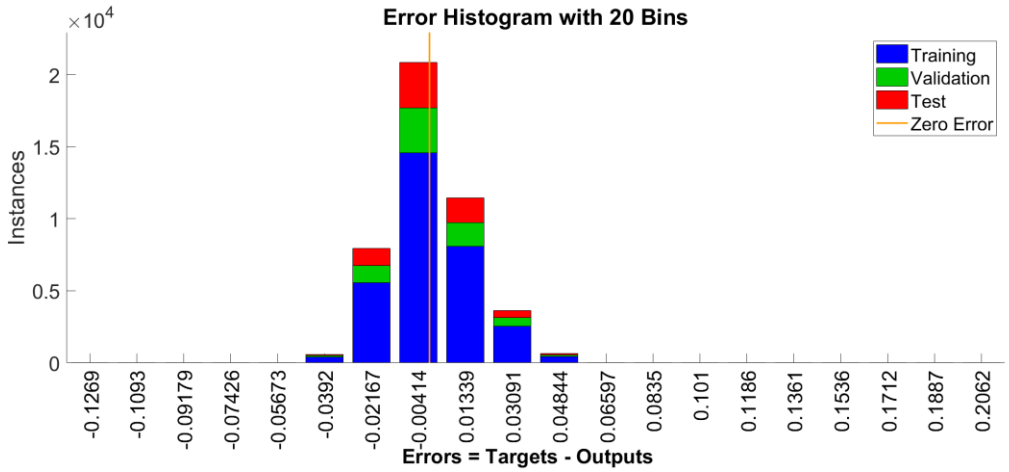

Figure H.2 Error histogram plot for bus Q(U) control at bus 11

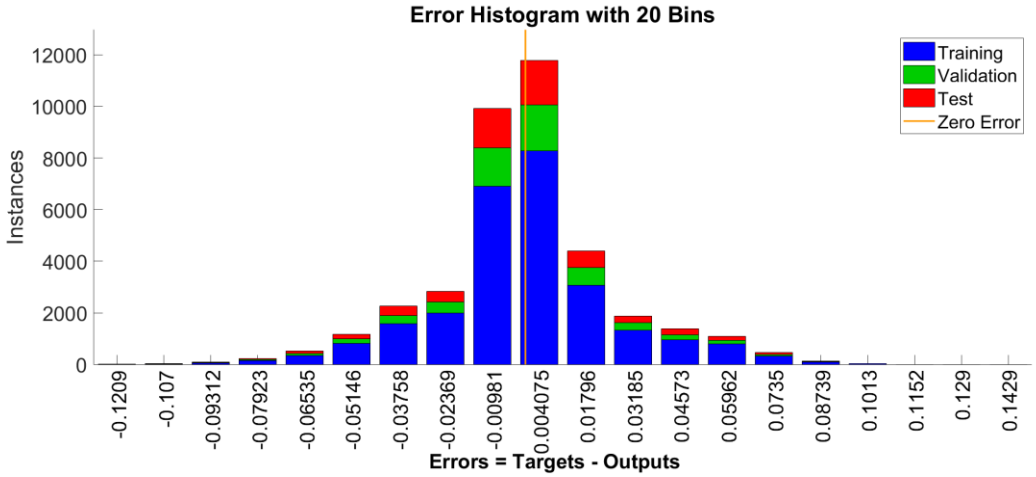

Figure H.3 Error histogram plot for bus Q(U) control at bus 16

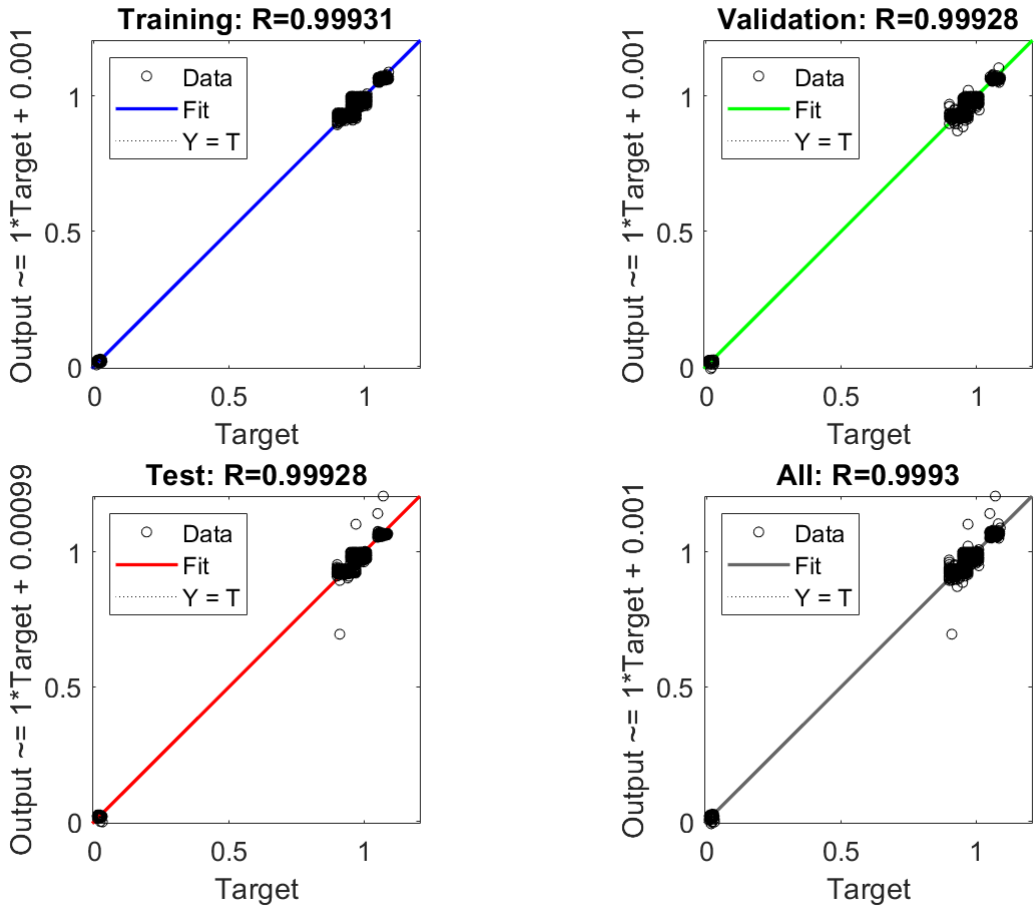

Figure H.4 Regression plot for bus Q(U) control at bus 11

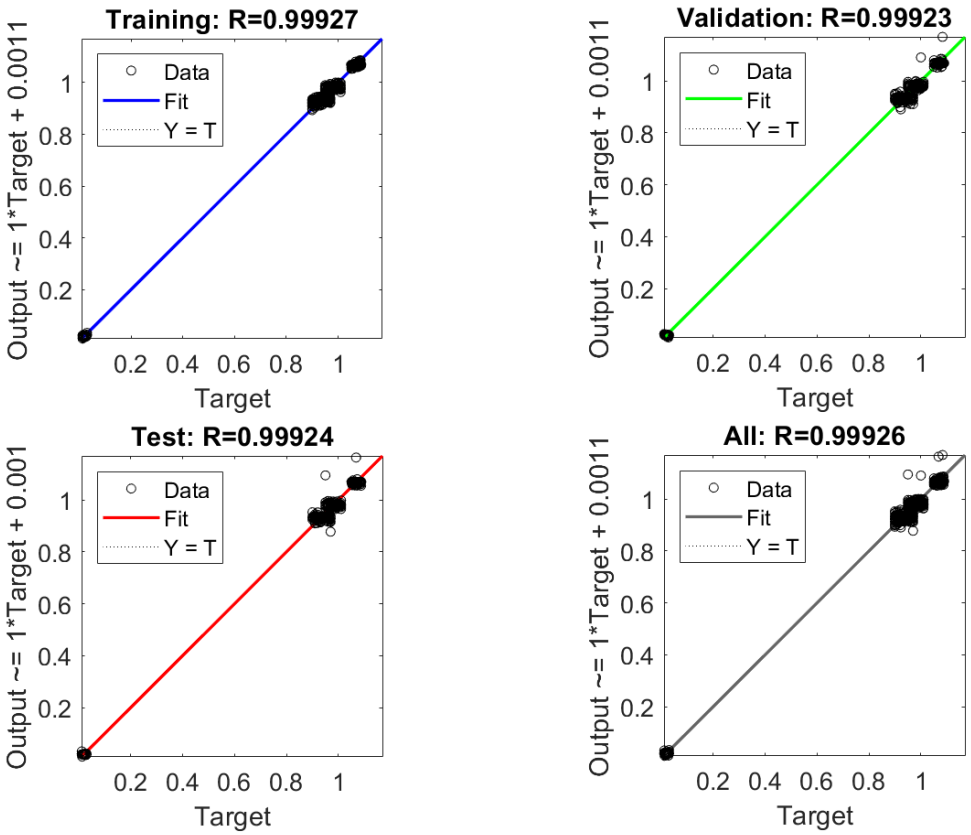

Figure H.5 Regression plot for bus Q(U) control at bus 10

References

[1] United Nations Framework Convention on Climate Change, “Paris Agreement.” Accessed: Jan. 25, 2021. [Online]. Available: https://unfccc.int/sites/default/files/english_paris_agreement.pdf.

[2] M. Z. Jacobson *et al.*, “100% clean and renewable wind, water, and sunlight all-sector energy roadmaps for 139 countries of the world,” *Joule*, vol. 1, no. 1, pp. 108–121, 2017.

[3] IRENA, “Global energy transformation: A roadmap to 2050,” 2018. Accessed: Jan. 26, 2021. [Online]. Available: https://www.irena.org/-/media/Files/IRENA/Agency/Publication/2018/Apr/IRENA_Report_GET_2018.pdf.

[4] EEG 2017, “Renewable Energy Sources Act.” Accessed: Jan. 26, 2021. [Online]. Available: https://www.bmwi.de/Redaktion/EN/Downloads/renewable-energy-sources-act-2017.pdf%3F__blob%3DpublicationFile%26v%3D3.

[5] Department of Business Energy and Industrial Strategy, “UK Energy in Brief,” 2020. Accessed: Jan. 26, 2021. [Online]. Available: https://assets.publishing.service.gov.uk/government/uploads/system/uploads/attachment_data/file/857027/UK_Energy_in_Brief_2019.pdf.

[6] Office of Gas and Electricity Markets, “Feed-in-Tariff (FIT) scheme.” https://www.ofgem.gov.uk/environmental-programmes/fit (accessed Jan. 26, 2021).

[7] IPCC (Intergovernmental Panel on Climate Change), “Global Warming of 1.5 °C, An IPCC Special Report on the impacts of global warming of 1.5 °C above pre-industrial levels and related global greenhouse gas emission pathways, in the context of strengthening the global response to the threat of climate chang.” Accessed: Jan. 26, 2021. [Online]. Available: https://www.ipcc.ch/sr15/.

[8] International Energy Agency, “World Energy Outlook 2019.” Accessed: Jan. 26, 2021. [Online]. Available: https://www.iea.org/reports/world-energy-outlook-2019.

[9] Energy Commission Ghana, “National Energy Statistics 2000-2019.” Accessed: Jan. 26, 2021. [Online]. Available: http://www.energycom.gov.gh/files/2020 ENERGY STATISTICS-revised.pdf.

[10] Energy Commission Ghana, “2020 Electricity Supply Plan for the Ghana Power System.” Accessed: Jan. 27, 2021. [Online]. Available: http://www.energycom.gov.gh/files/2020 Electricity Supply Plan.pdf.

[11] Energy Commission Ghana, “2019 Energy (Supply And Demand)Outlook For Ghana.” Accessed: Jan. 26, 2021. [Online]. Available: http://www.energycom.gov.gh/planning/data-center/energy-outlook-for-ghana.

[12] M. W. Asmah, J. Myrzik, and B. K. Ahunu, “Challenges in the Ghanaian

power system: the prospects of renewable energy sources," in *AFRICON 2015*, 2015, pp. 1–5.

[13] Energy Commission Ghana, "Strategic National Energy Plan 2006-2020." Accessed: Jan. 27, 2021. [Online]. Available: http://www.energycom.gov.gh/planning/snep.

[14] H. Yakubu, "National renewable energy report," Energy Commission, Accra, Ghana, Tech. Rep., Jan. 2014. Accra.

[15] Energy Commission, "Ghana: Sustainable Action for All, Action Plan," 2012. Accessed: Feb. 03, 2021. [Online]. Available: http://www.energycom.gov.gh/renewables/se4all.

[16] Parliament of the Republic of Ghana, Renewable Energy Act 2011. Ghana, 2011, Ghana, 2011, Act 832. GPCL/A663/350/12/2011.

[17] T. Ackermann, G. Andersson, and L. Söder, "Distributed generation: a definition," *Electr. power Syst. Res.*, vol. 57, no. 3, pp. 195–204, 2001.

[18] Power Systems Energy Consulting and Ghana Grid Company Limited, "Ghana Wholesale Power Reliablity Assessment 2010." Accessed: Feb. 03, 2021. [Online]. Available: http://www.ecowrex.org/system/files/repository/2010_ghana-wholesale-power-reliability-assessment-gridco.pdf.

[19] M. W. Asmah, J. M. A. Myrzik, and B. K. Ahunu, "Power system expansion using renewable energy sources in Ghana," in *2015 50th International Universities Power Engineering Conference (UPEC)*, 2015, pp. 1–6.

[20] Ministry of Energy-Ghana, "Power Distribution System Master Plan Study for Ghana." Accessed: Aug. 27, 2021. [Online]. Available: https://openjicareport.jica.go.jp/pdf/11897832.pdf.

[21] Tractebel Engineering GDF SUEZ, "Transmission System Master Plan for Ghana," Ghana Grid Company, Accra, Ghana, Final Rep., GH-GRID/4NT/195162/000/01, Feb.201.

[22] USAID and Energy Commission Ghana, "Integrated Power System Master Plan for Ghana Volume 3 (2018)." Accessed: Feb. 03, 2021. [Online]. Available: http://www.energycom.gov.gh/planning/ipsmp/ipsmp-2018.

[23] USAID and Energy Commission Ghana, "Integrated Power System Master Plan for Ghana (2019) Volume 2," 2019. Accessed: Feb. 03, 2021. [Online]. Available: http://www.energycom.gov.gh/planning/ipsmp/ipsmp-2019.

[24] Energy Commission Ghana, "Renewable Energy Sub-Code for DistributionNetwork connected Variable Renewable Energy Power Plants in Ghana." Accessed: Feb. 01, 2021. [Online]. Available: http://energycom.gov.gh/regulation/renewable-energy-grid-sub-codes.

[25] H. Ji *et al.*, "A centralized-based method to determine the local voltage control strategies of distributed generator operation in active distribution networks," *Appl. Energy*, vol. 228, pp. 2024–2036, 2018.

[26] G. Pepermans, J. Driesen, D. Haeseldonckx, R. Belmans, and W. D'haeseleer, "Distributed generation: definition, benefits and issues," *Energy Policy*, vol. 33, no. 6, pp. 787–798, 2005.

[27] Ministry of Energy, "Ghana Renewable Energy Master Plan," *2019*. http://energycom.gov.gh/rett/documents-downloads/category/29-re-master-plan (accessed Jan. 27, 2021).

[28] Distributed Generation and Sustainable Electrical Energy Centre, "United Kingdom generic distribution system (UKGDS)." http://github.com/sedg/ukgds. (accessed Feb. 01, 2016).

[29] M. J. Chihota, B. Bekker, and C. T. Gaunt, "Technical assessment of the impacts of distributed energy resources on distribution feeders," in *Uncertainties in Modern Power Systems*, Elsevier, 2021, pp. 397–439.

[30] T. Adefarati and R. C. Bansal, "Reliability assessment of distribution system with the integration of renewable distributed generation," *Appl. Energy*, vol. 185, pp. 158–171, 2017.

[31] M. J. H. Moghaddam, A. Kalam, J. Shi, S. A. Nowdeh, F. H. Gandoman, and A. Ahmadi, "A new model for reconfiguration and distributed generation allocation in distribution network considering power quality indices and network losses," *IEEE Syst. J.*, vol. 14, no. 3, pp. 3530–3538, 2020.

[32] K. Kawabe and K. Tanaka, "Impact of dynamic behavior of photovoltaic power generation systems on short-term voltage stability," *IEEE Trans. Power Syst.*, vol. 30, no. 6, pp. 3416–3424, 2015.

[33] S. Hashemi and J. Østergaard, "Methods and strategies for overvoltage prevention in low voltage distribution systems with PV," *IET Renew. power Gener.*, vol. 11, no. 2, pp. 205–214, 2016.

[34] T. Stetz, F. Marten, and M. Braun, "Improved low voltage grid-integration of photovoltaic systems in Germany," *IEEE Trans. Sustain. energy*, vol. 4, no. 2, pp. 534–542, 2012.

[35] Volta River Authority-Northern Electricity Department, "NEDCo Business Plan Presentation 2013." Accessed: Apr. 23, 2021. [Online]. Available: http://www.nedcogh.com/annual_reports.php.

[36] S. Maharjan, A. M. Khambadkone, and J. C.-H. Peng, "Integration of Centralized and Local Voltage Control Scheme in Distribution Network to Reduce the Operation of Mechanically Switched Devices," 2019.

[37] E. Liu and J. Bebic, "Distribution System Voltage Performance Analysis for High-Penetration Photovoltaics," 2008. Accessed: Feb. 18, 2021. [Online]. Available: https://www.nrel.gov/docs/fy08osti/42298.pdf.

[38] K. Turitsyn, P. Sulc, S. Backhaus, and M. Chertkov, "Options for control of reactive power by distributed photovoltaic generators," *Proc. IEEE*, vol. 99, no. 6, pp. 1063–1073, 2011.

[39] K. Turitsyn, P. Šulc, S. Backhaus, and M. Chertkov, "Distributed control of reactive power flow in a radial distribution circuit with high photovoltaic penetration," in *IEEE PES general meeting*, 2010, pp. 1–6.

[40] K. E. Antoniadou-Plytaria, I. N. Kouveliotis-Lysikatos, P. S. Georgilakis, and N. D. Hatziargyriou, "Distributed and decentralized voltage control of smart distribution networks: Models, methods, and future research," *IEEE Trans. Smart Grid*, vol. 8, no. 6, pp. 2999–3008, 2017.

[41] N. Mahmud and A. Zahedi, "Review of control strategies for voltage regulation of the smart distribution network with high penetration of

renewable distributed generation," *Renew. Sustain. Energy Rev.*, vol. 64, pp. 582–595, 2016.

[42] J. Dong, Y. Xue, M. Olama, T. Kuruganti, J. Nutaro, and C. Winstead, "Distribution Voltage Control: Current Status and Future Trends," in *2018 9th IEEE International Symposium on Power Electronics for Distributed Generation Systems (PEDG)*, 2018, pp. 1–7.

[43] Energy Commission, "National electricity grid code." Accessed: Feb. 05, 2017. [Online]. Available: http://www.energycom.gov.gh/files/National Electricity Grid Code.pdf.

[44] B. Green, "Grid strategy 2011: Conservation voltage reduction and volt var optimization in the smart grid," Electric Power Research Institude, Tech. Rep (2011).

[45] M. Madrigal, R. Uluski, and K. M. Gaba, *Practical Guidance for Defining a Smart Grid Modernization Strategy: The Case of Distribution (Revised Edition)*. World Bank Publications, 2017.

[46] V. C. Strezoski, N. A. Katic, and D. S. Janjic, "Voltage control integrated in distribution management system," *Electr. Power Syst. Res.*, vol. 60, no. 2, pp. 85–97, 2001.

[47] G. Valverde and T. Van Cutsem, "Model Predictive Control of Voltages in Active Distribution Networks," *IEEE Trans. Smart Grid*, vol. 4, no. 4, pp. 2152–2161, Dec. 2013.

[48] Y. Mavrocostanti and J. Berry, "Implementation and trial of centralised voltage control in 33kV and 11kV electricity distribution networks," in 25th International Conference on Electricity Distribution Conference, 2019.

[49] Z. Wang, H. Chen, J. Wang, and M. Begovic, "Inverter-Less Hybrid Voltage/Var Control for Distribution Circuits With Photovoltaic Generators," *IEEE Trans. Smart Grid*, vol. 5, no. 6, pp. 2718–2728, 2014.

[50] M. S. El Moursi, H. H. Zeineldin, J. L. Kirtley, and K. Alobeidli, "A Dynamic Master/Slave Reactive Power-Management Scheme for Smart Grids With Distributed Generation," *IEEE Trans. Power Deliv.*, vol. 29, no. 3, pp. 1157–1167, Jun. 2014.

[51] G. C. Kryonidis, C. S. Demoulias, and G. K. Papagiannis, "A new voltage control scheme for active medium-voltage (MV) networks," *Electr. Power Syst. Res.*, vol. 169, pp. 53–64, 2019.

[52] H. Sun *et al.*, "Review of challenges and research opportunities for voltage control in smart grids," *IEEE Trans. Power Syst.*, vol. 34, no. 4, pp. 2790–2801, 2019.

[53] H. Shahbazi and F. Karbalaei, "Decentralized Voltage Control of Power Systems Using Multi-Agent Systems," *J. Mod. Power Syst. Clean Energy*, vol. 8, no. 2, pp. 249–259, 2020.

[54] A. Bernstein, L. Reyes-Chamorro, J.-Y. Le Boudec, and M. Paolone, "A composable method for real-time control of active distribution networks with explicit power setpoints. Part I: Framework," *Electr. Power Syst. Res.*, vol. 125, pp. 254–264, 2015.

[55] L. Reyes-Chamorro, A. Bernstein, J.-Y. Le Boudec, and M. Paolone, "A composable method for real-time control of active distribution networks with explicit power setpoints. Part II: Implementation and validation,"

Electr. Power Syst. Res., vol. 125, pp. 265–280, 2015.

[56] O. Olatunde, M. Y. Hassan, M. P. Abdullah, and H. A. Rahman, "Real-time multiperiod voltage control algorithm with OLTC and switched capacitors for smart distribution networks in the presence of energy storage system," *Int. Trans. Electr. Energy Syst.*, vol. 30, no. 9, p. e12475, 2020.

[57] N. Yorino, Y. Zoka, M. Watanabe, and T. Kurushima, "An Optimal Autonomous Decentralized Control Method for Voltage Control Devices by Using a Multi-Agent System," *IEEE Trans. Power Syst.*, vol. 5, no. 30, pp. 2225–2233, 2015.

[58] F. Olivier, P. Aristidou, D. Ernst, and T. Van Cutsem, "Active Management of Low-Voltage Networks for Mitigating Overvoltages Due to Photovoltaic Units," *IEEE Trans. Smart Grid*, vol. 7, no. 2, pp. 926–936, 2016.

[59] P. N. Vovos, A. E. Kiprakis, A. R. Wallace, and G. P. Harrison, "Centralized and distributed voltage control: Impact on distributed generation penetration," *IEEE Trans. power Syst.*, vol. 22, no. 1, pp. 476–483, 2007.

[60] E. Demirok, P. C. González, K. H. B. Frederiksen, D. Sera, P. Rodriguez, and R. Teodorescu, "Local Reactive Power Control Methods for Overvoltage Prevention of Distributed Solar Inverters in Low-Voltage Grids," *IEEE J. Photovoltaics*, vol. 1, no. 2, pp. 174–182, 2011.

[61] M. Zeraati, M. E. H. Golshan, and J. M. Guerrero, "A Consensus-Based Cooperative Control of PEV Battery and PV Active Power Curtailment for Voltage Regulation in Distribution Networks," *IEEE Trans. Smart Grid*, vol. 10, no. 1, pp. 670–680, 2019.

[62] A. O'Connell and A. Keane, "Volt–var curves for photovoltaic inverters in distribution systems," *IET Gener. Transm. Distrib.*, vol. 11, no. 3, pp. 730–739, 2017.

[63] S. Maharjan, A. M. Khambadkone, and J. C. Peng, "Robust Constrained Model Predictive Voltage Control in Active Distribution Networks," *IEEE Trans. Sustain. Energy*, p. 1, 2020.

[64] Y. Xu, Z. Y. Dong, R. Zhang, and D. J. Hill, "Multi-Timescale Coordinated Voltage/Var Control of High Renewable-Penetrated Distribution Systems," *IEEE Trans. Power Syst.*, vol. 32, no. 6, pp. 4398–4408, Nov. 2017.

[65] H. S. Bidgoli and T. Van Cutsem, "Combined Local and Centralized Voltage Control in Active Distribution Networks," *IEEE Trans. Power Syst.*, vol. 33, no. 2, pp. 1374–1384, Mar. 2018.

[66] S. Karagiannopoulos, P. Aristidou, and G. Hug, "Hybrid approach for planning and operating active distribution grids," *IET Gener. Transm. Distrib.*, vol. 11, no. 3, pp. 685–695, 2017.

[67] M. Bello, D. Montenegro-Martinez, B. York, and J. Smith, "Optimal settings for multiple groups of smart inverters on secondary systems using autonomous control," *IEEE Trans. Ind. Appl.*, vol. 54, no. 2, pp. 1218–1223, 2017.

[68] P. Li, C. Zhang, X. Fu, G. Song, C. Wang, and J. Wu, "Determination of Local Voltage Control Strategy of Distributed Generators in Active

Distribution Networks Based on Kriging Metamodel," *IEEE Access*, vol. 7, pp. 34438–34450, 2019.

[69] E. Demirok, D. Sera, P. Rodriguez, and R. Teodorescu, "Enhanced local grid voltage support method for high penetration of distributed generators," in *IECON 2011 - 37th Annual Conference of the IEEE Industrial Electronics Society*, 2011, pp. 2481–2485.

[70] R. Heidari, M. M. Seron, and J. H. Braslavsky, "A Decentralised Adaptive Voltage Droop Control for Inverters in Power Distribution Networks," in *2018 IEEE PES Asia-Pacific Power and Energy Engineering Conference (APPEEC)*, 2018, pp. 577–582.

[71] E. K. Anto, P. Y. Okyere, and E. A. Frimpong, "Impact Assessment of Increasing Solar PV Penetrations on Voltage and Total Harmonic Distortion of a Distribution Network," *J. Multidiscip. Eng. Sci. Stud.*, vol. 1, no. 2, 2015.

[72] E. A. Kwofie, E. K. Anto, and G. Mensah, "Determination of the Optimal DG PV Interconnection Location Using Losses and Voltage Regulation as Assessment Indicators Case Study: ECG 33 kV Sub-Transmission Network," *Int. J. Energy Power Eng.*, vol. 11, no. 1, pp. 12–22, 2016.

[73] E. A. Kwofie, G. Mensah, and V. S. Antwi, "Post Commission Grid Impact Assessment of a 20 MWp Solar PV Grid Connected System on the ECG 33 kV Network in Winneba," in *2019 IEEE PES/IAS PowerAfrica*, 2019, pp. 521–526.

[74] E. A. Kwofie, G. Mensah, and E. K. Anto, "Determination of the Optimal power factor at which DG PV should be Operated," in *2017 IEEE PES PowerAfrica*, 2017, pp. 391–395.

[75] Energy Commission Ghana, "Renewable Energy Sub-Code for NITS connected Variable Renewable Energy Power Plants in Ghana," 2015. Accessed: Feb. 03, 2021. [Online]. Available: http://energycom.gov.gh.

[76] B. Nasiri, C. Wagner, U. Häger, and C. Rehtanz, "Distribution grid planning considering smart grid technologies," *CIRED - Open Access Proc. J.*, vol. 2017, no. 1, pp. 2228–2232, 2017.

[77] M. Aien, A. Hajebrahimi, and M. Fotuhi-Firuzabad, "A comprehensive review on uncertainty modeling techniques in power system studies," *Renew. Sustain. Energy Rev.*, vol. 57, pp. 1077–1089, 2016.

[78] L. A. Zadeh, "Fuzzy sets as a basis for a theory of possibility," *Fuzzy Sets Syst.*, vol. 100, pp. 9–34, 1999.

[79] A. Soroudi, M. Ehsan, R. Caire, and N. Hadjsaid, "Possibilistic evaluation of distributed generations impacts on distribution networks," *IEEE Trans. power Syst.*, vol. 26, no. 4, pp. 2293–2301, 2011.

[80] A. Soroudi, "Possibilistic-Scenario Model for DG Impact Assessment on Distribution Networks in an Uncertain Environment," *IEEE Trans. Power Syst.*, vol. 27, no. 3, pp. 1283–1293, 2012.

[81] A. Soroudi and T. Amraee, "Decision making under uncertainty in energy systems: State of the art," *Renew. Sustain. Energy Rev.*, vol. 28, pp. 376–384, 2013.

[82] H. Hernandez, "Multivariate probability theory: Determination of probability density functions," *ForsChem Res. Reports*, vol. 13, 2017.

[83] Joint Research Centre, “Photovoltaic geographical information system.” https://re.jrc.ec.europa.eu/pvg_tools/en/tools.html#MR (accessed Feb. 05, 2019).

[84] G. M. Masters, *Renewable and efficient electric power systems*. John Wiley & Sons, 2013.

[85] E. Skoplaki and J. A. Palyvos, “On the temperature dependence of photovoltaic module electrical performance: A review of efficiency/power correlations,” *Sol. energy*, vol. 83, no. 5, pp. 614–624, 2009.

[86] R. Al-Abri, “Voltage Stability Analysis with High Distributed Generation (DG) Penetration.” UWSpace, 2012, [Online]. Available: http://hdl.handle.net/10012/6853.

[87] X. Zeng, D. Wang, and J. Wu, “Evaluating the three methods of goodness of fit test for frequency analysis,” *J. Risk Anal. Cris. Response*, vol. 5, no. 3, pp. 178–187, 2015.

[88] M. E. Nassar and M. M. A. Salama, “A novel probabilistic load model and probabilistic power flow,” in *2015 IEEE 28th Canadian Conference on Electrical and Computer Engineering (CCECE)*, 2015, pp. 881–886.

[89] B. R. Prusty and D. Jena, “A critical review on probabilistic load flow studies in uncertainty constrained power systems with photovoltaic generation and a new approach,” *Renew. Sustain. Energy Rev.*, vol. 69, pp. 1286–1302, 2017.

[90] G. Carpinelli, P. Caramia, and P. Varilone, “Multi-linear Monte Carlo simulation method for probabilistic load flow of distribution systems with wind and photovoltaic generation systems,” *Renew. Energy*, vol. 76, pp. 283–295, 2015.

[91] J. M. Morales and J. Perez-Ruiz, “Point estimate schemes to solve the probabilistic power flow,” *IEEE Trans. power Syst.*, vol. 22, no. 4, pp. 1594–1601, 2007.

[92] D. Villanueva, J. L. Pazos, and A. Feijoo, “Probabilistic load flow including wind power generation,” *IEEE Trans. Power Syst.*, vol. 26, no. 3, pp. 1659–1667, 2011.

[93] P. S. Georgilakis and N. D. Hatziargyriou, “Optimal distributed generation placement in power distribution networks: models, methods, and future research,” *IEEE Trans. power Syst.*, vol. 28, no. 3, pp. 3420–3428, 2013.

[94] K. Christakou, D.-C. Tomozei, J.-Y. Le Boudec, and M. Paolone, “GECN: Primary Voltage Control for Active Distribution Networks via Real-Time Demand-Response,” *IEEE Trans. Smart Grid*, vol. 2, no. 5, pp. 622–631, 2014.

[95] W. L. Theo, J. S. Lim, W. S. Ho, H. Hashim, and C. T. Lee, “Review of distributed generation (DG) system planning and optimisation techniques: Comparison of numerical and mathematical modelling methods,” *Renew. Sustain. Energy Rev.*, vol. 67, pp. 531–573, 2017.

[96] M. P. HA, P. D. Huy, and V. K. Ramachandaramurthy, “A review of the optimal allocation of distributed generation: Objectives, constraints, methods, and algorithms,” *Renew. Sustain. Energy Rev.*, vol. 75, pp. 293–312, 2017.

[97] A. S. Chuang and F. Wu, “An extensible genetic algorithm framework for

problem solving in a common environment," *IEEE Trans. power Syst.*, vol. 15, no. 1, pp. 269–275, 2000.

[98] E. L. Da Silva, H. A. Gil, and J. M. Areiza, "Transmission network expansion planning under an improved genetic algorithm," *IEEE Trans. Power Syst.*, vol. 15, no. 3, pp. 1168–1174, 2000.

[99] J. H. Holland, *Adaptation in natural and artificial systems: an introductory analysis with applications to biology, control, and artificial intelligence*. MIT press, 1992.

[100] B. Singh, V. Mukherjee, and P. Tiwari, "Genetic algorithm for impact assessment of optimally placed distributed generations with different load models from minimum total MVA intake viewpoint of main substation," *Renew. Sustain. Energy Rev.*, vol. 57, pp. 1611–1636, 2016.

[101] M. Sedghi, A. Ahmadian, and M. Aliakbar-Golkar, "Assessment of optimization algorithms capability in distribution network planning: Review, comparison and modification techniques," *Renew. Sustain. Energy Rev.*, vol. 66, pp. 415–434, 2016.

[102] A. A. Abdelsalam and E. F. El-Saadany, "Probabilistic approach for optimal planning of distributed generators with controlling harmonic distortions," *IET Gener. Transm. Distrib.*, vol. 7, no. 10, pp. 1105–1115, 2013.

[103] W. Sheng, K. Liu, Y. Liu, X. Meng, and Y. Li, "Optimal Placement and Sizing of Distributed Generation via an Improved Nondominated Sorting Genetic Algorithm II," *IEEE Trans. Power Deliv.*, vol. 2, no. 30, pp. 569–578, 2015.

[104] S. Ganguly and D. Samajpati, "Distributed generation allocation with on-load tap changer on radial distribution networks using adaptive genetic algorithm," *Appl. Soft Comput.*, vol. 59, pp. 45–67, 2017.

[105] A. M. Tahboub, M. S. El Moursi, W. L. Woon, and J. L. Kirtley, "Multiobjective dynamic VAR planning strategy with different shunt compensation technologies," *IEEE Trans. Power Syst.*, vol. 33, no. 3, pp. 2429–2439, 2017.

[106] M. Furukakoi, O. B. Adewuyi, H. Matayoshi, A. M. Howlader, and T. Senjyu, "Multi objective unit commitment with voltage stability and PV uncertainty," *Appl. Energy*, vol. 228, pp. 618–623, 2018.

[107] K. Turitsyn, P. Sulc, S. Backhaus, and M. Chertkov, "Distributed control of reactive power flow in a radial distribution circuit with high photovoltaic penetration," *IEEE Power Energy Soc. Gen. Meet.*, 2009.

[108] A. Soroudi, M. Aien, and M. Ehsan, "A Probabilistic Modeling of Photo Voltaic Modules and Wind Power Generation Impact on Distribution Networks," *IEEE Syst. J.*, vol. 2, no. 6, pp. 254–259, 2012.

[109] P. Chiradeja and R. Ramakumar, "An approach to quantify the technical benefits of distributed generation," *IEEE Trans. energy Convers.*, vol. 19, no. 4, pp. 764–773, 2004.

[110] O. Marggraf, S. Laudahn, B. Engel, C. Aigner, M. Lindner, and R. Witzmann, "U-Control-Recommendations for Distributed and Automated Voltage Control in Current and Future Distribution Grids," in *7th Solar & 16th Wind Integration Workshop*, 2017.

[111] B. Bletterie, S. Kadam, R. Bolgaryn, and A. Zegers, "Voltage control with PV inverters in low voltage networks—In depth analysis of different concepts and parameterization criteria," *IEEE Trans. Power Syst.*, vol. 32, no. 1, pp. 177–185, 2016.

[112] P. Kundur *et al.*, "Definition and classification of power system stability IEEE/CIGRE joint task force on stability terms and definitions," *IEEE Trans. Power Syst.*, vol. 19, no. 3, pp. 1387–1401, 2004.

[113] M. Eremia and M. Shahidehpour, *Handbook of electrical power system dynamics: modeling, stability, and control*, vol. 92. John Wiley & Sons, 2013.

[114] G. Verbič and F. Gubina, "A new concept of voltage-collapse protection based on local phasors," *IEEE Trans. Power Deliv.*, vol. 19, no. 2, pp. 576–581, 2004.

[115] M. Paramasivam, A. Salloum, V. Ajjarapu, V. Vittal, N. B. Bhatt, and S. Liu, "Dynamic Optimization Based Reactive Power Planning to Mitigate Slow Voltage Recovery and Short Term Voltage Instability," *IEEE Trans. Power Syst.*, vol. 28, no. 4, pp. 3865–3873, 2013.

[116] J. Tang, J. Liu, F. Ponci, and A. Monti, "Adaptive load shedding based on combined frequency and voltage stability assessment using synchrophasor measurements," *IEEE Trans. power Syst.*, vol. 28, no. 2, pp. 2035–2047, 2013.

[117] J. Modarresi, E. Gholipour, and A. Khodabakhshian, "A comprehensive review of the voltage stability indices," *Renew. Sustain. Energy Rev.*, vol. 63, pp. 1–12, 2016.

[118] Y. Wang, W. Li, and J. Lu, "A new node voltage stability index based on local voltage phasors," *Electr. Power Syst. Res.*, vol. 79, no. 1, pp. 265–271, 2009.

[119] T. He, S. Kolluri, S. Mandal, F. Galvan, and P. Rasigoufard, "Identification of weak locations in bulk transmission systems using voltage stability margin index," in *IEEE Power Engineering Society General Meeting, 2004.*, 2004, pp. 1814–1819.

[120] V. Balamourougan, T. S. Sidhu, and M. S. Sachdev, "Technique for online prediction of voltage collapse," *IEE Proc. - Gener. Transm. Distrib.*, vol. 151, no. 4, pp. 453–460, 2004.

[121] S. Pérez-Londoño, L. F. Rodríguez, and G. Olivar, "A Simplified Voltage Stability Index (SVSI)," *Int. J. Electr. Power Energy Syst.*, vol. 63, pp. 806–813, 2014.

[122] I. Smon, G. Verbic, and F. Gubina, "Local voltage-stability index using tellegen's Theorem," *IEEE Trans. Power Syst.*, vol. 21, no. 3, pp. 1267–1275, 2006.

[123] B. D. H. Tellegen, "A general network theorem, with applications," *Philips Res Rep*, vol. 7, pp. 256–269, 1952.

[124] S. Director and R. Rohrer, "The generalized adjoint network and network sensitivities," *IEEE Trans. Circuit Theory*, vol. 16, no. 3, pp. 318–323, 1969.

[125] F. Gubina, R. Golob, and A. S. Debs, "Fast contingency evaluation by means of the improved adjoint network method," *Int. J. Electr. Power*

Energy Syst., vol. 18, no. 6, pp. 377–383, 1996.

[126] L. A. F. M. Ferreira, "A network-based approach to power system security assessment and control." Georgia Institute of Technology, 1986.

[127] P. Penfield, R. Spence, and S. Duinker, "A generalized form of Tellegen's theorem," *IEEE Trans. Circuit Theory*, vol. 17, no. 3, pp. 302–305, 1970.

[128] Q. Zhou and J. Bialek, "Simplified calculation of voltage and loss sensitivity factors in distribution networks," in *Proc. 16th Power Syst. Comput. Conf.(PSCC2008)*, 2008.

[129] T. Sansawatt, L. F. Ochoa, and G. P. Harrison, "Smart decentralized control of DG for voltage and thermal constraint management," *IEEE Trans. power Syst.*, vol. 27, no. 3, pp. 1637–1645, 2012.

[130] Z. Zhang, L. F. Ochoa, and G. Valverde, "A Novel Voltage Sensitivity Approach for the Decentralized Control of DG Plants," *IEEE Trans. Power Syst.*, vol. 33, no. 2, pp. 1566–1576, 2018.

[131] P. Dierckx, *Curve and surface fitting with splines*. Oxford University Press, 1995.

[132] The Mathworks, "Curve Fitting Toolbox User's Guide." [Online] Available: http://cda.psych.uiuc.edu/matlab_pdf/curvefit.pdf.

[133] S. A. Kalogirou, "Artificial neural networks in renewable energy systems applications: a review," *Renew. Sustain. energy Rev.*, vol. 5, no. 4, pp. 373–401, 2001.

[134] K. S. Garud, S. Jayaraj, and M. Lee, "A review on modeling of solar photovoltaic systems using artificial neural networks, fuzzy logic, genetic algorithm and hybrid models," *Int. J. Energy Res.*, vol. 45, no. 1, pp. 6–35, 2021.

[135] S. Fischer, P. Frey, and H. Drück, "A comparison between state-of-the-art and neural network modelling of solar collectors," *Sol. energy*, vol. 86, no. 11, pp. 3268–3277, 2012.

[136] T. C. McCandless, S. E. Haupt, and G. S. Young, "A regime-dependent artificial neural network technique for short-range solar irradiance forecasting," *Renew. Energy*, vol. 89, pp. 351–359, 2016.

[137] M. Q. Raza and A. Khosravi, "A review on artificial intelligence based load demand forecasting techniques for smart grid and buildings," *Renew. Sustain. Energy Rev.*, vol. 50, pp. 1352–1372, 2015.

[138] H. Hahn, S. Meyer-Nieberg, and S. Pickl, "Electric load forecasting methods: Tools for decision making," *Eur. J. Oper. Res.*, vol. 199, no. 3, pp. 902–907, 2009.

[139] H. A. Malki, N. B. Karayiannis, and M. Balasubramanian, "Short-term electric power load forecasting using feedforward neural networks," *Expert Syst.*, vol. 21, no. 3, pp. 157–167, 2004.

[140] W. Chine, A. Mellit, V. Lughi, A. Malek, G. Sulligoi, and A. M. Pavan, "A novel fault diagnosis technique for photovoltaic systems based on artificial neural networks," *Renew. Energy*, vol. 90, pp. 501–512, 2016.

[141] D. E. Rumelhart, G. E. Hinton, and R. J. Williams, "Learning internal representations by error propagation," California Univ San Diego La Jolla Inst for Cognitive Science, 1985.

[142] A. Mellit and S. A. Kalogirou, “Artificial intelligence techniques for photovoltaic applications: A review,” *Prog. energy Combust. Sci.*, vol. 34, no. 5, pp. 574–632, 2008.

[143] A. Cichocki, R. Unbehauen, and R. W. Swiniarski, *Neural networks for optimization and signal processing*, vol. 253. wiley New York, 1993.

[144] J. Li, J. Cheng, J. Shi, and F. Huang, “Brief introduction of back propagation (BP) neural network algorithm and its improvement,” in *Advances in computer science and information engineering*, Springer, 2012, pp. 553–558.

[145] S. A. Kalogirou and M. Bojic, “Artificial neural networks for the prediction of the energy consumption of a passive solar building,” *Energy*, vol. 25, no. 5, pp. 479–491, 2000.

[146] J. Heaton, *Introduction to neural networks with Java*. Heaton Research, Inc., 2008.

[147] L. Xia, Z. Ma, G. Kokogiannakis, Z. Wang, and S. Wang, “A model-based design optimization strategy for ground source heat pump systems with integrated photovoltaic thermal collectors,” *Appl. Energy*, vol. 214, pp. 178–190, 2018.

[148] A. R. Moghadassi, M. R. Nikkholgh, F. Parvizian, and S. M. Hosseini, “Estimation of thermophysical properties of dimethyl ether as a commercial refrigerant based on artificial neural networks,” *Expert Syst. Appl.*, vol. 37, no. 12, pp. 7755–7761, 2010.

[149] S. Al-Dahidi, M. Louzazni, and N. Omran, “A local training strategy-based artificial neural network for predicting the power production of solar photovoltaic systems,” *IEEE Access*, vol. 8, pp. 150262–150281, 2020.

[150] S. Li, Y. Sun, M. Ramezani, and Y. Xiao, “Artificial Neural Networks for Volt/VAR Control of DER Inverters at the Grid Edge,” *IEEE Trans. Smart Grid*, vol. 10, no. 5, pp. 5564–5573, 2018.

[151] T. Liu, Q. Li, Q. Tong, Q. Zhang, and K. Liu, “An adaptive strategy to compensate nonlinear effects of voltage source inverters based on artificial neural networks,” *IEEE Access*, vol. 8, pp. 129992–130002, 2020.

Curriculum Vitae

Personal Data

Place of birth:	Nkawkaw, Ghana
Marital status:	Single
Nationality:	Ghanaian

Education

04.2018 – 08 2022 **Electrical Power Engineering (PhD)**

University of Bremen, Bremen, Germany

Thesis: Enhancing Voltage Regulation in Medium Voltage Distribution Grids in Ghana using Distributed Generation

08.2013 - 05.2015 **Electrical Power Engineering (Masters)**

Masdar Institute of Science and Technology, Abu Dhabi, United Arab Emirates

Thesis: Optimal Active Network Management Scheme with Efficient Utilization of Renewable Power Generation Ancillary Services

08.2005 - 06.2009 **Electrical and Electronic Engineering (Bachelors)**

Kwame Nkrumah University of Science and Technology, Kumasi, Ghana

Thesis: Construction of High Power Domestic Solar System of 500VA

Professional Experience

04.2018 - today **PhD Research Assistant**

	Institute of Automation Technology, University of Bremen, Bremen, Germany
01.2016 - 04.2017	**Assistant Lecturer**
	University of Energy and Natural Resources – Sunyani, Ghana
09.2013 - 05.2015	**Research Assistant**
	iEnergy Center, Masdar Institute, United Arab Emirates
01.2011 - 08.2013	**Transmission Engineer**
	Glo Mobile Ghana, Accra, Ghana
11.2009 - 08.2010	**Graduate Electrical Engineer**
	Northern Electricity Company (NEDCo)-Volta River Authority, Ghana

Software Skills

Simulation Software	DigSilent Powerfactory, PSCAD, MATLAB/Simulink, Matpower
Programming	Python, Matlab